

12-2014

FAST FISSION NEUTRON DETECTION USING THE CHERENKOV EFFECT

Matthew Millard

Clemson University, mjmilla@clemson.edu

Follow this and additional works at: https://tigerprints.clemson.edu/all_theses

 Part of the [Environmental Engineering Commons](#), [Nuclear Engineering Commons](#), and the [Physics Commons](#)

Recommended Citation

Millard, Matthew, "FAST FISSION NEUTRON DETECTION USING THE CHERENKOV EFFECT" (2014). *All Theses*. 2047.
https://tigerprints.clemson.edu/all_theses/2047

This Thesis is brought to you for free and open access by the Theses at TigerPrints. It has been accepted for inclusion in All Theses by an authorized administrator of TigerPrints. For more information, please contact kokeefe@clemson.edu.

FAST FISSION NEUTRON DETECTION USING THE CHERENKOV EFFECT

A Thesis
Presented to
the Graduate School of
Clemson University

In Partial Fulfillment
of the Requirements for the Degree
Master of Science
Environmental Engineering and Earth Science

by
Matthew James Millard
December 2014

Accepted by:
Timothy A. DeVol, Committee Chair
Zane W. Bell
Lindsay Shuller-Nickles

ABSTRACT

The Cherenkov effect in optically clear media of varying indices of refraction and composition was investigated for quantification of fast neutrons. The ultimate application of the proposed detection system is criticality monitoring. The optically clear medium, composed of select target nuclei, was coupled to a photomultiplier tube. Neutron reaction products of the target nuclei contained within the optical medium emit beta particles and gamma rays that produce Cherenkov photons within the medium which can be detected. Assessed media include quartz (SiO_2), sapphire (Al_2O_3), spinel (MgAl_2O_4), and zinc sulfide (ZnS), which were irradiated with un-moderated ^{252}Cf . Monte Carlo N-Particle (MCNP) code simulations were conducted to quantify the neutron flux incident on the media. High resolution gamma-ray spectroscopic measurements of the samples were conducted to verify the MCNP estimate. The threshold reactions of interest were $^{28}\text{Si}(\text{n}, \text{p})^{28}\text{Al}$, $^{27}\text{Al}(\text{n}, \text{p})^{27}\text{Mg}$, $^{24}\text{Mg}(\text{n}, \text{p})^{24}\text{Na}$, and $^{64}\text{Zn}(\text{n}, \text{p})^{64}\text{Cu}$ which have neutron reaction cross sections in the 1 to 10 MeV range on the order of 0.1 barn. The detection system offers a unique way to measure a criticality event; it can count in place, making retrieval by emergency personnel unnecessary.

ACKNOWLEDGEMENTS

Thanks go to:

Dr. Timothy DeVol, for taking a chance and hiring me as one of his students (I promise it will pay off some day). Without his guidance, this research would not have been possible.

Dr. Lindsay Shuller-Nickles, for teaching me about the nuclear fuel cycle, giving me her input and words of encouragement throughout this process, and lending me books that I will likely never return.

Dr. Zane Bell, for developing this detection technique, allowing me to work with him at ORNL, showing me how interesting scientific research can be, and most importantly, for teaching me how to build match stick rockets.

Dr. Lynn Boatner, for developing this detection technique with Dr. Bell and creating the glass that I worked with at ORNL.

Dr. John Ballato, for introducing me to the idea of using crystal samples.

Amy Meldrum, for helping me learn how to use GATE software.

Dr. Elizabeth Carraway, for allowing me to use her spectrofluorometer.

My friends, for making every day a little better.

TABLE OF CONTENTS

	Page
ABSTRACT	ii
ACKNOWLEDGEMENTS	iii
LIST OF FIGURES	vi
LIST OF TABLES	ix
INTRODUCTION	1
BACKGROUND.....	3
Nuclear Criticality Accidents	3
Nuclear Accident Dosimetry.....	5
THEORY	9
Cherenkov Radiation.....	9
Neutron Activation.....	12
Recent Research.....	14
Preliminary Data.....	16
Target Material Properties.....	18
1) Shape of the Cross Section.....	18
2) Magnitude of the Cross Section	18
3) Decay Constant of the Induced Activity	19
4) Purity and Interfering Activities	19
5) Nature of the Induced Activity.....	20
6) Physical Properties	20
RESEARCH OBJECTIVE	22
Hypotheses.....	22
MATERIALS AND METHODS	23
Target Nuclides.....	23
Ideal Media	25
Neutron Source.....	26
Procedure.....	27
Fluorescence Discrimination.....	27
Irradiation.....	31

TABLE OF CONTENTS (CONTINUED)

	Page
LLD and ULD	33
Time Series Measurements	34
Calculating Efficiency	35
Simulations	36
RESULTS AND DISCUSSION	38
Experimental Half-Life	38
Calculation of the Reaction Rate	41
Measured Counting Efficiency for Cherenkov Radiation	43
GATE Simulations	44
CONCLUSIONS	66
Future Work	66
Applicability for a Criticality Event	68
APPENDICES	71
Appendix A: Raw Data	72
Al ₂ O ₃	72
SiO ₂	74
MgAl ₂ O ₄ (30 s bins)	77
MgAl ₂ O ₄ (10 min bins)	79
ZnS	82
Appendix B: Input Files	83
Example MCNP Input (Al ₂ O ₃)	83
Example GATE Input Macro (SiO ₂)	86
Appendix C: ²⁵² Cf Source Information	110
Appendix D: Gamma Ray Spectra	113
Appendix E: SpectroFluorometer Measurements	117
Appendix F: Neutron Reaction Target Search Program	122
REFERENCES	126

LIST OF FIGURES

	Page
Figure 1 <i>An ORNL PNAD. (Kerr and Mei 1993) TLDs 1 and 2 are exposed to a neutron flux with the slow component removed due to captures by the cadmium shield. TLDs 3 and 4 are placed under plastic to simulate dose received by tissue deeper in the body.</i>	7
Figure 2 <i>Hanford Fixed Nuclear Accident Dosimeter with multiple activation foils and TLDs. An algorithm reconstructs the neutron spectra based on the radioactivity of the foils and readout from the TLDs (Rathbone 2010).</i>	8
Figure 3 <i>Beta particle and Compton scattering Cherenkov thresholds as a function of index of refraction</i>	10
Figure 4 <i>Steps of neutron activation analysis. A sample is irradiated, producing a radioactive reaction product with activity $A(t)$, removed from irradiation, and counted</i>	14
Figure 5 <i>a) Decay of ^{116m}In in $\text{Pb}_2\text{P}_2\text{O}_7:\text{In}$ glass. The MCS used 1 second bins (Bell and Boatner 2010) b) Neutron cross sections of $^{115}\text{In}(n, \gamma)$ and $^{31}\text{P}(n, p)$ from 1 to 20 MeV. (National Nuclear Data Center 2013)</i>	16
Figure 6 <i>Time series spectrum of $\text{Pb}_2\text{P}_2\text{O}_7:\text{In}$ glass after irradiation by an Am-Be source. The data is fit to exponentials with decay constants of ^{31}Si and ^{116m}In.</i>	17
Figure 7 <i>Neutron reaction cross sections of selected target nuclides (National Nuclear Data Center 2013).</i>	25
Figure 8 <i>Watt function representative of fission spectra taken from the MCNP5 manual. The shape of the spectra of ^{252}Cf, ^{235}U, and ^{239}Pu are almost indistinguishable.</i>	27
Figure 9 <i>Time series comparison of the spinel sample exposed to room light and the spinel sample kept in the dark box. The initial count rate of the spinel exposed to room light is approximately 100 times greater than the spinel left in the dark box and the signal from the spinel exposed to room light decays according to at least two time components .</i>	29
Figure 10 <i>Pulse height spectrum comparison of spinel exposed to room light vs. spinel kept in darkness. At lower channels the difference in counts is orders of magnitude. The lower level discriminator was set to the lowest channel which had net counts less than L_c; channel 11 in this case</i>	31
Figure 11 <i>Geometry of irradiation of samples by ^{252}Cf. The edge of the sample was lined up with the edge of the ^{252}Cf capsule for easy replication of the experiment.</i>	32
Figure 12 <i>Counting electronics of detection method. Cherenkov photons from the sample produce a pulse in the PMT which is amplified by the amplifier and recorded by the MCS before being displayed by a computer.</i>	33
Figure 13 <i>Pulse height spectrum of Al_2O_3 irradiated by ^{252}Cf. Only the net counts in channels 6 through 22 were greater than the critical value, N_d.</i>	34
Figure 14 <i>GATE simulation model of a sample coupled to photomultiplier tube</i>	37
Figure 15 <i>Time series spectrum of SiO_2 after having been irradiated by ^{252}Cf. The half-life value calculated by Solver (2.14 minutes) was very close to the accepted half-life value for ^{28}Al (2.24 minutes), which was the radionuclide of interest.</i>	38
Figure 16 <i>Decay of ^{24}Na in MgAl_2O_4 after irradiation by unmoderated ^{252}Cf. The red line is a regression fit where all parameters were decided by Solver. The green line corresponds to the theoretical half-life of ^{24}Na.</i>	40

LIST OF FIGURES (CONTINUED)

	Page
Figure 17 <i>GATE/GEANT4 simulation results of a 0.5 MeV electron source distributed homogeneously in a fused silica disc that is coupled to a photomultiplier tube. A) Density with a constant index of refraction of 1.4 and b) index of refraction with a constant density of 2.2 g/cm³ were varied to show the effect on counting efficiency.</i>	47
Figure 18 <i>Counting Efficiency as a function of lower level discriminator. Results are from GATE simulations of quartz, sapphire, spinel, and zinc sulfide with identical dimensions exposed to a 1.0 MeV electron source and coupled to a photomultiplier tube with 100% quantum efficiency.</i>	49
Figure 19 <i>Counting Efficiency as a function of lower level discriminator. Results are from GATE simulations of quartz, sapphire, spinel, and zinc sulfide each irradiated by a neutron reaction product and coupled to a photomultiplier tube.</i>	50
Figure 20 <i>Pulse height spectrum of a bismuth germanate (BGO) crystal exposed to gamma ray sources. The peak channels correspond to the maximum number of photoelectrons emitted for a particular energy.</i>	53
Figure 21 <i>Comparison of the efficiency vs lower level discriminator for GATE simulations and experimental data. a) ²⁸Al in SiO₂, B) ²⁷Mg in Al₂O₃, C) ²⁷Mg in MgAl₂O₄, D) ²⁴Na in MgAl₂O₄, E) ⁶⁴Cu in ZnS</i>	56
Figure 22 <i>Pulse height spectrum of samples irradiated by ²¹⁰Po. a) SiO₂, B) Al₂O₃,</i>	59
Figure 23 <i>Approximate Quantum Efficiency vs. Wavelength spectrum for a standard Hamamatsu R268 PMT (Hamamatsu Photonics K.K., Electron Tube Center 1996)</i>	61
Figure 24 <i>Comparison of the efficiency vs lower level discriminator for GATE simulations with varying parameters that affect light collection of the PMT. a) ²⁸Al in SiO₂, B) ²⁷Mg in Al₂O₃, C) ²⁷Mg in MgAl₂O₄, D) ²⁴Na in MgAl₂O₄, E) ⁶⁴Cu in ZnS</i>	64
Figure 25 <i>Wavelength spectrum of Cherenkov photons that reach the PMT in a GATE simulation of ²⁷Mg in Al₂O₃</i>	65
Figure 26 <i>a), b), c) Time series data showing the exponential decay of ²⁷Mg produced as a result of neutron irradiation of Al₂O₃. d) Time series data showing a lack of signal after the Cherenkov photons were prevented from reaching the PMT. The background count rate decreases when the PMT is covered by foil. This suggests that that background gamma-ray radiation may be interacting with the Al₂O₃ sample, producing Cherenkov or fluorescence photons.</i>	73
Figure 27 <i>Pulse height spectrum of Al₂O₃ after irradiation by ²⁵²Cf</i>	74
Figure 28 <i>a), b), c) Time series data showing the exponential decay of ²⁸Al produced as a result of neutron irradiation of SiO₂. d) Time series data showing a lack of signal after the Cherenkov photons were prevented from reaching the PMT. The background count rate of the covered and uncovered PMT are the same</i>	76
Figure 29 <i>Pulse height spectrum of irradiated SiO₂ after irradiation by ²⁵²Cf</i>	76
Figure 30 <i>a), b), c) Time series data showing the exponential decay of ²⁷Mg produced as a result of neutron irradiation of MgAl₂O₄. d) Time series data showing a lack of signal after the Cherenkov photons were prevented from reaching the PMT. Just as with Al₂O₃ the background count rate decreases when the PMT is covered by foil. The MgAl₂O₄ sample may be scintillating or producing Cherenkov photons from ambient gamma-ray radiation.</i>	78
Figure 31 <i>Pulse height spectrum of irradiated MgAl₂O₄ after irradiation by ²⁵²Cf</i>	79

LIST OF FIGURES (CONTINUED)

	Page
Figure 32 a), b), c) Time series data showing the exponential decay of ^{24}Na produced as a result of neutron irradiation of MgAl_2O_4 . d) Time series data showing a lack of signal after the Cherenkov photons were prevented from reaching the PMT.....	81
Figure 33 Pulse height spectrum of irradiated MgAl_2O_4 after irradiation by ^{252}Cf	81
Figure 34 Pulse height spectrum of ZnS irradiated by ^{252}Cf vs Background. No signal due to irradiation is visible.....	82
Figure 35 Time series data showing a lack of signal from ^{64}Cu in ZnS.....	82
Figure 36 Three day background count. The 511 keV peak from positron annihilation, 1460 keV peak from ^{40}K , and 2614 keV peak from ^{208}Tl are present.....	113
Figure 37 Al_2O_3 irradiated by ^{252}Cf and counted for 30 minutes. The gamma ray peaks from the decay of ^{27}Mg and ^{24}Na are present.....	114
Figure 38 SiO_2 irradiated by ^{252}Cf and counted for 15 minutes. Counts were present at 1778 keV, however MAESTRO (the MCA software) was not able to distinguish them from background.....	114
Figure 39 MgAl_2O_4 irradiated by ^{252}Cf and counted for 30 minutes. The gamma ray peaks from the decay of ^{27}Mg and ^{24}Na are present.....	115
Figure 40 MgAl_2O_4 irradiated by ^{252}Cf and counted for 2 days. The gamma ray peaks from the decay of ^{24}Na are present.....	115
Figure 41 ZnS irradiated by ^{252}Cf and counted for 3 days. The 511 keV gamma ray peak from positron annihilation is present; the net area from the 3 day background count was subtracted out of the net area value.....	116
Figure 42 Geometry of the spectrofluoroscopic measurements taken of the samples. The $^{90}\text{Sr}/^{90}\text{Y}$ source and the x-ray tube did not irradiate the samples simultaneously.....	118
Figure 43 Wavelength spectra of A) Background (only the source, no sample) B) SiO_2 C) Al_2O_3 D) MgAl_2O_4 , and E) ZnS when irradiated by a $^{90}\text{Sr}/^{90}\text{Y}$ source and a 40 keV x-ray source. The $^{90}\text{Sr}/^{90}\text{Y}$ source spectrum should be a combination of Cherenkov and fluorescence photons while the x-ray source spectrum should only contain fluorescence photons. The Cherenkov spectrum from a GATE simulation of each sample has been plotted using the right-hand axis.....	121
Figure 44 User interface for target reaction search tool used for finding neutron reactions for Cherenkov based neutron activation analysis. The program takes the specified criteria of the target nuclide and reaction product and outputs a list of reactions that meet those criteria.....	123
Figure 45 Flow chart describing the execution of the target reaction search tool used for finding reactions for Cherenkov based neutron activation analysis.....	125

LIST OF TABLES

	Page
Table 1 Target Isotope Properties.....	24
Table 2 Reaction Product Properties.....	25
Table 3 Target Material Properties.....	26
Table 4 Comparison of Theoretical and Experimental Values of Half-life.....	40
Table 5 Solver's estimate of ^{24}Na half-life as a function of time.....	41
Table 6 Initial Activity of MCNP Simulation and Measurement with a High-Resolution Gamma-ray Spectroscopy System.....	43
Table 7 Measured Counting Efficiency.....	44
Table 8 Comparison of GATE and Experimental Efficiency.....	51

INTRODUCTION

One of the greatest safety concerns at nuclear reactors and processing facilities is the risk of exposure to harmful radiation. Because of stringent safety measures, workers will likely only receive a harmful dose of radiation in the event of an accident. Of all the accidents that take place, an uncontrolled criticality event will produce the greatest amount of radiation dose in the shortest time. The level of radiation that results from a typical criticality can easily surpass the LD₅₀ (lethal dose to 50% of the population) of 4 Gy, with most of the radiation emitted during a criticality event being neutron and gamma-ray radiation. Both forms of radiation can cause serious biological effects in tissue; however neutrons cause 5 to 20 times more damage in the body than gamma rays of similar energy.

Existing detectors designed to measure the neutron flux near a criticality accident primarily consist of thermoluminescent dosimeters (TLDs) and activation foils. The response of thermoluminescent dosimeters to radiation is proportional to the response of tissue in the human body. Therefore, TLDs can be used to estimate the total neutron dose received by a person. By utilizing activation foils with different neutron cross sections, an approximate neutron energy spectrum at the detector (Kerr and Mei 1993) can be deduced. TLDs must be retrieved so that they can be read by a TLD reader, while the activation foils must be retrieved to be counted with a high-resolution gamma-ray spectroscopy system. Retrieval of these detectors can be hazardous due to the neutron activation that takes place in the

surrounding material and because the criticality event has the potential to take place again.

A detection method that measures neutron flux and does not require retrieval has been developed. The detection method offers fast data acquisition, and its operation is based on the principles of the Cherenkov effect and neutron activation analysis. It also features materials activated by fast neutrons via (n, p) reactions leading to residual beta-gamma radioactivity which produces Cherenkov light, which can then be detected by a photosensitive instrument. The function of this research is to determine the utility of various neutron sensitive materials incorporated in this detection method by exposing them to a fast fission neutron flux with energy between 1 and 10 MeV.

BACKGROUND

NUCLEAR CRITICALITY ACCIDENTS

A criticality event results when a fissile material reaches a critical mass – a mass of fissile material in a suitable geometry such that a self-sustained fission reaction can take place. It can occur when a sufficient amount of fissile material is concentrated into a small volume. If free neutrons are present within or near the material, they can interact with the nuclei of the material (e.g., ^{239}Pu or ^{235}U), causing them to fission. A self-sustained chain reaction can then be initiated, where each neutron produced in a fission reaction can produce two or more neutrons and an equal number of neutrons leak out of the critical mass as cause additional fissions. This self-sustained reaction generates a large number of fissions; typically between 10^{15} and 10^{20} total fissions take place during an accidental criticality event, with each fission leaking 2 to 3 neutrons (McLaughlin 2000). The reaction will terminate once enough fissile material has been consumed to make the mass subcritical, or until the fissile material's geometry becomes unfavorable for the reaction to continue. Therefore, whenever it is necessary for people to handle fissile material, the prevention and detection (if prevention fails) of a criticality event is of great concern.

Uranium enrichment is an important process in the nuclear fuel cycle. Enriching uranium means increasing the concentration of ^{235}U relative that that of ^{238}U . This is commonly done by gaseous diffusion or gaseous centrifugation where

UF₆ gas is sent through multiple refinement stages until the requisite isotopic enrichment is reached. In each stage, the ratio of ²³⁵U to ²³⁸U increases in the UF₆ gas.

Despite the systems and procedures that enrichment facilities have in place to prevent the possibility of an accidental criticality, accidents have occurred. In 1961, at a uranium enrichment facility in Siberia, a desublimation vessel used in a UF₆ purification process was not properly cooled, which allowed a large increase in the rate and amount of enriched UF₆ passing through the tank and into the next vessel in the process. Eventually, the purification process led to a vacuum pump with an oil reserve where UF₆ tended to accumulate. Under normal operating conditions, the oil in the vacuum pump was replaced every 15 days. The increased buildup of UF₆ in the oil was not taken into account by the operators, and once a critical mass of ²³⁵U had accumulated in the vacuum pump's oil reservoir (later analysis showed a concentration of 173 grams per liter of uranium enriched to 22.6% in the reservoir), a criticality event took place. The first excursion produced approximately 2×10^{14} fissions. The only person to be significantly exposed was the operator, who received a dose of approximately 2 Gy and experienced mild radiation sickness. (McLaughlin 2000).

Reprocessing of spent nuclear fuel to extract ²³⁹Pu and the residual ²³⁵U is another important process in the nuclear fuel cycle in several countries, especially Japan. It involves chemically separating plutonium and uranium from the rest of the fuel and fission products. A nuclear accident involving reprocessing happened

at a Fuel Conversion Test Building in Tokai-mura, Ibaraki prefecture in Japan in 1999. Workers added solutions of uranyl nitrate (enriched to between 16% and 20% ^{235}U) directly into a precipitation tank instead of sending it through a column as prescribed in the formal procedure. Unfortunately, the uranium enrichment of the uranyl nitrate concentration added to the precipitation tank was significantly higher than the rating of the tank, and a criticality ensued. One worker received a dose between 16 and 20 Gy and another received a dose between 6 and 10 Gy. Both died months later as a result of the dose from the accident (McLaughlin 2000).

NUCLEAR ACCIDENT DOSIMETRY

The Department of Energy's (DOE) national laboratories have detection protocols for nuclear accident dosimetry. In the event of an accident, it is important to triage exposed workers for medical treatment. Geiger-Mueller (GM) probes are used to measure the induced beta particle or gamma ray radiation from activated indium foil inside a worker's security badge. If it is determined from the count rate of the GM probe that the person received a dose greater than 0.25 Gy, they are sent to the laboratory's medical department for blood collection and analysis (Kerr and Mei 1993).

The foil measurement may indicate a dose that is lower than what the person actually received because the activity of the foil will vary based on the person's orientation during exposure. Therefore, people whose indium foil dose measures less than 0.25 Gy undergo a second quick sort measurement. Geiger-Mueller probes

will detect the beta particles and gamma rays from ^{38}Cl and ^{24}Na which are produced in the body by $^{37}\text{Cl}(n, \gamma)^{38}\text{Cl}$ and $^{23}\text{Na}(n, \gamma)^{24}\text{Na}$ reactions. For the second quick sort measurement, a GM probe is placed against the abdominal area and the person is asked to bend over the probe to increase its sensitivity. Those determined to have the highest dose from this measurement will be next to be sent for blood collection and analysis. Eventually, all of those suspected of being exposed will have their blood collected and analyzed. Quantification of neutron reactions in the blood is done by liquid scintillation counting of a 20 mL blood sample to determine the presence of ^{24}Na . (Kerr and Mei 1993).

For rapid screening for fast neutron reactions in the body, the presence of ^{32}P in hair from the $^{32}\text{S}(n, p)^{32}\text{P}$ reaction is quantified. The concentration of sulfur in human hair is about 45 mg/g (Kerr and Mei 1993). The activity from ^{32}P is counted using liquid scintillation counting after preparing the hair sample by chemical dissolution or ashing (Kerr and Mei 1993). The advantage of using hair is that samples from different parts of the body can be taken and their activity measured, which can give an idea of the orientation of the person's body when the irradiation took place.

In addition to measuring the activity of activated radionuclides within the body, both ORNL (Oak Ridge National Laboratory) and PNNL (Pacific Northwest National Laboratory) make use of personal nuclear accident dosimeters (PNADs) and fixed nuclear accident dosimeters (FNADs). At ORNL, a neutron PNAD is

composed of a thermo-luminescent dosimeter TLD-600/TLD-700 pair (natural LiF and LiF enriched in ^6Li for neutron sensitivity) under 300 mg/cm² of plastic and another TLD-600/TLD-700 pair under a cadmium filter, which captures slow neutrons before they can reach the TLDs, allowing for the fast neutron flux to be measured (Kerr and Mei 1993). A schematic of the PNAD is shown below in Figure 1.

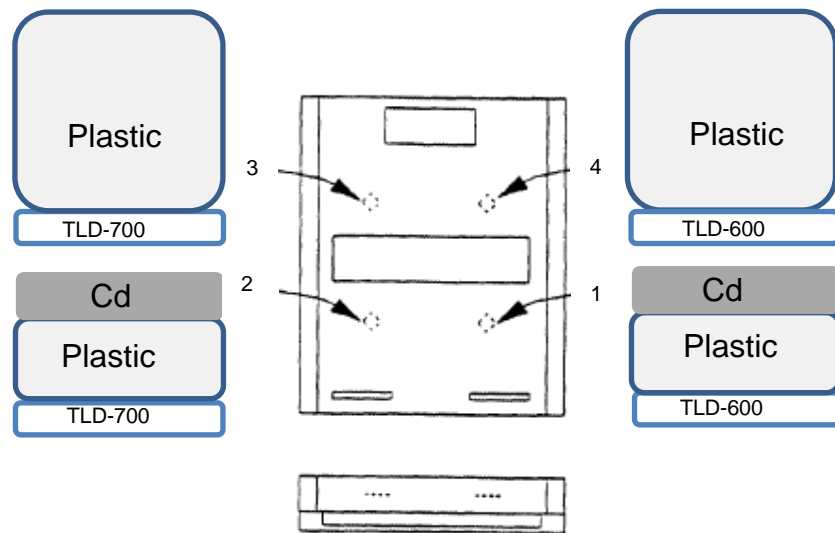


Figure 1 An ORNL PNAD. (Kerr and Mei 1993) TLDs 1 and 2 are exposed to a neutron flux with the slow component removed due to captures by the cadmium shield. TLDs 3 and 4 are placed under plastic to simulate dose received by tissue deeper in the body.

At PNNL, fixed nuclear accident dosimeters are more accurate than the personal nuclear accident dosimeters. The FNADs at PNNL are able to measure neutron energies in six ranges, including between 1.2 MeV and 2.9 MeV and greater than 2.9 MeV, which are regions of interest in this research. Figure 2 shows a schematic of the FNAD:

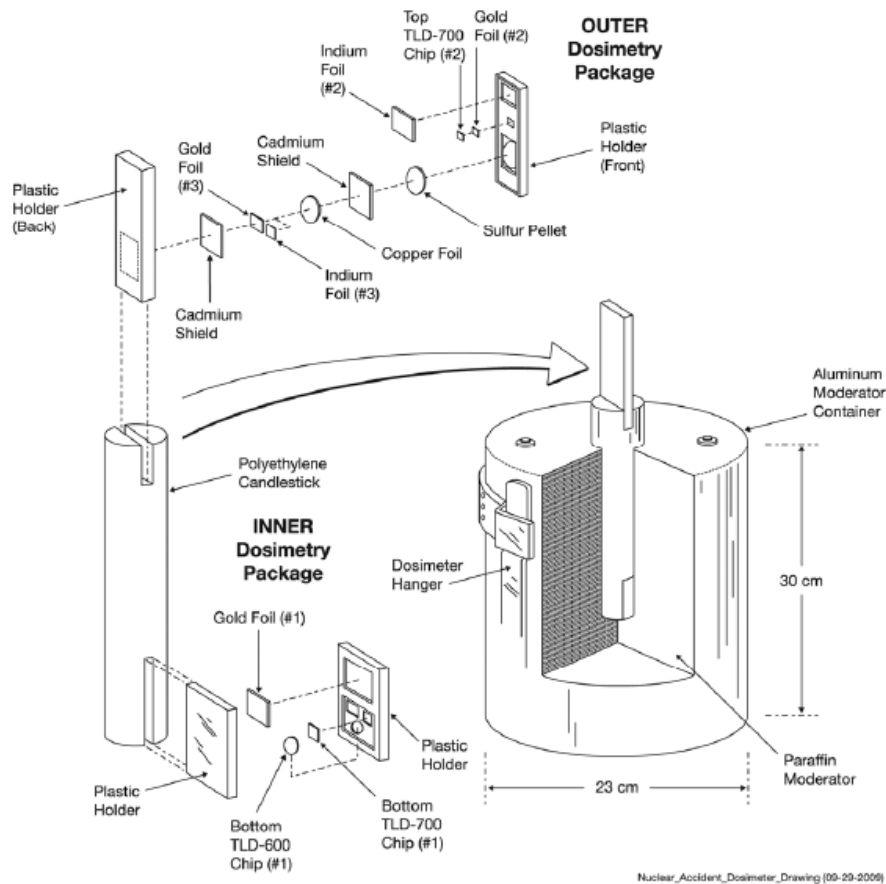


Figure 2 Hanford Fixed Nuclear Accident Dosimeter with multiple activation foils and TLDs. An algorithm reconstructs the neutron spectra based on the radioactivity of the foils and readout from the TLDs (Rathbone 2010).

Both PNADs and FNADs must meet standards defined by the Department of Energy's *DOE Standard Radiological Control* report. In the case of a nuclear accident, both PNADs and FNADs must be able to measure a dose of at least 0.1 Gy. PNADs must be able to detect up to 10 Gy, FNADs up to 100 Gy, and both must be accurate to within $\pm 25\%$ of the actual dose (U.S. Department of Energy 2008).

THEORY

CHERENKOV RADIATION

Frank and Tamm (Frank and Tamm 1937) demonstrated that in order to produce Cherenkov photons, a charged particle passing through a transparent medium must satisfy the equation

$$\beta n > 1 \quad (1)$$

where $\beta=v/c$, where v is the velocity of the particle, c is the speed of light in a vacuum, and n is the index of refraction of the medium. The velocity of the charged particle is related to its kinetic energy, T , by the equation (Taylor 2005, 641)

$$T = m_o c^2 \left[\frac{1}{\sqrt{1 - \beta^2}} - 1 \right] \quad (2)$$

where m_o is the rest mass of the particle. By combining the equations 1 and 2, an equation for the threshold kinetic energy needed to produce Cherenkov photons can be written as

$$T = m_o c^2 \left[\frac{1}{\sqrt{1 - \frac{1}{n^2}}} - 1 \right] \quad (3)$$

Gamma rays produce Cherenkov photons indirectly through their interactions with electrons. A gamma ray transfers energy to an electron via Compton scattering or the photoelectric effect. The energy of the gamma ray, E_g ,

needed to produce Cherenkov radiation if interacting with an electron via the photoelectric effect is

$$E_g = E + E_b \quad (4)$$

where E is the Cherenkov threshold energy of an electron and E_b is the binding energy of the electron. If interacting via Compton scattering, the energy threshold to produce Cherenkov photons is

$$E_g = \frac{1}{2} m_e \left(-1 + \frac{n + 1}{\sqrt{n^2 - 1}} \right) \quad (5)$$

where m_e is the rest mass of an electron. The energy thresholds for electrons and gamma rays (via Compton scattering) are shown in Figure 3.

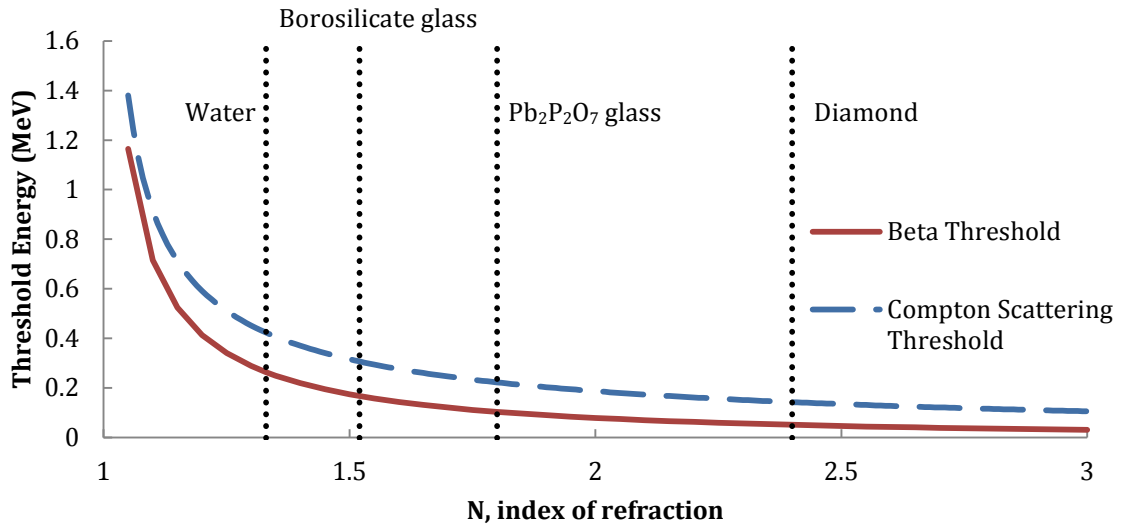


Figure 3 Beta particle and Compton scattering Cherenkov thresholds as a function of index of refraction

Frank and Tamm showed that the energy W radiated by the electron through the surface of a cylinder of length l is

$$W = \frac{e^2 l}{c^2} \int_{\beta n > 1} \omega d\omega \left(1 - \frac{1}{\beta^2 n^2}\right) \quad (6)$$

where ω is the angular frequency of the Cherenkov radiation, $\omega = 2\pi c/\lambda$, and λ is the wavelength at which the Cherenkov radiation is emitted. In order to simplify the problem, this equation makes several assumptions (Jelley 1958, 15):

- The conductivity of the medium is zero, the magnetic permeability $\mu = 1$, and there is no absorption of Cherenkov radiation.
- The particle moves at constant velocity through the medium.
- The medium is infinite.
- The length l should be large in comparison to the wavelength of the radiation emitted.

Assuming that l is also small compared to the total path length of the particle, Frank and Tamm deduced from equation 6 the quantity M – the number of photons emitted over the total path length between wavelengths λ_2 and λ_1 – as

$$M = 2\pi\alpha \left(\frac{1}{\lambda_2} - \frac{1}{\lambda_1}\right) \int_{1/n}^{\beta^{max}} \left(\frac{1}{(\beta(l)n)^2} - 1\right) dl \quad (7)$$

where α , the fine structure constant, is $\frac{e^2}{hc}$. Equations 7 shows that the number of Cherenkov photons emitted by a charged particle traveling in a medium increases with the speed of the charged particle and the index of refraction of the medium.

NEUTRON ACTIVATION

The likelihood that a neutron will interact with the nucleus of an atom is quantified by the neutron cross section. Different reactions are possible, and correspond to the target nucleus and to the energy of the neutron. The reaction rate between neutrons and the material they are irradiating is given by (Knoll, 2012, p. 767)

$$R = \Phi \sigma N_t \quad \text{(10)}$$

where R (s^{-1}) is the reaction rate, Φ ($s^{-1}cm^{-2}$) is the neutron flux, σ (cm^2) is the microscopic neutron cross section, and N_t is the number of target atoms. The neutron flux and the neutron cross section are energy dependent. The neutron flux also changes as it travels through the material.

Assuming the reaction of interest is the only one that will add to the number of reaction product atoms, and that the reaction product is radioactive with decay constant λ (s^{-1}), the buildup of product radioactive nuclei caused by this reaction is given by

$$\frac{dN}{dt} = R - \lambda N \quad \text{(11)}$$

where N is the number of radioactive atoms. Assuming the neutron flux to be constant and neglecting the number of target nuclides transmuted during the irradiation, the reaction rate R can be taken to be constant. The solution of (11) is

$$N(t) = \frac{R}{\lambda}(1 - e^{-\lambda t}) \quad (12)$$

where t is the time since the onset of irradiation in seconds. When irradiation by neutrons stops at time t_o , the activity of the radionuclide can be written as

$$A_o = R(1 - e^{-\lambda t_o}) \quad (13)$$

where A_o (s^{-1}) is the activity of the radionuclide at time t_o . Accounting for the number of background counts B during $t_2 - t_1$, and integrating from time t_1 to time t_2 , as shown in the Figure 4, one can get an estimate of the number of counts expected

$$C = \varepsilon \int_{t_1}^{t_2} A_o e^{-\lambda(t-t_o)} dt + B = \varepsilon \frac{A_o}{\lambda} e^{\lambda t_o} (e^{-\lambda t_1} - e^{-\lambda t_2}) + B \quad (14)$$

where ε is the counting efficiency. The counting efficiency is the number of radionuclide decays divided by the number of counts between t_1 and t_2 . Equation 14 combined with equation 13 can be re-written as

$$\varepsilon = \frac{\lambda(C-B)}{N_T \sigma \Phi (1 - e^{-\lambda t_o}) e^{\lambda t_o} (e^{-\lambda t_1} - e^{-\lambda t_2})} \quad (\text{Knoll 2012, 768}) \quad (15)$$

The counting efficiency for a Cherenkov-based neutron detection method depends on several factors, including the energy of the reaction product(s), the index of refraction of the material, the light transmission of the material, light escaping from the material, and the quantum efficiency (QE) of the photo-multiplier tube (PMT),

$$QE = \frac{\text{number of photoelectrons emitted}}{\text{number of incident photons}}.$$

Alternatively, once the counting efficiency is known, and the material is placed in a neutron field where the neutron flux is unknown, the flux on the material can be found from

$$\Phi = \frac{\lambda(C-B)}{\varepsilon N_T \sigma (1 - e^{-\lambda t_0}) e^{\lambda t_0} (e^{-\lambda t_1} - e^{-\lambda t_2})}. \quad (16)$$

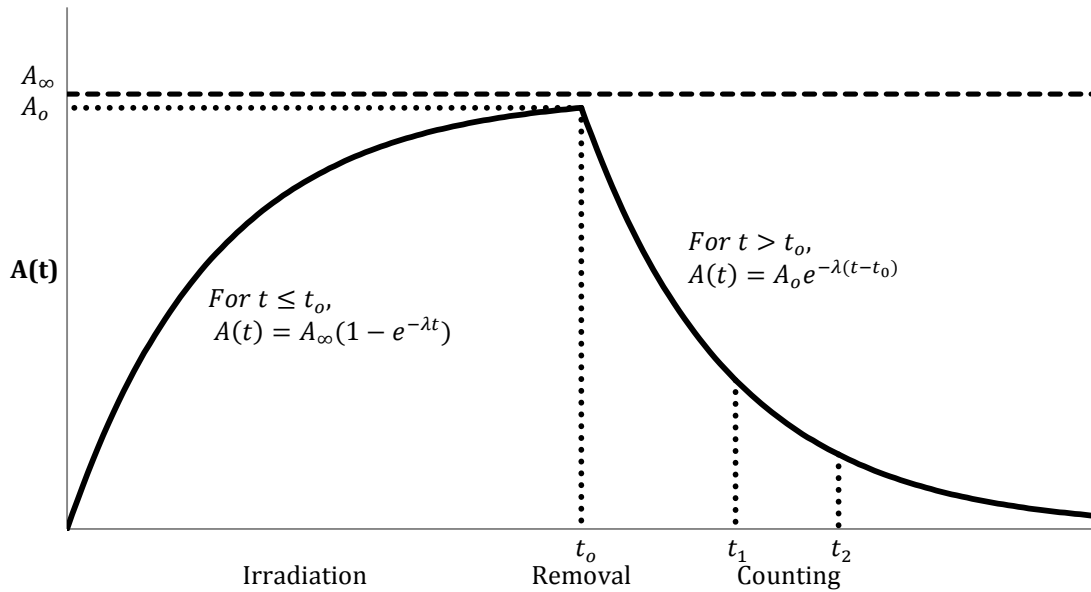


FIGURE 4 Steps of neutron activation analysis. A sample is irradiated, producing a radioactive reaction product with activity $A(t)$, removed from irradiation, and counted

RECENT RESEARCH

Bell and Boatner (2010) reported the use of the Cherenkov effect for thermal neutron detection in $Pb_2P_2O_7$ glass doped with indium (III) oxide (approximately 10% by weight). The isotope ^{115}In comprises 95.7% of natural Indium and has an (n, γ) neutron cross section of approximately 200 barns ($200 \times 10^{-24} \text{ cm}^2$) for

thermal (room temperature) neutrons (0.025 eV). When ^{115}In captures a neutron via an γ reaction, it will most likely enter into a metastable state of $^{116\text{m}}\text{In}$, which has a half-life of approximately 54 minutes and emits energetic beta particles and gamma rays. The energies of these beta particles and gamma rays are well above the threshold for producing Cherenkov photons in most liquids and solids. Bell and Boatner irradiated the indium doped glass with a $570,000 \text{ n s}^{-1}$ moderated Americium-Lithium source which yielded a thermal neutron flux of approximately $100 \text{ n cm}^{-2}\text{s}^{-1}$, and counted the resulting Cherenkov radiation with a PMT and a multi-channel scaler (MCS). The results shown in Figure 5 demonstrate the detection of neutrons via the Cherenkov effect.

Using MCNP5, Bell and Boatner calculated the reaction rate of the $^{115}\text{In}(n, \gamma)^{116\text{m}}\text{In}$ reaction within the glass to be approximately 992 s^{-1} . From measurements, they estimated the initial count rate to be $130 \text{ counts s}^{-1}$. Dividing the initial count rate by the reaction rate, Bell and Boatner found the efficiency to be approximately 13% for their 2 cm diameter, 1 cm thick $\text{Pb}_2\text{P}_2\text{O}_7:\text{In}$ glass (Bell and Boatner 2010).

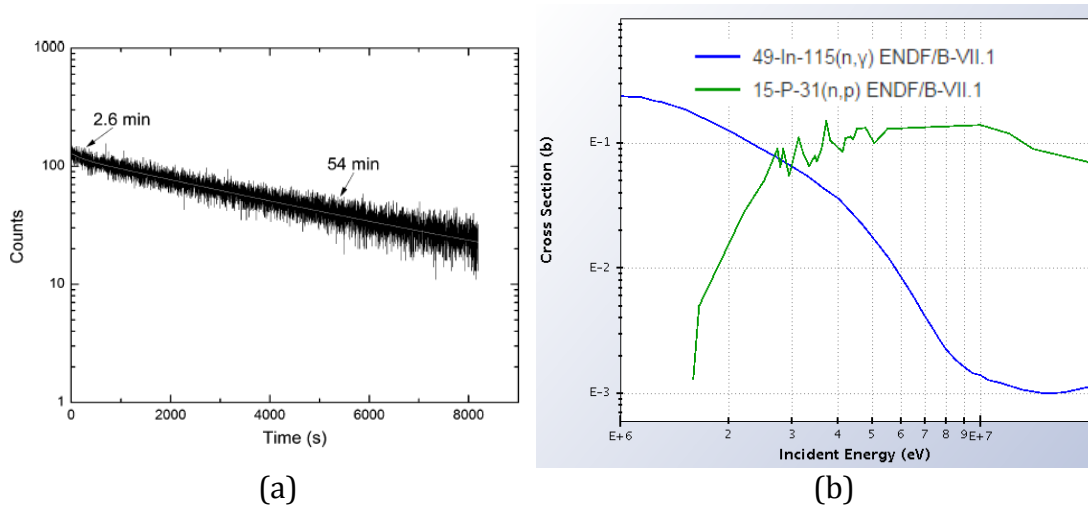


Figure 5 a) Decay of ^{116m}In in $\text{Pb}_2\text{P}_2\text{O}_7:\text{In}$ glass. The MCS used 1 second bins (Bell and Boatner 2010) b) Neutron cross sections of $^{115}\text{In}(n, \gamma)$ and $^{31}\text{P}(n, p)$ from 1 to 20 MeV. (National Nuclear Data Center 2013)

PRELIMINARY DATA

Bell and Boatner's $\text{Pb}_2\text{P}_2\text{O}_7:\text{In}$ glass was irradiated with an unmoderated Americium-Beryllium (Am-Be) source and counted using their method. The source emitted approximately 1.15×10^5 neutrons per second, with approximately 5,000 to 10,000 n/s incident on the sample. The reactions of interest were $^{115}\text{In}(n, \gamma)^{116m}\text{In}$ and $^{31}\text{P}(n, p)^{31}\text{Si}$. Figure 6 shows the count rate as a function of time due to the $\text{Pb}_2\text{P}_2\text{O}_7:\text{In}$ glass after irradiation. The data appears to correspond to an exponential decay with the decay constant of ^{31}Si ($\frac{\chi^2}{\nu} = 1.042$), which has a half life of 2.62 hours. The sum of the Silicon-31 and ^{116m}In exponentials were also fit to the data with similar results ($\frac{\chi^2}{\nu} = 1.032$). The reduced chi-squared statistic is only different by 0.01, suggesting that adding the ^{116m}In exponential does not contribute

significantly to achieving a good fit. The $^{31}\text{P}(n, p)^{31}\text{Si}$ reaction has a cross section of approximately 0.1 barn between 3 and 10 MeV (Figure 5b). Since the signal produced was relatively small (less than twice background), future target reactions exposed to the same or a similar source likely needed to have cross sections with a similar magnitude or proportionally smaller if the mass of the target material is increased in order to produce a measurable signal. Also recall that a greater neutron flux would also allow for a proportionally smaller cross section and/or target mass.

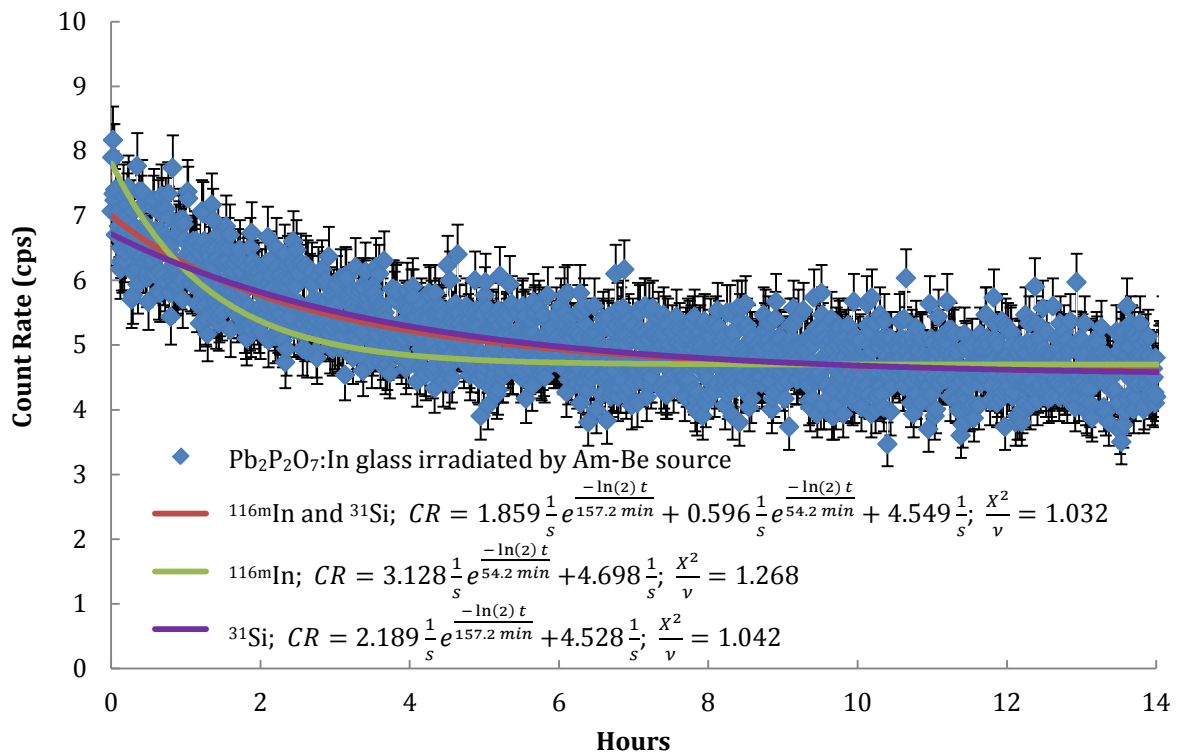


FIGURE 6 Time series spectrum of $\text{Pb}_2\text{P}_2\text{O}_7:\text{In}$ glass after irradiation by an Am-Be source. The data is fit to exponentials with decay constants of ^{31}Si and $^{116\text{m}}\text{In}$.

TARGET MATERIAL PROPERTIES

In his book, Knoll (2012, p769) lists 6 qualities of the detection medium that must be taken into consideration when designing a neutron activation detector. These qualities have been amended to reflect the needs of a Cherenkov-based neutron activation detection method.

1) SHAPE OF THE CROSS SECTION

The shape of the target nuclide's cross section must be similar to the shape of the energy spectrum of the neutron flux that is to be detected. The reactions utilized in the work presented here are relevant to the unmoderated neutron energy spectrum of fission. In this energy range, threshold reactions are possible. A threshold reaction has the advantage of giving a lower limit on the energy of the neutrons being detected, making it easier to assign a radiation weighting factor when estimating dose.

2) MAGNITUDE OF THE CROSS SECTION

The magnitude of the neutron reaction rate is directly proportional to the cross section of a target nuclide. In the case of most neutron detector applications, a very high neutron reaction rate in the detection medium is desirable. Neutron reactions that result in a radioactive reaction product (which are necessary for an activation detector) generally have cross sections that are below 1 barn in the 1 to 10 MeV energy range.

3) DECAY CONSTANT OF THE INDUCED ACTIVITY

It is necessary to know the decay constant of the radioactivity in order to verify that the counts are due to the radionuclide of interest i.e., the product of a specific neutron-induced reaction. This can be done by modeling the count rate as a sum of exponentials. Determining which counts belong to each radionuclide can be difficult if radioactive reaction products with similar decay constants are present.

A radionuclide's activity will be reduced by 99.9% after 7 half-lives. Having a target isotope that will produce a radioisotope with a half-life on the order of minutes to hours is preferable in order to decrease the amount of time needed to count the activity. This will enable quicker estimation of the neutron flux that induced the activity.

4) PURITY AND INTERFERING ACTIVITIES

Most elements are poly-isotopic and most materials comprise multiple elements. This makes it likely that there will be multiple activated radionuclides within the material. Therefore, the resulting counts may be modeled as a sum of decaying exponentials that correspond to the decay constants of different activated radionuclides within the material. The count rate as a function of time is,

$$CR(t) = CR_1e^{-\lambda_1t} + CR_2e^{-\lambda_2t} + \dots + CR_je^{-\lambda_jt} + \dots + CR_ne^{-\lambda_nt} + BR \quad (17)$$

where BR is the background count rate and CR_j is the initial count rate due to a specific radionuclide with decay constant λ_j . The coefficients in Equation 17 are most easily found when the difference between the radionuclides' half-lives is large.

If the half-lives are very similar, knowledge of the cross section, number, and natural abundance of each target nuclide, along with the resulting reaction product's beta particle branching ratio and energy may be used to estimate the ratio between initial count rates of different radionuclides.

5) NATURE OF THE INDUCED ACTIVITY

The induced activity must be able to produce (with high probability) beta particles, positrons, or gamma rays (which can produce Compton electrons and photoelectrons) that are at least as energetic as the Cherenkov energy threshold. Since the energy of a charged particle needed for producing Cherenkov radiation increases with the mass of the particle, and the energy of radiation produced by radioactive decay will be at most a few MeV, only electrons and positrons will be capable of producing Cherenkov radiation.

6) PHYSICAL PROPERTIES

The medium must have a high enough index of refraction so that the induced activity may produce Cherenkov photons. The medium must be able to transmit those photons so that they can travel far enough to enter the PMT or photon collecting device that will be attached to the medium. If a light pipe is not used, the medium should also have a diameter that is equal to or smaller than the diameter of the PMT photocathode in order to prevent the Cherenkov light from escaping over the edge of the photocathode. A reflector, e.g. aluminum foil, may also be placed

around the material at the air-medium interface in order to prevent light from escaping from all of the sides that do not face the PMT.

RESEARCH OBJECTIVE

This research explores the capabilities of the Cherenkov-based neutron detection technique developed by Bell and Boatner for quantifying the fast neutron flux from fission. In particular, this research focuses on identifying target isotopes and optical materials that would be optimal for such a detection system. The optimal target isotope is one that becomes radioactive and emits beta particles or gamma rays following a fast neutron reaction. The optimal optical material is one that is comprised of a high percentage of the target isotope and allows for the production and transmission of Cherenkov radiation. A properly chosen material should produce a measurable signal when irradiated by a fast fission neutron flux.

HYPOTHESES

1. The neutron detection technique developed by Bell and Boatner, which has been tested at thermal neutron energies, can be effective at fast neutron energies, 1 - 10 MeV.
2. A properly chosen target isotope and medium, when irradiated by neutrons of these energies, will produce a sufficient signal such that the neutron flux in the medium can be quantified.

MATERIALS AND METHODS

Target Nuclides

The neutron reaction cross sections of all naturally abundant stable isotopes in the neutron energy range of 1 to 10 MeV were examined. . The magnitudes for each type of reaction, e.g. (n, γ), (n, p), (n, α), were obtained from the National Nuclear Database Center's (NNDC) Evaluated Nuclear Data Files (ENDF). Based on preliminary experiments done at Oak Ridge National Laboratory, cross section values of interest were on the order of 0.1 barn or greater.

For reactions that had a sufficient cross section magnitude, the reaction products were queried for beta particles or gamma ray emitters – the only radiation from a radioisotope that can cause the emission of Cherenkov photons in normal materials. If the reaction product emitted beta particles or gamma rays that had energies of at least a few hundred keV, and these emissions had a high probability of occurring, then the half-life of the reaction product was evaluated to determine if it was long enough to be counted sufficiently and short enough to be counted so that an evaluation of the data could be made within a suitable time frame. If the half-life of the radionuclide is too short, on the order of a few seconds or less, then the radionuclide may decay away before it can be counted. If the half-life of the radionuclide is too long, on the order of a few days or more, then the length of time required to measure the radioactivity may not be worth the effort if other methods are available that take less time. It was decided that an ideal half-life would be on

the order of minutes to hours. A computer program was written to help sort through potential candidates. The interface for the program and a flow chart of the decision process is located in Appendix F.

The properties of the target isotopes chosen for this research are shown in Table 1, their neutron reaction cross sections are seen in Figure 7, and their reaction products are shown in Table 2.

TABLE 1 Target Isotope Properties

Target Isotope	Reaction	Cross Section Maximum, 1 -10 MeV	Natural Abundance
^{28}Si	$^{28}\text{Si}(n, p)^{28}\text{Al}$	0.36 barns	92.22%
^{27}Al	$^{27}\text{Al}(n, p)^{27}\text{Mg}$	0.09 barns	100%
^{24}Mg	$^{24}\text{Mg}(n, p)^{24}\text{Na}$	0.15 barns	78.99%
^{64}Zn	$^{64}\text{Zn}(n, p)^{64}\text{Cu}$	0.26 barns	49.17%

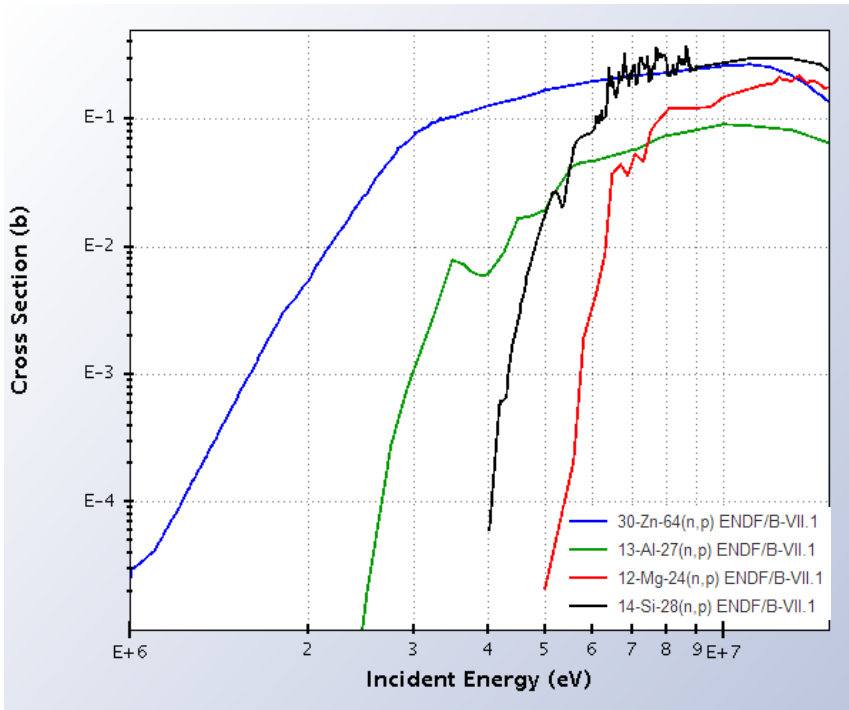


FIGURE 7 Neutron reaction cross sections of selected target nuclides (National Nuclear Data Center 2013).

TABLE 2 Reaction Product Properties

Reaction Product	Half-Life	Beta Particle Endpoint Energy (keV)	Beta Intensity (%)	Gamma Ray Energy (keV)	Gamma Ray Intensity %
²⁸ Al	2.241 min	2863	99.99	1779	99.99
²⁷ Mg	9.458 min	1596, 1767	29.06, 70.94	843.8, 1014	71.80, 28.20
²⁴ Na	14.99 hr	1392.56	99.86	1369, 2754	99.99, 99.86
⁶⁴ Cu	12.70 hr	653.0*, 579.4	17.60*, 38.5	511.0	35.2

*Positron emission; two annihilation photons (511 keV) produced per positron

IDEAL MEDIA

Once the target nuclei were chosen, the next step was to choose the proper media. Ideal media would have a high index of refraction and good transmittance at

Cherenkov light wavelengths, namely the UV to near UV region. Media chosen with these characteristics were specimens of quartz, sapphire, spinel, and zinc sulfide, all one inch in diameter in order to couple them to a one inch diameter photomultiplier tube. The properties of these materials are shown in Table 3.

TABLE 3 Target Material Properties

Material	Target Isotope	Index of Refraction at 420 nm**	Internal Transmittance At 420 nm*	Sample Thickness (cm)	Sample Density (g/cm ³)
Quartz (SiO ₂)	²⁸ Si	1.56	>99%	0.635	2.27
Sapphire (Al ₂ O ₃)	²⁷ Al	1.79	>99%	1.07	3.98
Spinel(Mg Al ₂ O ₄)	²⁷ Al, ²⁴ Mg	1.74	91%	1.27	3.72
Zinc Sulfide (ZnS)	⁶⁴ Zn	2.54	>99%	0.60	4.23

*Peak wavelength of the photomultiplier tube used in the experiments
 + (Bass et. al 1995)

NEUTRON SOURCE

A ²⁵²Cf neutron source emitting about 200,000 neutrons per second was used for irradiation. The source was manufactured according to the Certificate of Competent Authority USA/0018/S-96: a seal welded cylinder, doubly encapsulated, with the inner encapsulation made of a platinum-rhodium alloy and the outer encapsulation made of Type 304L stainless steel or Zircalloy-2. At its creation, it contained no more than 5.2 Ci of ²⁵²Cf in oxide form (Radioactive Material Packaging 2014). A diagram of the source capsule can be found in Appendix C. An approximation of the ²⁵²Cf fission neutron energy spectrum is shown Figure 8. The encapsulation materials will not have a noticeable effect on the ²⁵²Cf fission spectrum, nor reduce its magnitude via neutron absorption. The ²⁵²Cf

fission neutron spectrum is an appropriate representation of the spectrum of other fissile material, e.g. plutonium or uranium.

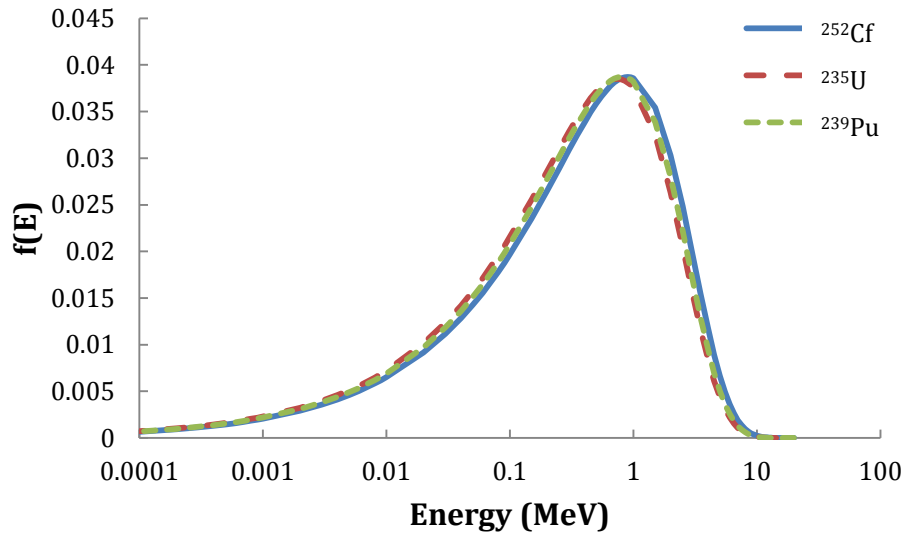


FIGURE 8 Watt function representative of fission spectra taken from the MCNP5 manual (X-5 Monte Carlo Team 2003). The shape of the spectra of ^{252}Cf , ^{235}U , and ^{239}Pu are almost indistinguishable.

PROCEDURE

FLUORESCENCE DISCRIMINATION

The light detection device used was a Hamamatsu R268 28mm diameter, 11 stage, head-on type photomultiplier tube with a borosilicate glass window and a bialkali photocathode. Since PMTs inherently exhibit background noise, it was first necessary to find lower level and upper level pulse height discriminators in order to exclude some of the low-energy background counts. When the LLD was set at channel 1 on the multi-channel analyzer (discriminating against approximately 3

photoelectrons), preliminary background counts showed that the un-irradiated MgAl_2O_4 and ZnS samples exhibited a signal that decayed with time, eventually reaching a constant count rate after many hours, as seen in Figure 9. It was noticed that this only happened when the sample had been exposed to room light before counting. The PMT was always kept in the dark, even when the dark box (discussed later) door was opened to mount the sample onto the PMT. This indicated that the unknown signal may be due to some type of fluorescence of the sample caused by exposure to room light. To discriminate against the fluorescence signal in MgAl_2O_4 and ZnS , a lower level discriminator (LLD) was selected while observing the pulse height spectrum. This LLD was then used during the collection of the time-series data.

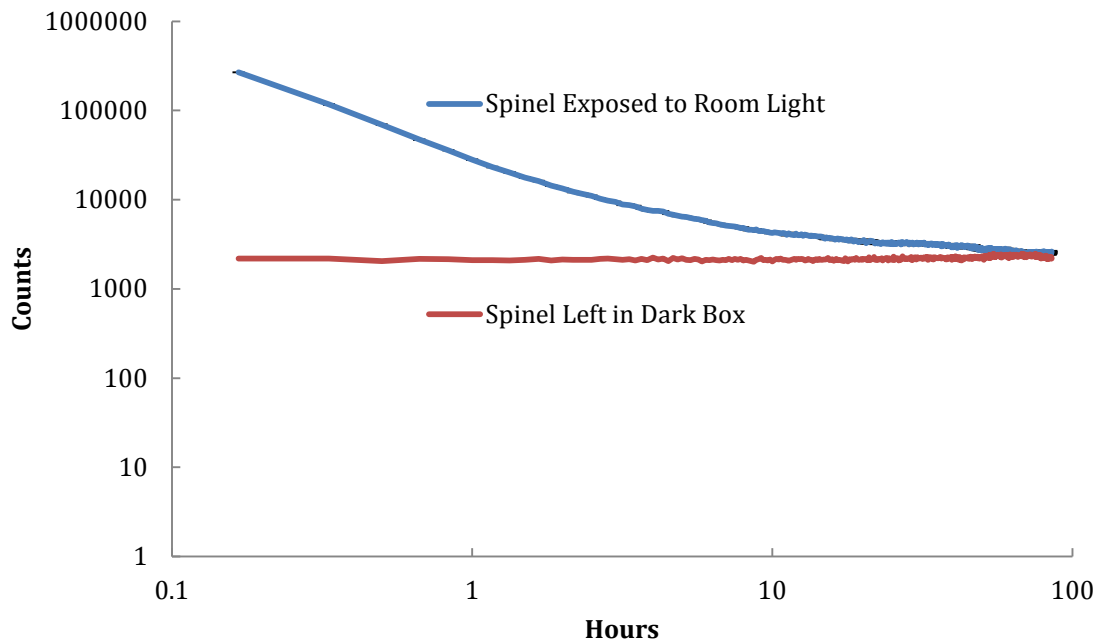


FIGURE 9 Time series comparison of the spinel sample exposed to room light and the spinel sample kept in the dark box. The initial count rate of the spinel exposed to room light is approximately 100 times greater than the spinel left in the dark box and the signal from the spinel exposed to room light decays according to at least two time components.

First, in order to find the true background count rate (no fluorescence), each un-irradiated sample was removed from the PMT (the PMT was not exposed to room light), exposed to room light for approximately 10 minutes (or about 10 times longer than it would be exposed when transferring the sample from the source closet to the dark box), replaced on the PMT, and then counted using a multichannel scaler with a very low lower level discriminator. A multichannel scaler recorded the count rate as a function of time for approximately 85 hours for MgAl_2O_4 and 10 minutes for ZnS . When the multichannel scaler spectrum showed that the signal had decayed to a constant level, which was assumed to be the true background

count rate, a pulse height spectrum was taken. Then, the sample was exposed to room light again and another pulse height spectrum was taken while the signal decayed to look for differences between the background spectrum and the spectrum taken immediately after the sample was exposed to room light. The counting time for the each pulse height spectrum was 3 hours. In each channel of the pulse height measurement of fluorescence, if the net counts were less than L_c , where

$$L_c = 2.33\sigma_B \text{ (Currie 1968),} \quad \mathbf{(18)}$$

and σ_B = standard deviation of background counts in each channel, then with 95% confidence, there was no signal due to fluorescence in that channel. If the counts were greater than L_c , then that channel was discriminated against. Among the different samples, the lower level discriminators were set between channels 6 and 12 out of a total of 512 channels. A pulse height spectrum of spinel exposed to room light and spinel kept in a dark box is shown in Figure 10.

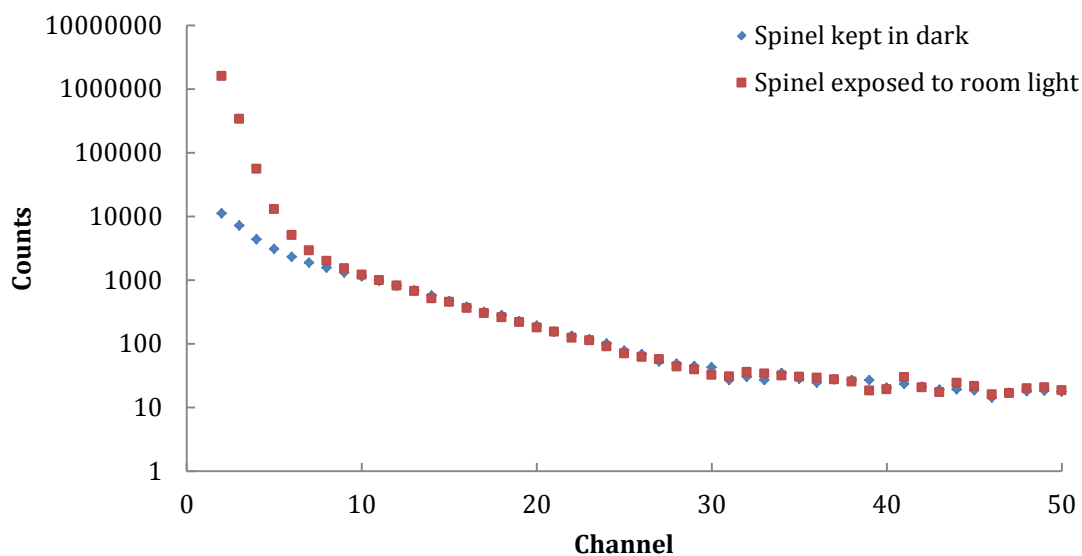


FIGURE 10 Pulse height spectrum comparison of spinel exposed to room light vs. spinel kept in darkness. At lower channels the difference in counts is orders of magnitude. The lower level discriminator was set to the lowest channel which had net counts less than L_c ; channel 11 in this case. The one sigma error bars are smaller than the data points

IRRADIATION

To irradiate each sample, the ^{252}Cf capsule and sample were placed on a lead block to increase reflection of neutrons; with samples placed flush against the side of capsule. The irradiation configuration is shown in Figure 11. Samples were irradiated for at least two half-lives of the expected reaction product, reaching more than 75% of its maximum possible activity, or saturation activity.

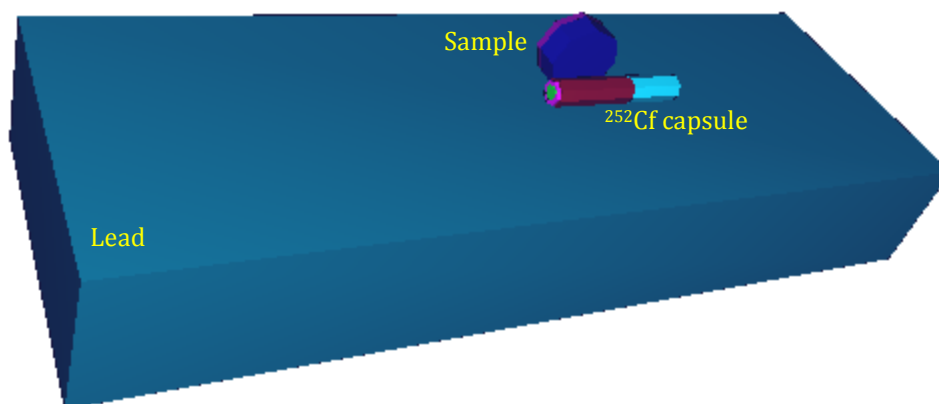


FIGURE 11 *Geometry of irradiation of samples by ²⁵²Cf. The edge of the sample was lined up with the edge of the ²⁵²Cf capsule for easy replication of the experiment.*

Samples were then removed from the source and counted. The side of the sample that faced the source was positioned to face the PMT window. Optical grease (GE Visc-60M polydimethylsiloxane) was daubed onto the PMT window to increase light transmission, and the sample and top edge of the PMT were covered with aluminum foil to increase reflection of light into the PMT. The PMT and sample were placed inside a light-tight box (dark box). The schematic of the detection system is shown in Figure 12.

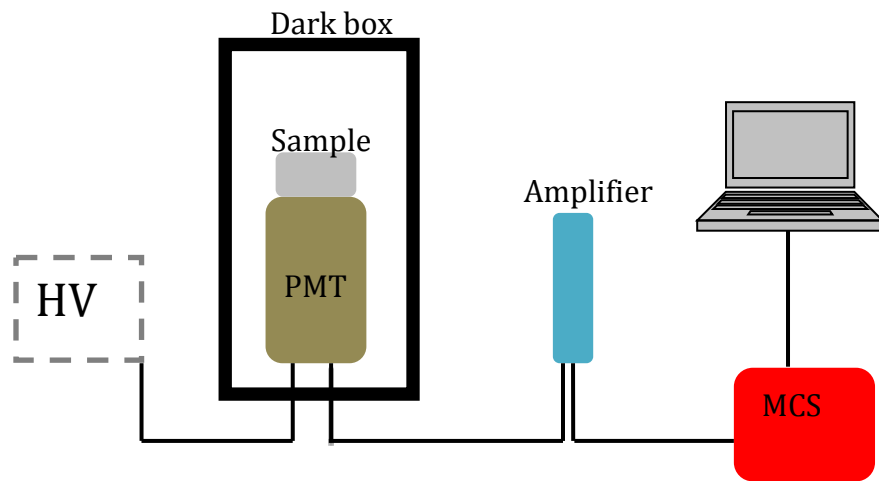


FIGURE 12 *Counting electronics of detection method. Cherenkov photons from the sample produce a pulse in the PMT which is amplified by the amplifier and recorded by the MCS before being displayed by a computer.*

LLD AND ULD

The pulse height spectrum of irradiated samples was compared to the spectrum of the un-irradiated sample to find a quantitative signal due to radiation from reaction products in the sample. In each channel, if the net counts exceeded N_D where,

$$N_D = 4.65\sqrt{N_B} + 2.71 \text{ (Currie 1968)} \quad (19)$$

and N_B = number of background counts, then with 95% confidence, some counts in that channel were due to signal caused by the reaction products from neutron irradiation. There was found to be a small range of channels where the number of counts exceeded N_D . The lowest channel in this range was taken to be the new lower level discriminator (as long as it was greater than or equal to the lower level

discriminator established earlier) and the highest channel in this range was taken to be the upper level discriminator, as seen in Figure 13.

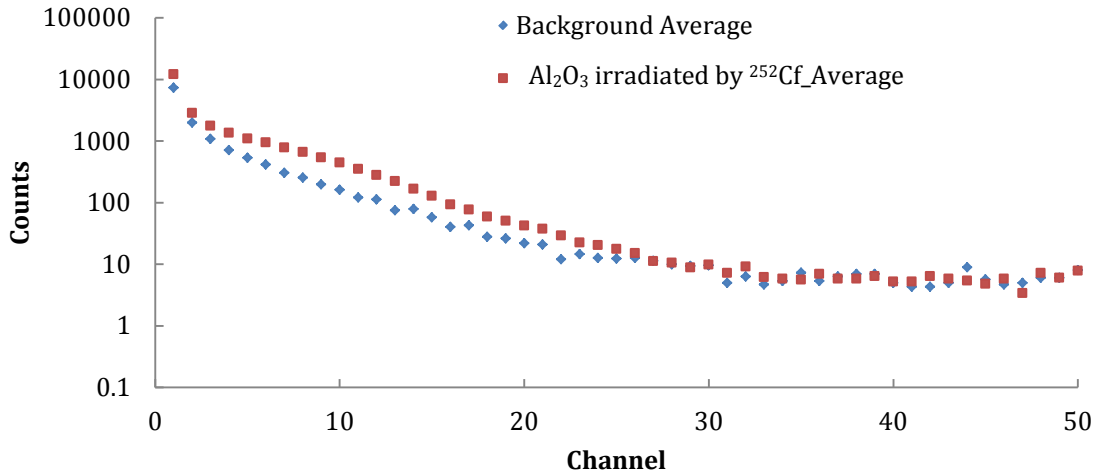


FIGURE 13 Pulse height spectrum of Al_2O_3 irradiated by ^{252}Cf . Only the net counts in channels 6 through 22 were greater than the critical value, N_D . The one sigma error bars are smaller than the data points

TIME SERIES MEASUREMENTS

Each sample was irradiated with the ^{252}Cf source and counted using the data acquisition system in multichannel scaler mode. The product radionuclides with half-lives on the order of minutes, ^{28}Al and ^{27}Mg , were counted with time bins of 20 and 30 seconds, respectively, while radionuclides with half-lives on the order of hours, ^{24}Mg and ^{64}Cu , were counted with 10 minute time bins. There were 512 total time bins used in each measurement.

CALCULATING EFFICIENCY

Solutions for the parameters of equation 17 were obtained using Solver, a Microsoft Excel tool. Solver utilizes a Levenberg-Marquardt algorithm (Marquardt 1963) to minimize the difference between the data and the theoretical equation by adjusting the independent variables designated by the user. All time series measurements in this research were assumed to have only one decay constant, therefore equation 17 reduced to

$$CR(t) = CR_1 e^{-\lambda_1 t} + BR . \quad (20)$$

Therefore, the variables that Solver had to calculate were CR_1 , λ_1 , and BR .

First, the decay constant was found in order to verify that the correct reaction product was being measured. To do that, all of the variables were allowed to be determined by Solver. The target was set as the sum (over all time bins) of the squares of the differences between the count rate of the data and the count rate of equation 20, divided by the variances of the data, i.e. the target was the chi-squared statistic, χ^2 . Solver was then used to solve for CR_1 , and BR , with λ_1 held constant at the known theoretical value. The total count rate, $CR(t)$, and the background count rate, BR , were integrated from the counting start time, t_1 , to the counting stop time, t_2 , (becoming the values “C” and “B”, respectively) and used in equation 15 to calculate the counting efficiency.

Samples were also counted with a high-resolution gamma-ray spectroscopy system in an effort to determine the initial activity of the product radionuclide after irradiation. A 0.250 $\mu\text{Ci/L}$ standard solution of ^{152}Eu in 0.1 N HCL was used to make an efficiency calibration. The solution filled a volume in its vial similar to the volume of the samples. MCNP simulations showed that the difference in absolute efficiency between the vial and the samples should have been less than 5%. The samples were counted for at least 4 half-lives of the expected reaction product.

SIMULATIONS

A set of GEANT4 Application Tomographic Emission (GATE) simulations of the beta, gamma ray, and Cherenkov photon interactions within each sample were performed to better understand which factors affect the counting efficiency. A diagram of the geometry a GATE simulation is shown in Figure 14.

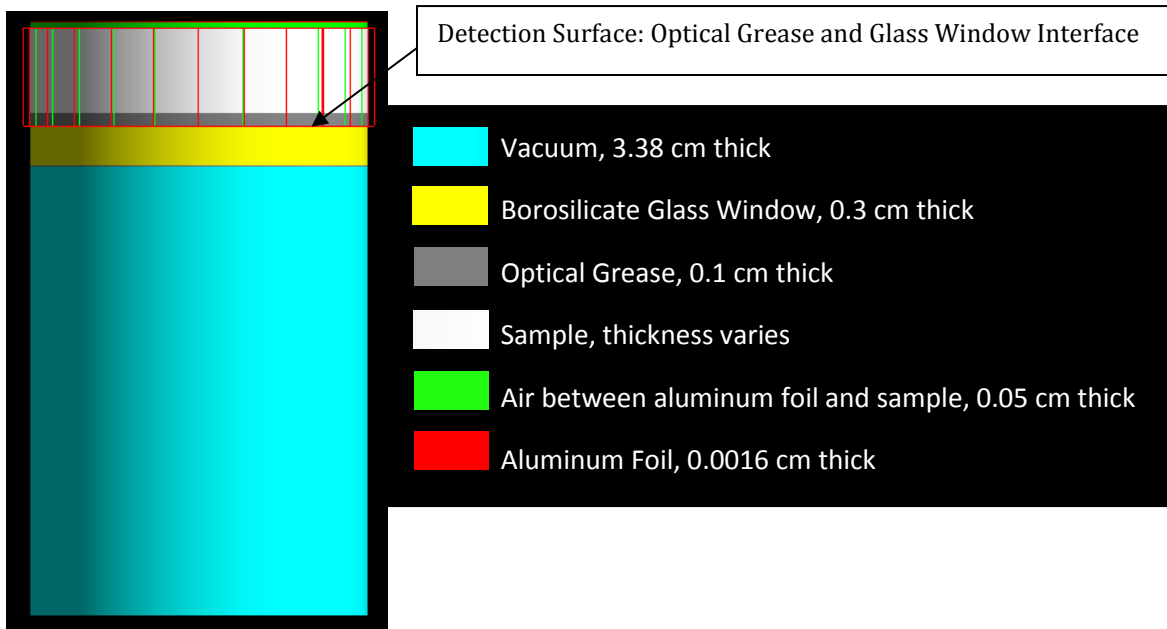


FIGURE 14 *GATE simulation model of a sample coupled to photomultiplier tube*

The simulations took into account the presence of a specular reflector (100% reflective aluminum foil) surrounding the sample, the optical grease coupling the sample to the PMT, absorption lengths, the indices of refraction, and the quantum efficiency of the PMT. Each simulation ran 10^6 particle histories. Transmission measurements taken with a Varian Cary 50 Bio UV/Visible Spectrophotometer were used to calculate the absorption lengths. The dispersion equations for each medium (used to calculate the indices of refraction) were obtained from the Handbook of Optics (Bass et. al 1995).

RESULTS AND DISCUSSION

EXPERIMENTAL HALF-LIFE

After irradiation by ^{252}Cf , samples were counted using the data acquisition system in multichannel scaler mode as seen in Figure 12. The MgAl_2O_4 sample was counted with time bins of 30 seconds for approximately 30 minutes to measure ^{27}Mg and subsequently with 10 minute time bins for a few days to measure ^{24}Na . Equation 20, which gives count rate as function of time, was used as a model to calculate the decay constants in the data. An example of multichannel scaler data is presented in Figure 15. The reduced chi-squared statistic,

$$\frac{\chi}{\nu} = \frac{\chi^2}{\text{Number of observations} - \text{number of fitted parameters} - 1}, \text{ was calculated to show goodness of fit.}$$

Values close to 1.0 are considered acceptable.

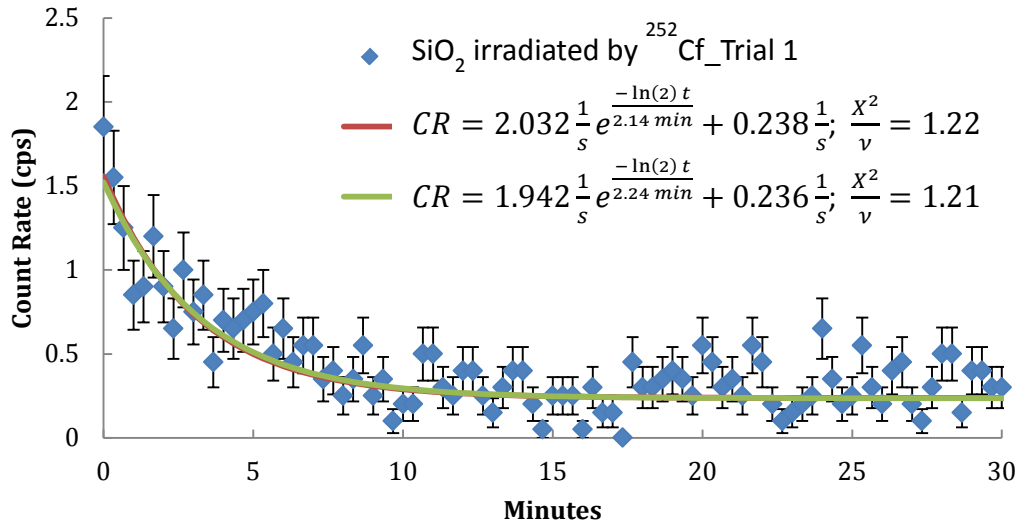


FIGURE 15 Time series spectrum of SiO_2 after having been irradiated by ^{252}Cf . The half-life value calculated by Solver (2.14 minutes) was very close to the accepted half-life value for ^{28}Al (2.24 minutes), which was the radionuclide of interest.

Table 4 shows the theoretical half-lives of the reaction products and the means of the measured half-lives calculated using equation 20, allowing CR_1 , BR, and λ_1 to be determined by Solver. All of the experimental values fall within one standard deviation of the generally accepted values as found at NNDC, with the exception of ^{64}Cu which was not measurable. The inability to detect ^{64}Cu was likely due to the relatively small branching ratio and low energy of its beta decays. Copper-64 decays by beta emission only about 53% of the time with a maximum energy of 653 keV, whereas the other reaction products decay by beta emission 100% of the time and have maximum energies of greater than 1000 keV, allowing them to cause the emission of more Cherenkov photons.

The estimation of the half-life of ^{24}Na from the experimental data was relatively poor compared to half-life estimates of other radionuclides in Table 4. One measurement of irradiated MgAl_2O_4 was only counted for 33 hours, or two half-lives of ^{24}Na . After 33 hours, the ^{24}Na had not decayed significantly enough for the background count rate to be seen in the multichannel scaler data (Figure 16). As a result, Solver found a background count rate significantly smaller than its actual value, which affected Solver's calculation of the initial count rate and half-life. This outcome conveys the importance of counting samples long enough to produce more accurate and precise results. Table 5 shows how the half-life estimated by Solver changes as the count time increases. The data is from another measurement of ^{24}Na in MgAl_2O_4 where the predicted half-life was 15.1 hours after a total count time of

85 hours. The increase in count time of the sample leads to an increase in the accuracy of Solver's calculation.

TABLE 4 Comparison of Theoretical and Experimental Values of Half-life

Sample	Reaction	Theoretical $t_{1/2}$	Experimental $t_{1/2}$
SiO ₂	²⁸ Si(n, p) ²⁸ Al	2.241 min	2.07 ± 0.143 min
Al ₂ O ₃	²⁷ Al(n, p) ²⁷ Mg	9.458 min	9.457 ± 0.317 min
MgAl ₂ O ₄	²⁷ Al(n, p) ²⁷ Mg	9.458 min	8.492 ± 2.953 min
	²⁴ Mg(n, p) ²⁴ Na + ²⁷ Al(n, α) ²⁴ Na	14.99 hr	20.60 ± 9.16 hr
ZnS	⁶⁴ Zn(n, p) ⁶⁴ Cu	12.701 hr	Not Detectable

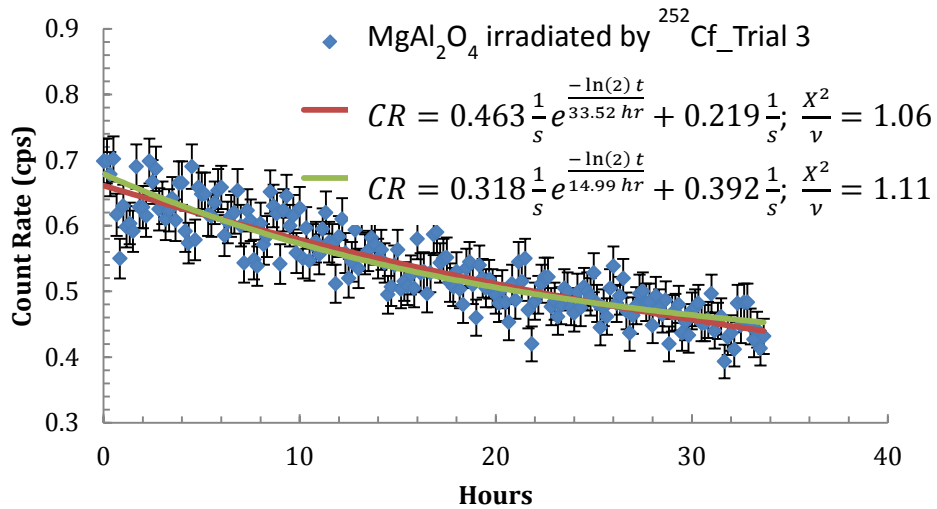


Figure 16 Decay of ²⁴Na in MgAl₂O₄ after irradiation by unmoderated ²⁵²Cf. The red line is a regression fit where all parameters were decided by Solver. The green line corresponds to the theoretical half-life of ²⁴Na.

TABLE 5 Solver’s estimate of ^{24}Na half-life as a function of time

Count Time (hours)	Solver Estimated Half-life (hours)	Percentage Error of Actual Half-life (14.99 hours)
20	7.07	52.8
40	11.65	22.3
60	12.67	15.5
80	14.82	1.1
85	15.1	0.7

Calculation of the Reaction Rate

An MCNP model of the ^{252}Cf source capsule was created based on the IAEA Certificate of Competent Authority Special Form Radioactive Materials Certificate Number USA/0018/S, Revision 6. After taking into account how much the ^{252}Cf had decayed, its daughter products, and that the source contained ^{250}Cf , it was found that the source produced approximately 2×10^5 neutrons per second. The full isotopic makeup of the source can be found in Appendix C. The MCNP simulation estimated a reaction rate for each reaction within the sample, and an incident neutron flux of approximately $9400 \text{ neutrons cm}^{-2}\text{s}^{-1}$, about half of which had energies greater than 1 MeV. The MCNP models were run for 10^8 particle histories; Table 6 shows the results of the simulations.

In order to corroborate the MCNP simulation results, each sample was irradiated until the reaction products reached saturation activity and then counted using a high-resolution gamma-ray spectroscopy system. Because the samples were irradiated to the saturation activity, the initial activity is equivalent to the reaction rate, which was calculated using equation 14. Table 6 also shows the results of the

high-resolution gamma-ray spectroscopy system measurements. Gamma-ray spectroscopy measurements were taken once for each sample; the uncertainty was calculated by Ortec's MAESTRO software by taking the square root of the sum of the squares of the uncertainty of the gross counts and the weighted error of the estimated background counts (Ortec 2012). Pulse height spectra of the gamma-ray spectroscopy data are contained in Appendix D. The activity of the ^{28}Al ($t_{1/2} = 2.24$ minutes) produced by the $^{28}\text{Si} (n, p) ^{28}\text{Al}$ reaction was not measurable because of the low efficiency ($\sim 3\%$) of the detection system and because much of the radioactivity had decayed away before the sample could be counted. The $^{24}\text{Mg} (n, p) ^{24}\text{Na}$ and $^{27}\text{Al} (n, \alpha) ^{24}\text{Na}$ reactions in MgAl_2O_4 are indistinguishable in the experimental results because both produce ^{24}Na . The reaction rates determined by MCNP and the gamma-ray spectroscopy system were different by about 25% or less. This confirmed that the reaction rates calculated by MCNP were reasonably accurate. The gamma ray spectra are presented in Appendix D.

TABLE 6 Initial Activity of MCNP Simulation and Measurement with a High-Resolution Gamma-ray Spectroscopy System.

Sample	Reaction	Gamma-ray Spectroscopy Activity (Bq)	MCNP Activity (Bq)	Difference (%)
SiO ₂	²⁸ Si(n, p) ²⁸ Al	Not Detectable	8.07 ± 0.00807	N.A.
Al ₂ O ₃	²⁷ Al(n, p) ²⁷ Mg	11.9 ± 0.223	10.4 ± 0.00652	14.4
MgAl ₂ O ₄	²⁷ Al(n, p) ²⁷ Mg	7.33 ± 0.143	7.46 ± 0.0127	1.7
	²⁴ Mg(n, p) ²⁴ Na + ²⁷ Al(n, α) ²⁴ Na	2.41 ± 0.0624	3.03 ± 0.00347	20.5
ZnS	⁶⁴ Zn(n, p) ⁶⁴ Cu	12.1 ± 0.268	16.6 ± 0.00680	26.8

MEASURED COUNTING EFFICIENCY FOR CHERENKOV RADIATION

The measured counting efficiencies calculated using equation 15 are shown in Table 7. Graphical data are shown in Appendix A. Magnesium-27 in Al₂O₃ had the highest efficiency, followed by ²⁸Al in SiO₂, ²⁷Mg in MgAl₂O₄, ²⁴Na in MgAl₂O₄, and ⁶⁴Cu in ZnS. As mentioned earlier, ⁶⁴Cu in ZnS was undetectable because of the small branching ratio and energy of the beta particles. MgAl₂O₄ likely had a lower efficiency than did SiO₂ and Al₂O₃ for this measurement because its lower level discriminator was set higher, discriminating against decay events where only a few photoelectrons were emitted in the PMT. Transmission of visible light through the MgAl₂O₄ sample is also significantly less than it is through the SiO₂ or Al₂O₃ samples. Detection of ²⁷Mg in MgAl₂O₄ was easier than detection of ²⁴Na in MgAl₂O₄ likely because ²⁷Mg has higher energy beta particles.

After three efficiency measurements were taken of each sample, they were irradiated once more to determine if any of the signal was due to electrons or gamma rays interacting inside of the PMT and causing the release of photoelectrons directly. To measure this, a layer of aluminum foil was placed between the PMT window and the sample. The layer of foil was thin enough to allow energetic beta particles and gamma rays to pass through, but not Cherenkov photons. The results, shown in Appendix A, imply that no measurable amount of the signal was due to gamma rays or beta particles interacting directly with the PMT.

TABLE 7 Measured Counting Efficiency

Sample	Radionuclide	LLD - ULD (channel)	Measured Efficiency (%)
SiO ₂	²⁸ Al	6.988 - 17.095	21.56 ± 3.60
Al ₂ O ₃	²⁷ Mg	6.114 - 22.087	37.89 ± 3.39
MgAl ₂ O ₄	²⁷ Mg	11.105 - 28.950	15.63 ± 5.26
	²⁴ Na	12.104 - 32.943	10.91 ± 0.49
ZnS	⁶⁴ Cu	N.A.	Not Measurable

GATE SIMULATIONS

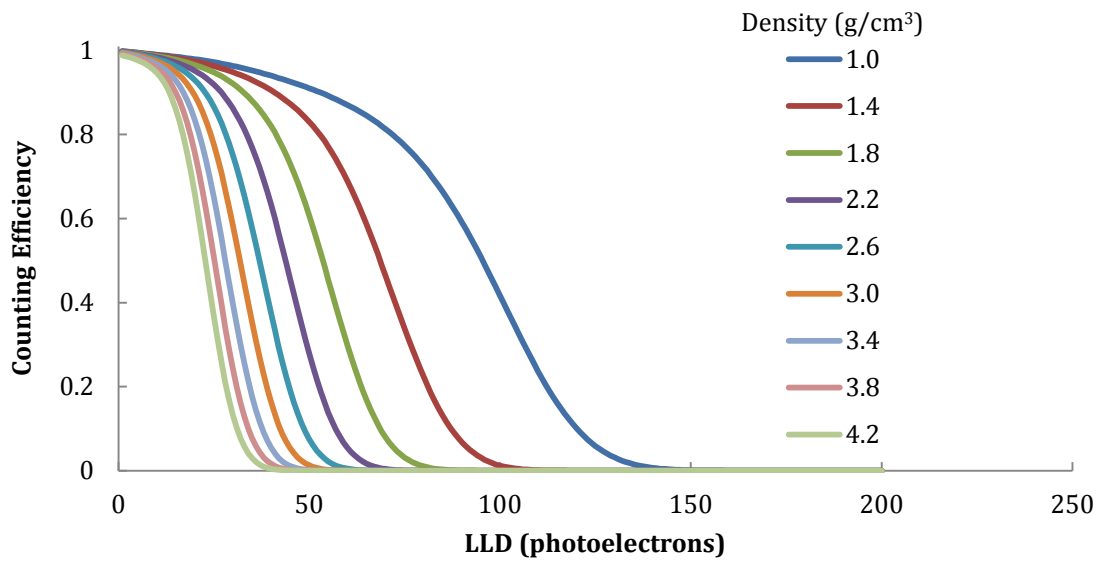
GATE simulations were run with the goal of understanding the parameters that affect the production and propagation of Cherenkov photons in media. Changes in density and index of refraction were simulated to investigate the effect on light collection efficiency. Then, simulations of the media used in the experiments were

done, first with the identical dimensions, and then with the actual dimensions of each sample.

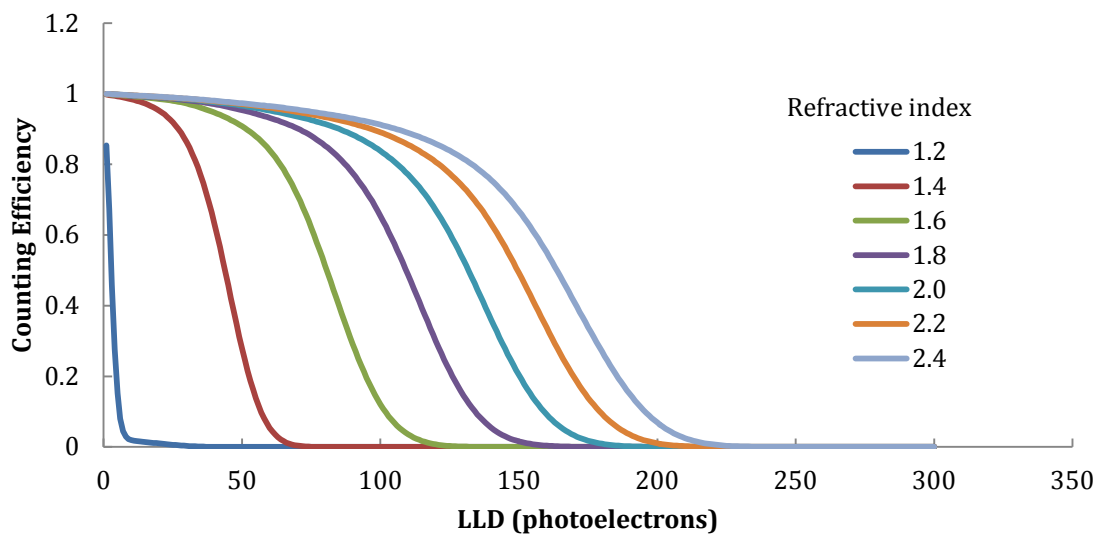
A 6 mm thick by 25.4 mm diameter sample of SiO₂ was modeled with a 0.5 MeV electron source that was homogeneous throughout the sample. The model geometry is shown in Figure 14. Except for aluminum, the absorption length for all optical photons was set to 50 m, and the detection surface efficiency was set to 100%. First, the density of the SiO₂ was varied from 1.0 g/cm³ to 4.2 g/cm³ in intervals of 0.4 g/cm³ with the index of refraction kept constant at 1.4. Then, the index of refraction was varied from 1.2 to 2.4 in intervals of 0.2 with the density kept constant at 2.2 g/cm³. Figure 17 shows the efficiency as a function of lower level discriminator in photoelectrons. In Figure 17, part A), the number of photoelectrons created increases as the density is decreased. This happens because the electron will travel farther in a less dense material. A longer path length will result in more Cherenkov photons produced. Below a density of about 2 g/cm³, a small change in density causes a substantial difference in the number of photoelectrons produced.

The number of photoelectrons produced has a significant dependence on the index of refraction, especially at lower refractive indices. When the index of refraction is increased, the threshold energy needed to produce Cherenkov photons decreases, making it possible for an electron to cause the production of Cherenkov photons at low energies, increasing the total number of Cherenkov photons

produced. In Figure 17, part B), a change from an index of refraction from 1.2 to 1.4 increases the photoelectrons created by approximately a factor of 10. At higher refractive indices the effect is diminished, a change from 2.2 to 2.4 results in only about a factor of 1/10 difference in photoelectron production. Therefore, more Cherenkov photons will be produced in low density materials with a relatively high index of refraction.



A)



B)

FIGURE 17 GATE/GEANT4 simulation results of a 0.5 MeV electron source distributed homogeneously in a fused silica disc that is coupled to a photomultiplier tube. A) density with a constant index of refraction of 1.4 and b) index of refraction with a constant density of 2.2 g/cm³ were varied to show the effect on counting efficiency.

Next, the media measured in the experiments were modeled, each with the same dimensions, 6mm thick by 25.4 mm in diameter. A 1.0 MeV electron source was placed homogeneously throughout the sample. Figure 18 shows that the most

efficient material is quartz; followed by sapphire, spinel, and zinc sulfide. Both spinel and zinc sulfide are less efficient due to their poorer transmittance, however it is interesting that quartz was far more efficient at creating photoelectrons than sapphire. Both had similar transmittances; however quartz (2.2 g/cm^3) is about half as dense as sapphire (4.0 g/cm^3). The density difference could cause the difference in photoelectron production if it were the only factor to consider, however the index of refraction of quartz is about 1.45 compared to 1.8 for sapphire. Taking into account the indices of refraction in addition to the density, and assuming a similar stopping power for quartz and sapphire, according to the data in Figure 17, one might guess that the efficiencies should be about equal; however that is not the case. This may suggest that density may have a larger effect on Cherenkov photon production at lower refractive indices (1.56 for quartz) than at higher refractive indices (1.79 for sapphire). The index of refraction at 420 nm for each material is in Table 3. A full analysis of how these parameters affect Cherenkov photon production and detection would be valuable, but is beyond the scope of this research.

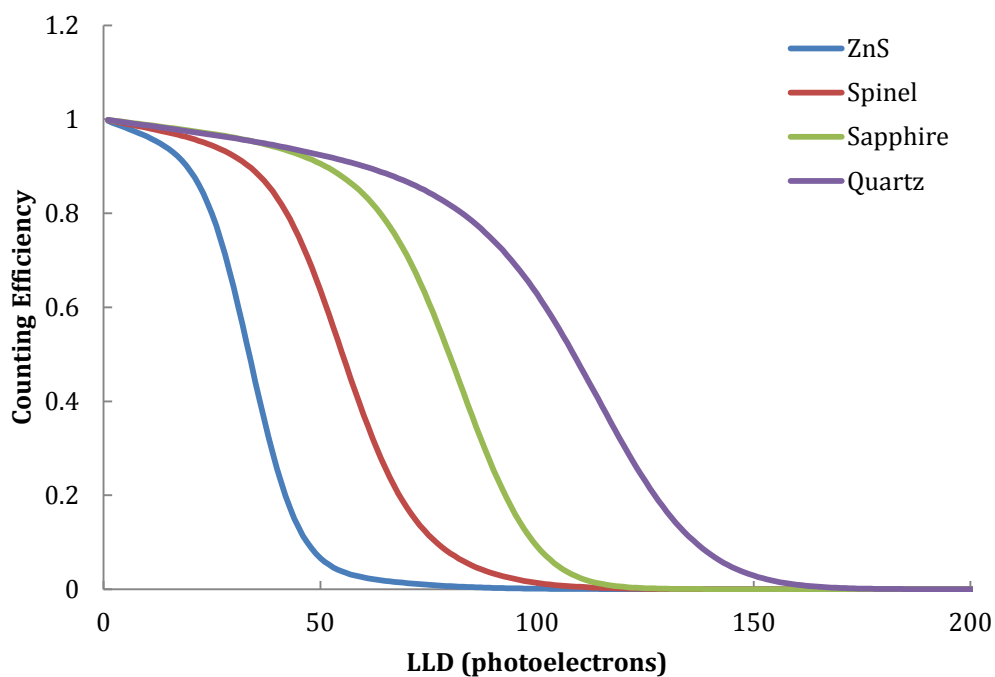


FIGURE 18 *Counting Efficiency as a function of lower level discriminator. Results are from GATE simulations of quartz, sapphire, spinel, and zinc sulfide with identical dimensions exposed to a 1.0 MeV electron source and coupled to a photomultiplier tube with 100% quantum efficiency.*

Simulations of the sample media with their actual dimensions were also run, so that they could be compared to the experimental results. Beta particle events and gamma-ray events occur simultaneously from the perspective of a PMT. Therefore, beta particle events and gamma-ray events were run in separate simulations and separate histograms of beta-induced photoelectrons and gamma-ray induced photoelectrons were generated. Then, two numbers of photoelectrons drawn from those distributions were added to realize the “total” histogram. The radionuclides produced by fast neutron activation in the samples were used as the sources, ^{28}Al in SiO_2 , ^{27}Mg in Al_2O_3 , ^{27}Mg and ^{24}Na in MgAl_2O_4 , and ^{64}Cu in ZnS . With the exception of

^{64}Cu , each radionuclide emitted gamma rays as well as beta particles. As expected, ^{28}Al in quartz is the most efficient combination for producing photoelectrons (Figure 19).

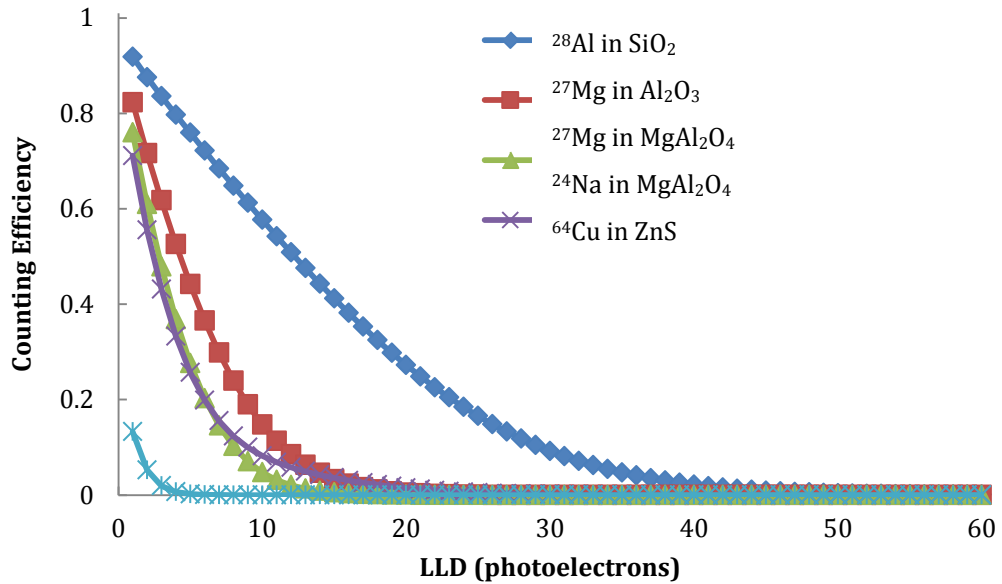


FIGURE 19 Counting Efficiency as a function of lower level discriminator. Results are from GATE simulations of quartz, sapphire, spinel, and zinc sulfide each irradiated by a neutron reaction product and coupled to a photomultiplier tube.

Table 8 shows the efficiency calculated from the GATE models defined as the number of events (decays) that produce at least one photoelectron in the PMT divided by the total number of events. The detection efficiencies are determined for the beta only, the gamma-ray only, and the total histograms. Note that almost all of the total efficiency came from the beta particles. This result is not surprising considering the higher threshold needed for gamma rays to produce Cherenkov photons and that these high energy gamma rays will not interact with the sample as

much as the beta particles, because of the low atomic number and density of the materials.

The efficiencies calculated from the GATE simulations were significantly greater than the measured efficiencies. This is likely due to discrimination against counts caused by only a few photoelectrons in the experimental data, i.e. a lower level discriminator. As shown earlier, this discrimination was necessary in order to minimize experimental background noise. Therefore, it can be assumed that the presence of background noise will have a great effect on the counting efficiency. By reducing the background so that single photoelectrons from the desired signal can be distinguished from background, the counting efficiency can be greatly increased.

TABLE 8 Comparison of GATE and Experimental Efficiency

Sample	Radionuclide	GATE Beta Efficiency %	GATE Gamma ray Efficiency %	GATE Total Efficiency %	Measured Efficiency %
SiO ₂	²⁸ Al	91.3	5.8	91.8	21.56 ± 3.60
Al ₂ O ₃	²⁷ Mg	80.3	10.3	82.3	37.89 ± 3.39
MgAl ₂ O ₄	²⁷ Mg	73.7	8.8	75.9	15.63 ± 5.26
	²⁴ Na	64.1	19.5	71.1	10.91 ± 0.49
ZnS	⁶⁴ Cu	6.8*, 7.8	N.A.	13.3	Not measurable

* Positron emission

The analyzed data from the GATE simulations is in terms of counting efficiency per number of photoelectrons emitted; the experimental data is in terms of counts per channel. Therefore, the channel to photoelectron ratio must be found. To do this, a bismuth germinate (BGO) crystal was irradiated by ²⁴¹Am, ⁵⁷Co, and

^{137}Cs , and counted under the same conditions as the samples. Knowing the photon yield of BGO, the approximate quantum efficiency of the PMT, and the location of the full energy peak of the radionuclides, an estimate of photoelectrons per channel can be made:

$$\frac{\text{photoelectrons}}{\text{channel}} = \frac{\text{gamma ray energy}}{\text{peak channel}} \times \left(\frac{\text{photon yield}}{\text{energy}} \right) \times \text{Quantum Efficiency}.$$

In the case of BGO, the photoelectron yield for bialkali photocathodes is approximately 10 to 15% of sodium iodide (NaI). Therefore,

$$\frac{\text{photoelectrons}}{\text{channel}} = \frac{\text{gamma ray energy}}{\text{peak channel}} \times \left(\frac{38 \text{ photons}}{\text{keV}} \right) \times (0.20) \times (0.10 \text{ to } 0.15).$$

Using the data in Figure 20, it was found that there are about 3 photoelectrons per channel. This value is only an estimate; the counts from single, double, triple, etc. photoelectron events have mean values and may be distributed over many channels.

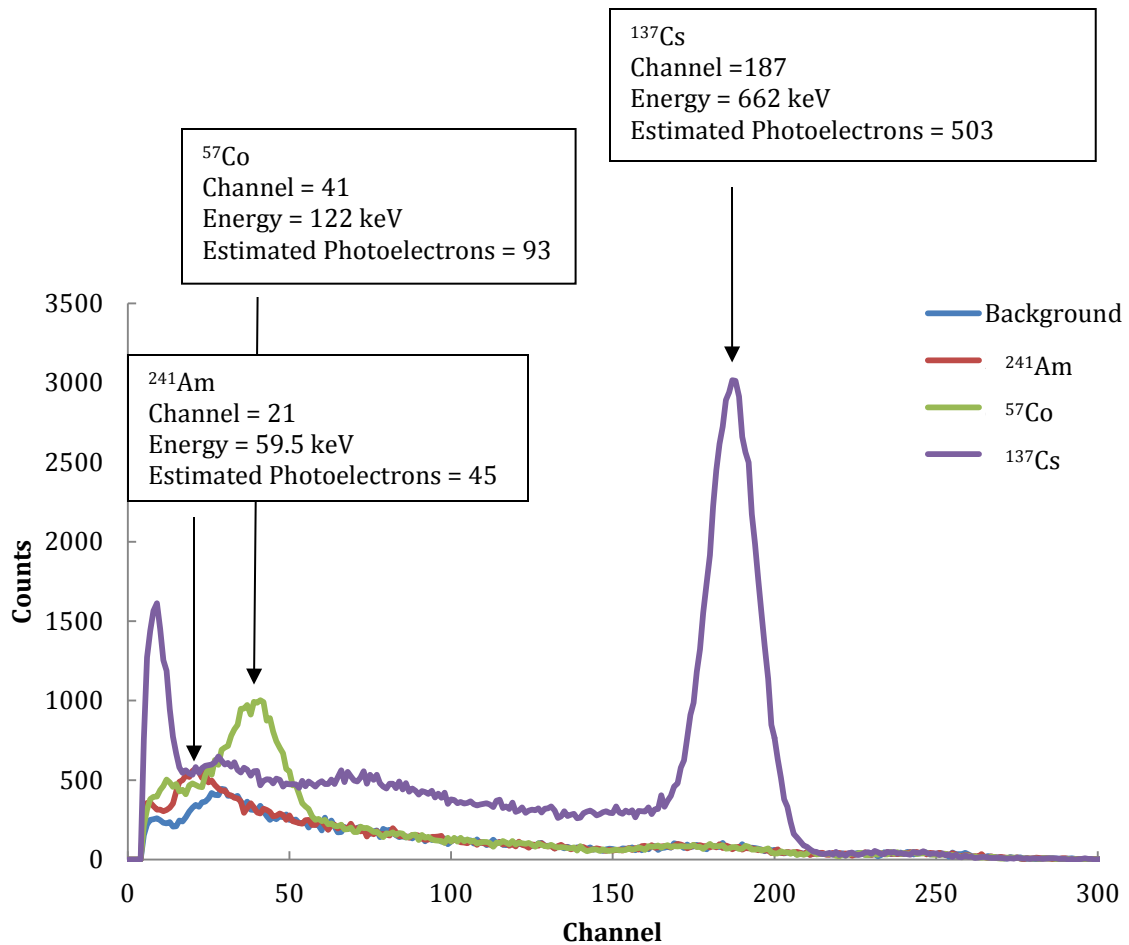
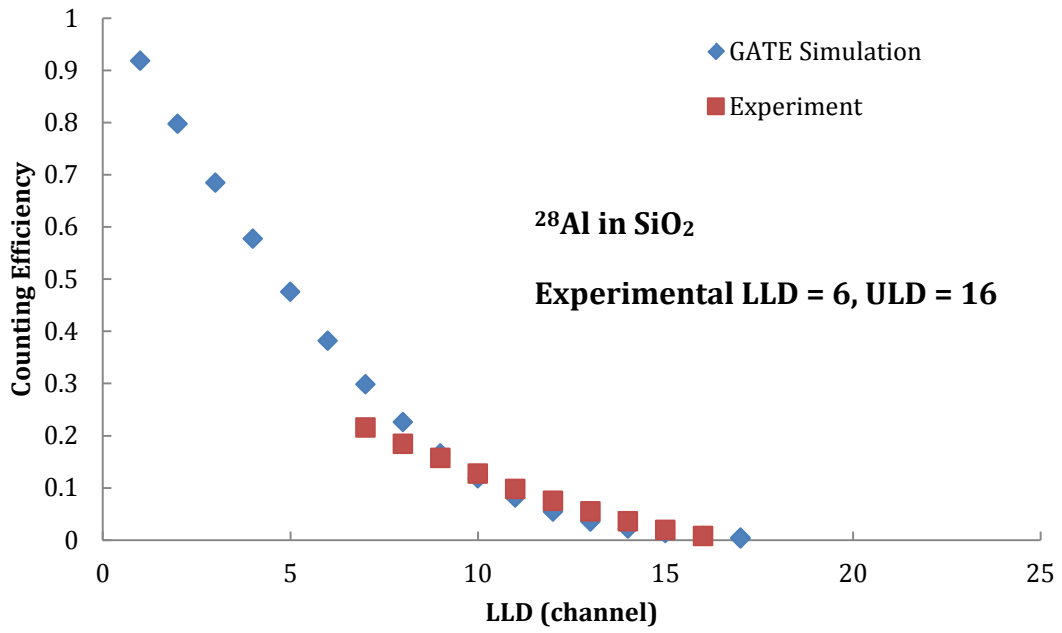


FIGURE 20 Pulse height spectrum of a bismuth germanate (BGO) crystal exposed to gamma ray sources. The peak channels correspond to the maximum number of photoelectrons emitted for a particular energy.

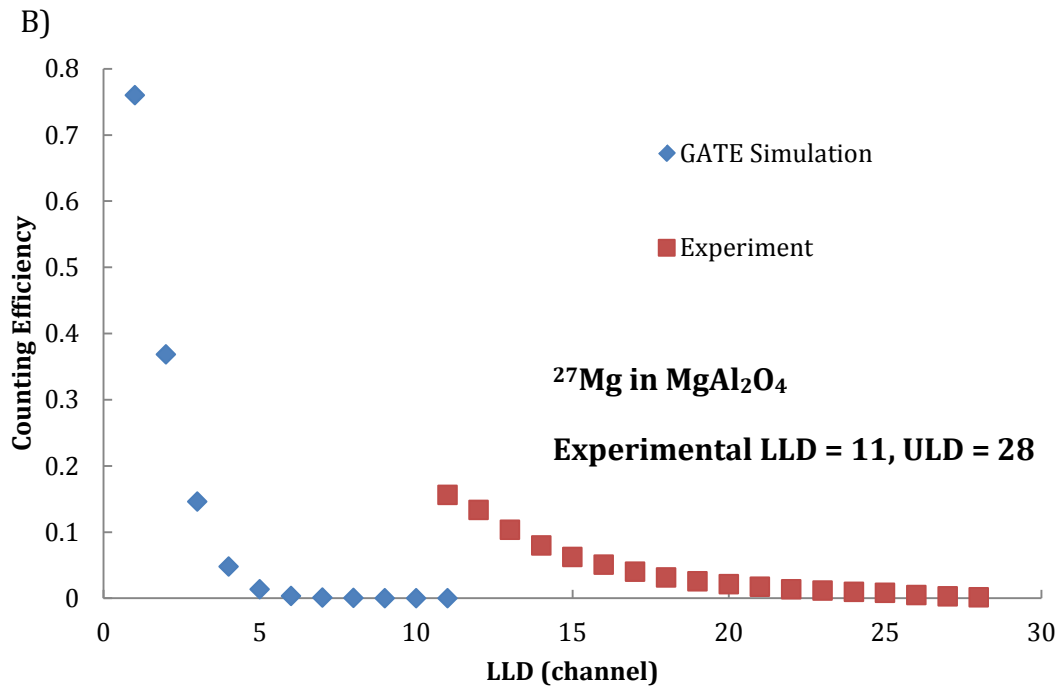
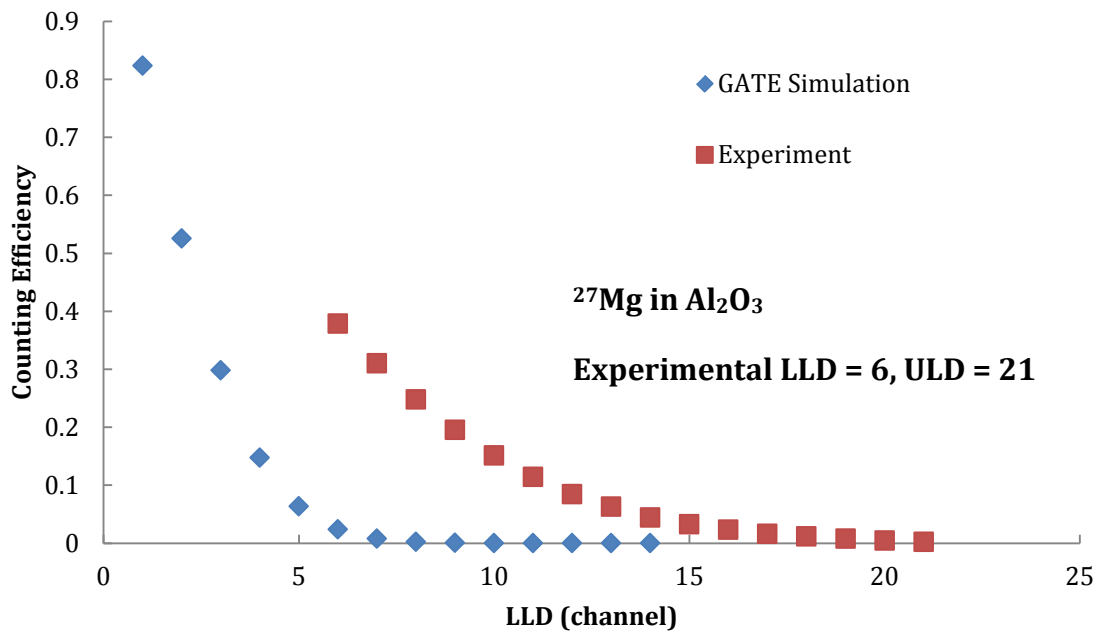
A comparison of the experimental data and data from GATE simulations is shown in Figure 21. Knowing that there are about 3 photoelectrons per channel, the fraction of simulated events that produced at least 1 photoelectron was graphed at channel 1, the fraction of simulated events that produced at least than 3 photoelectrons was graphed at channel 2, the fraction of simulated events that

produced at least 6 photoelectrons at channel 3, and so on. The experimental data shows the counting efficiency for the lower level discriminator values used in Table

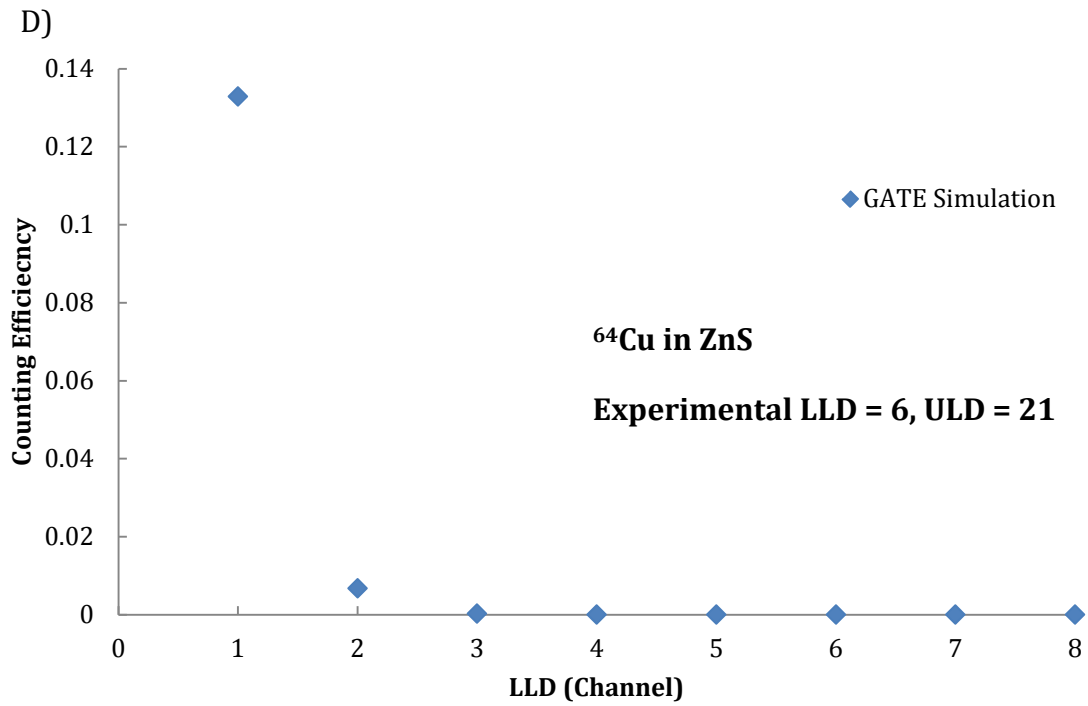
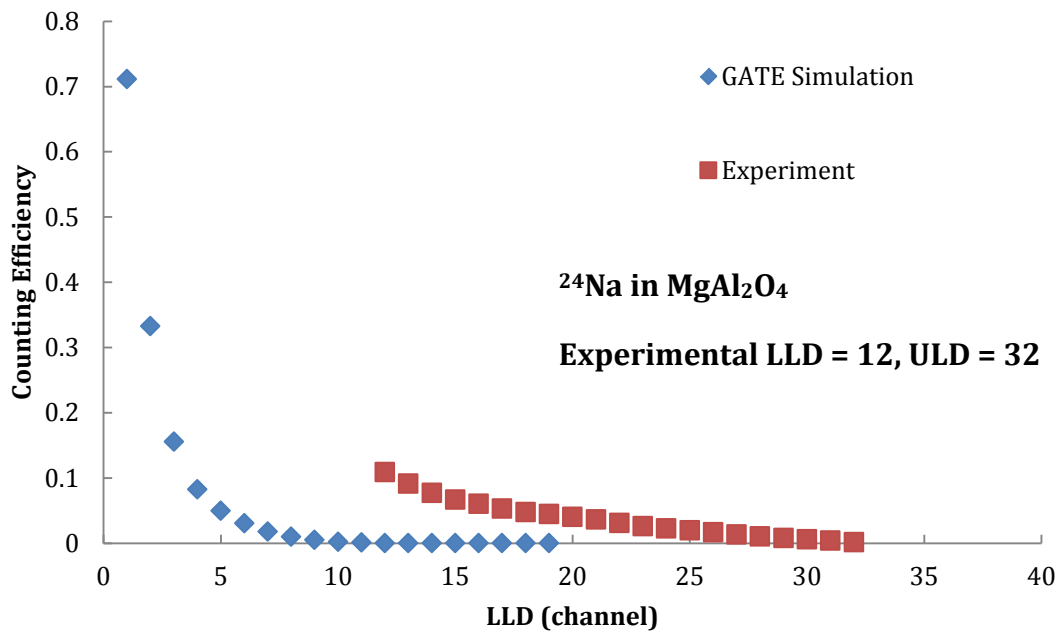
7.



A)



C)

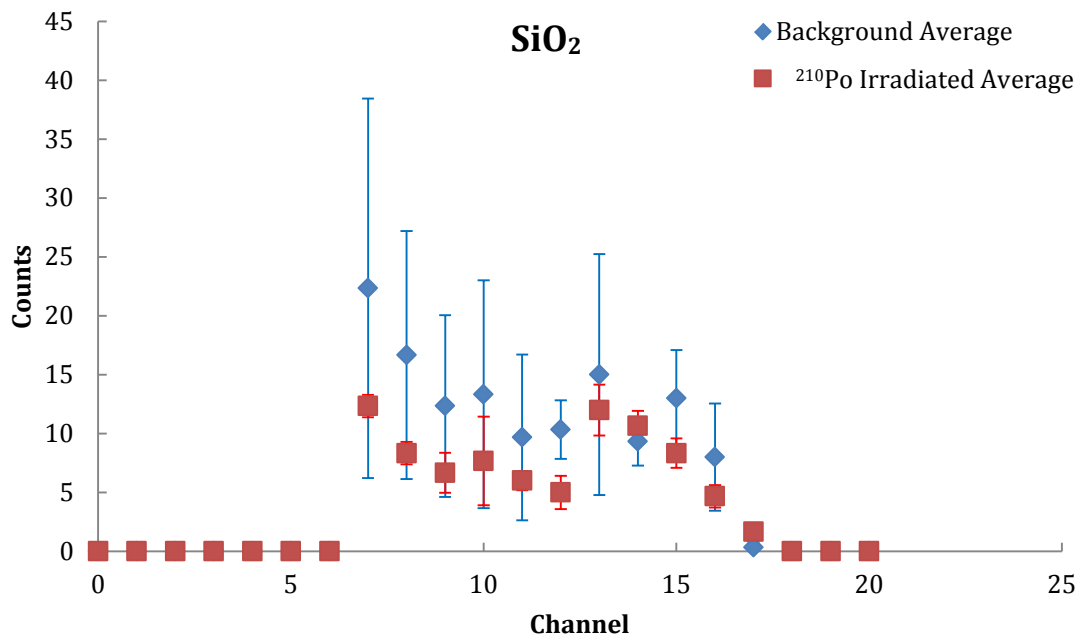


E)

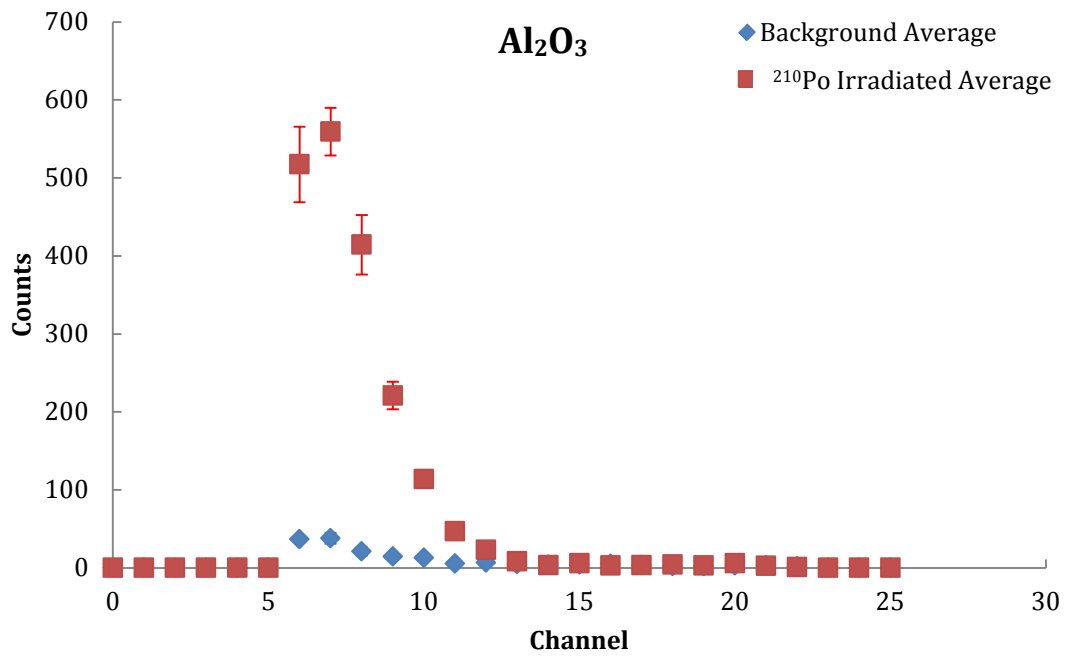
FIGURE 21 Comparison of the efficiency vs lower level discriminator for GATE simulations and experimental data. A) ^{28}Al in SiO_2 , B) ^{27}Mg in Al_2O_3 , C) ^{27}Mg in MgAl_2O_4 , D) ^{24}Na in MgAl_2O_4 , E) ^{64}Cu in ZnS

The data in Figure 21, B), C), and D) shows that for the LLDs set for Al_2O_3 and MgAl_2O_4 , the counting efficiency should have been very low, about 2% for Al_2O_3 , and less than 0.1% for MgAl_2O_4 . Since the recorded experimental efficiency was much higher than this, it implies that the signal seen from Al_2O_3 and MgAl_2O_4 does not only come from Cherenkov radiation caused by the decay particles of activated nuclides in the sample, but may be a result of another form of fluorescence.

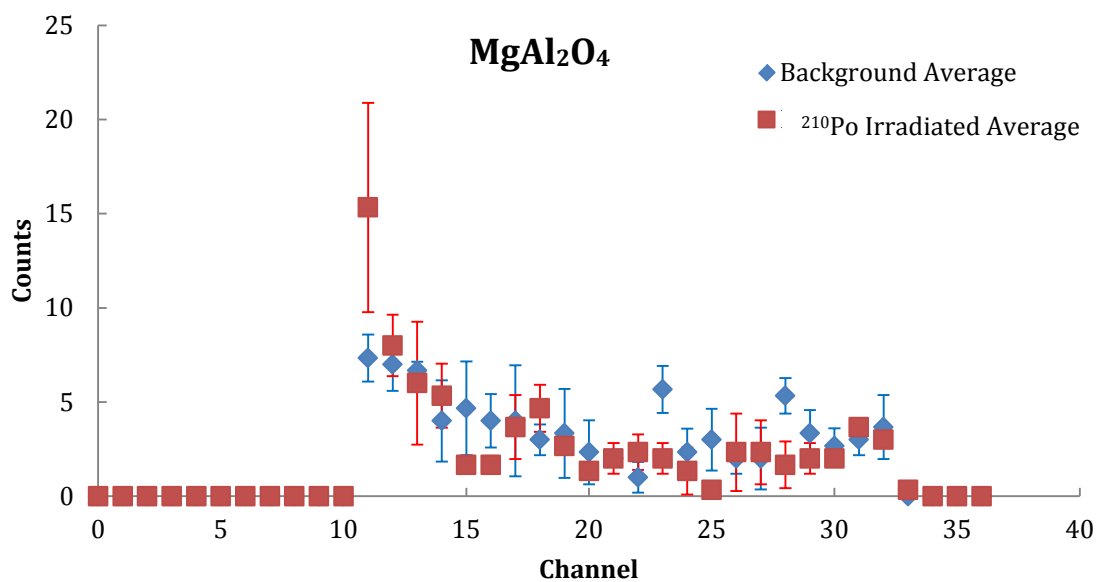
To corroborate this, a 2 nCi ^{210}Po (which emits 5.3 MeV alpha particle) disk source was placed on the samples while the samples were counted for 10 minutes. The threshold energy for Cherenkov photon production depends on the mass of the particle as well as the index of refraction of the medium. Because alpha particles are much more massive than electrons, a 5.3 MeV alpha particle will not be able to produce Cherenkov photons in the samples. Therefore, if the samples exhibit a signal from exposure to alpha particles, then some fluorescence is taking place. The results of these experiments (Figure 22) show that a significant signal appears when aluminum oxide is irradiated by alpha particles; the same is true for magnesium aluminate to a lesser extent. An attempt was made to distinguish between the signal due to Cherenkov radiation and fluorescence of the samples by examining the wavelength of Cherenkov photons compared to fluorescence photons. The results are shown in Appendix E.



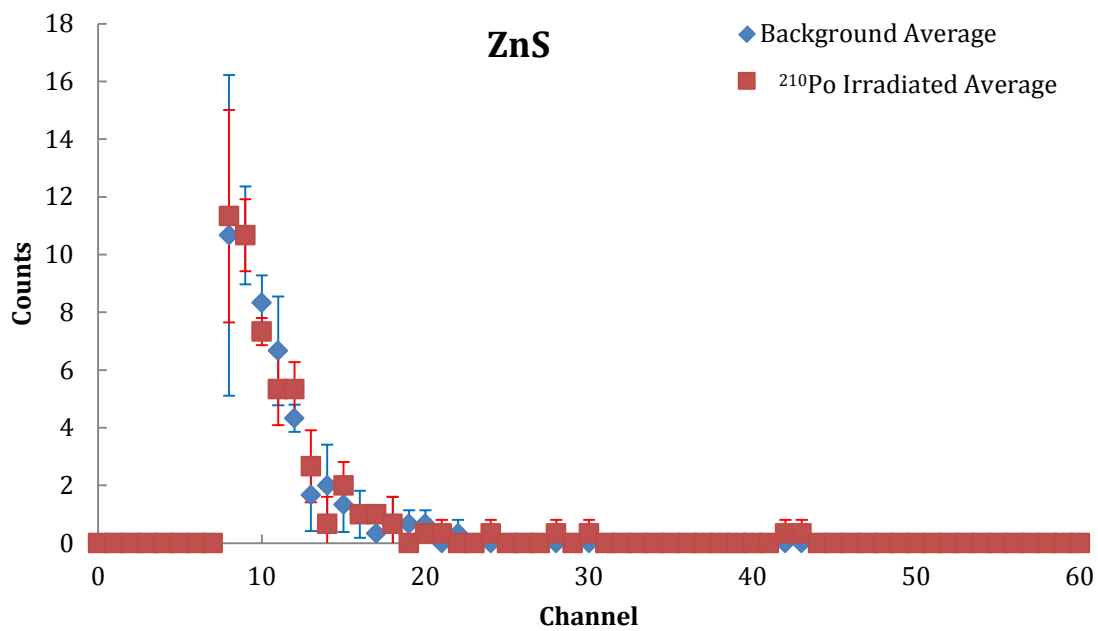
A)



B)



C)



D)

FIGURE 22 Pulse height spectrum of samples irradiated by ²¹⁰Po. A) SiO₂, B) Al₂O₃, C) MgAl₂O₄, and D) ZnS.

Simulations were also run to test how the quantum efficiency of the PMT, the presence of a reflector, and the presence of optical grease affected the counting efficiency. To quantify how the quantum efficiency of the PMT might affect the measured counting efficiency, the quantum efficiency was set to 100% for all wavelengths from 177 nm to 1240 nm. For comparison, the standard quantum efficiency of the type of PMT used in these experiments and in the simulations in Figure 21 is shown in Figure 23. Additionally, the reflector and optical grease were replaced with air in separate simulations to quantify how the presence of a reflector and optical coupling grease might affect the counting efficiency. The results are shown in Figure 24.

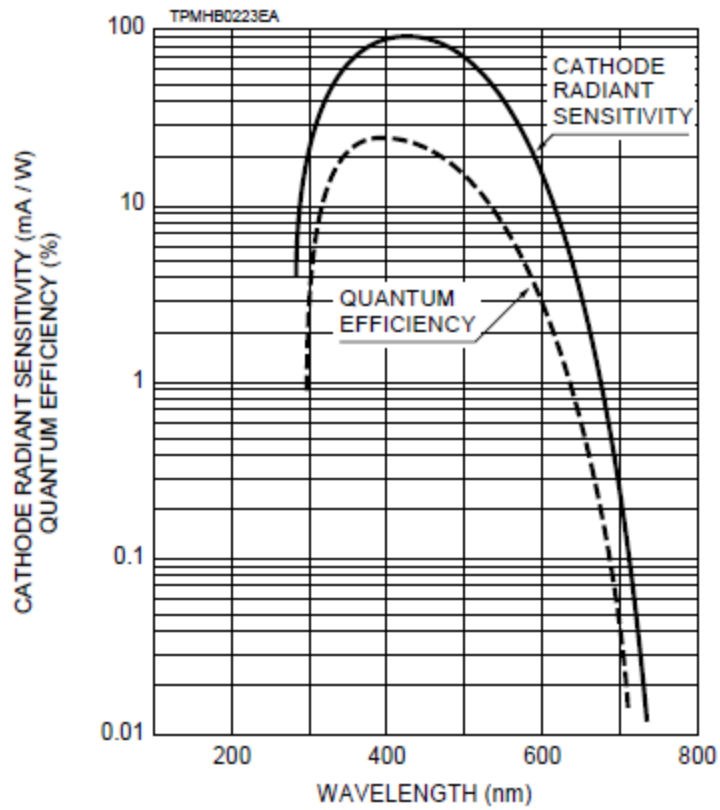
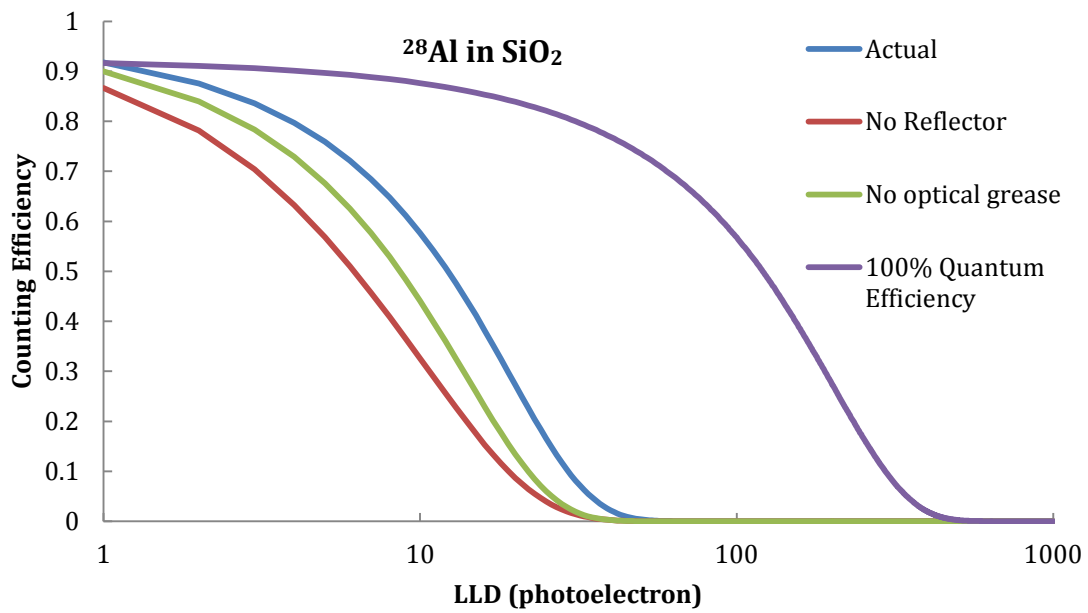
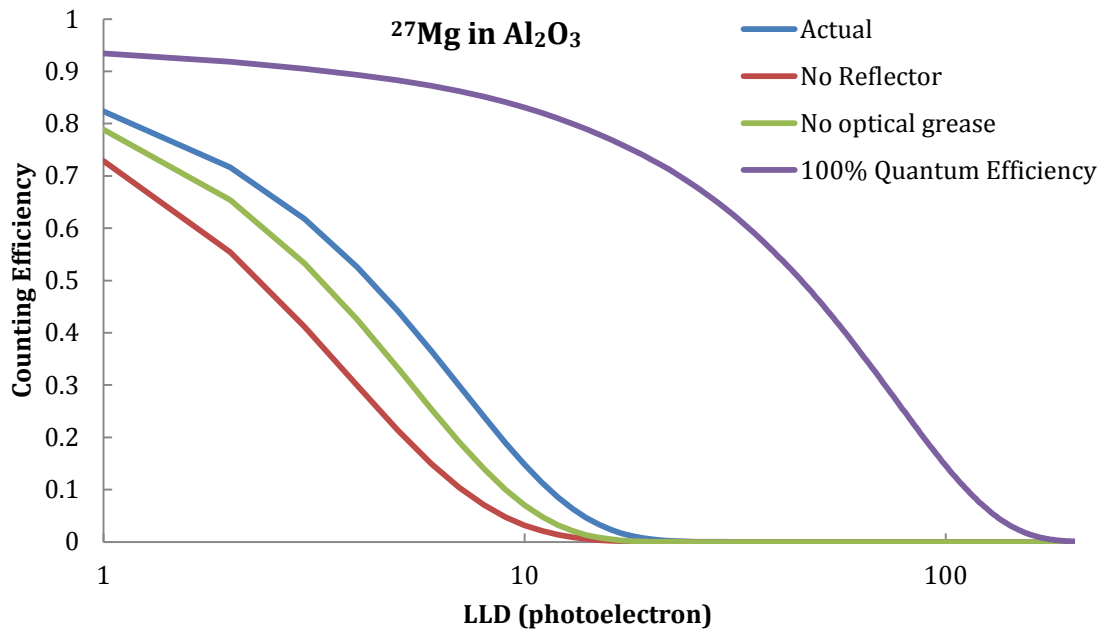


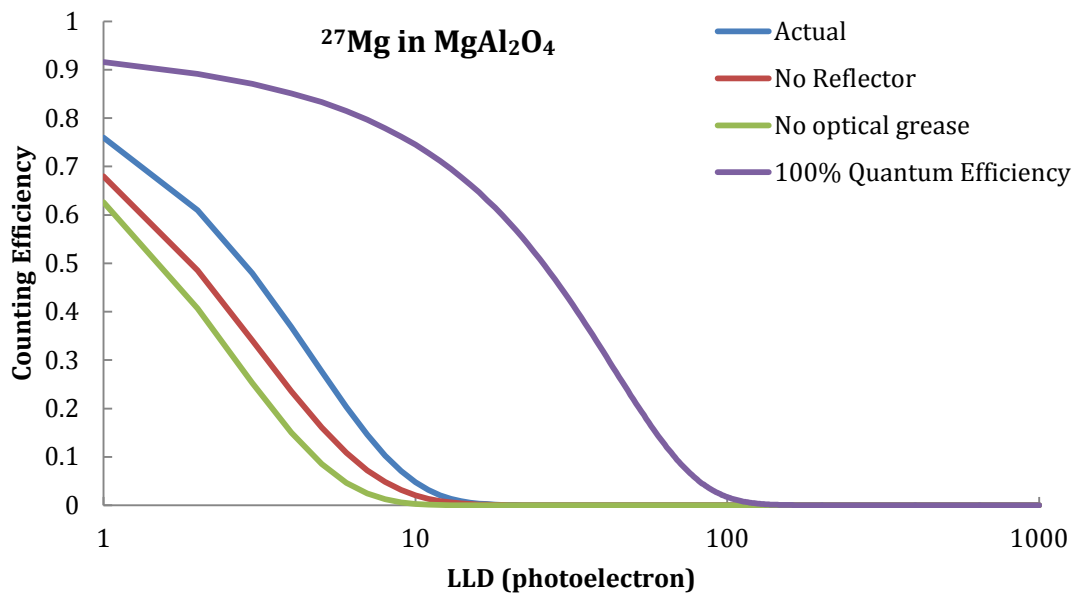
FIGURE 23 *Approximate Quantum Efficiency vs. Wavelength spectrum for a standard Hamamatsu R268 PMT (Hamamatsu Photonics K.K., Electron Tube Center 1996)*



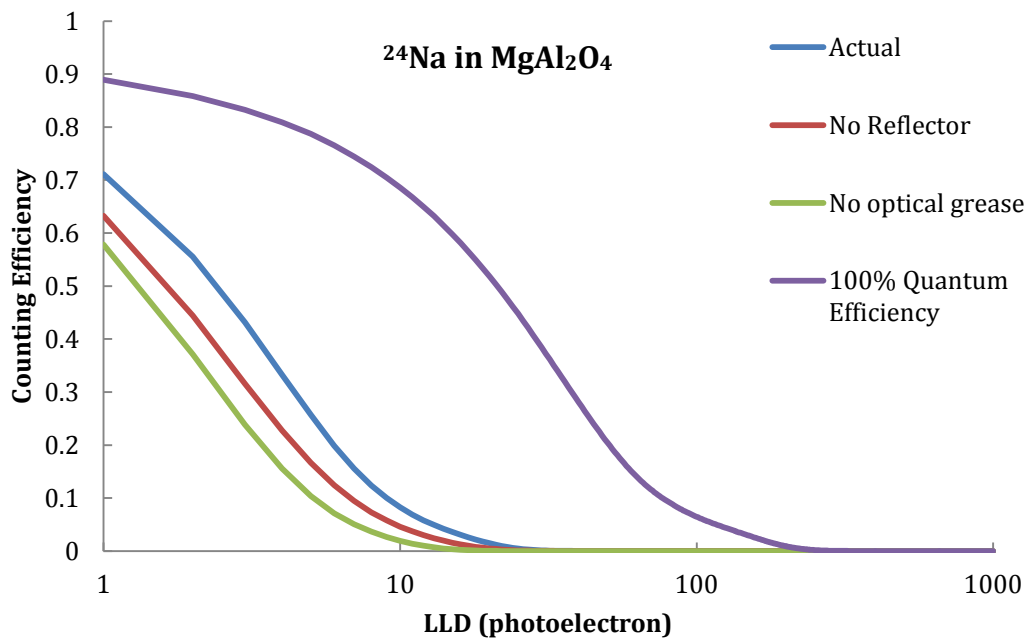
A)



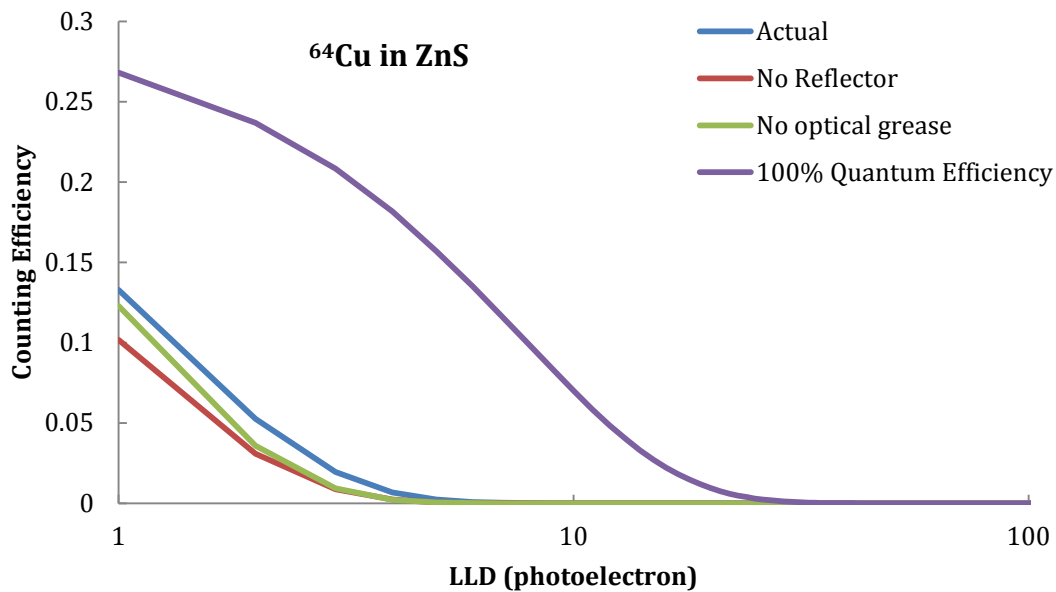
B)



C)



D)



E)

FIGURE 24 Comparison of the efficiency vs lower level discriminator for GATE simulations with varying parameters that affect light collection of the PMT. A) ^{28}Al in SiO_2 , B) ^{27}Mg in Al_2O_3 , C) ^{27}Mg in MgAl_2O_4 , D) ^{24}Na in MgAl_2O_4 , E) ^{64}Cu in ZnS

The PMT used in these experiments was sensitive to a photon wavelength range of 300 to 650 nm (Figure 23). The large increase in counting efficiency when the quantum efficiency was increased to 100% implies that a significant number of Cherenkov photons entering the PMT had wavelengths smaller than 300 nanometers or greater than 650 nanometers. Figure 25 shows the wavelength spectrum of photons that make it to the PMT during a simulation of ^{27}Mg in Al_2O_3 . Approximately 35% of incident photons have wavelengths shorter than 300 nm and 12.5% have wavelengths longer than 600 nm. For future experiments, using PMTs with a wider spectral response may increase efficiency. Removing the reflector reduced the counting efficiency significantly, as did removing the optical grease.

This result confirms the value of wrapping the sample in a reflector to reflect outgoing light back into the PMT, and coupling the sample to the PMT using optical gel for better light transmission. The true quantum efficiency of the PMT employed in these experiments and future experiments should also be quantified using tunable lasers and wavelength filters. It is possible that the standard quantum efficiency curve used in the aforementioned GATE simulations may not be truly representative of the actual quantum efficiency of the PMT, and therefore could have affected the results.

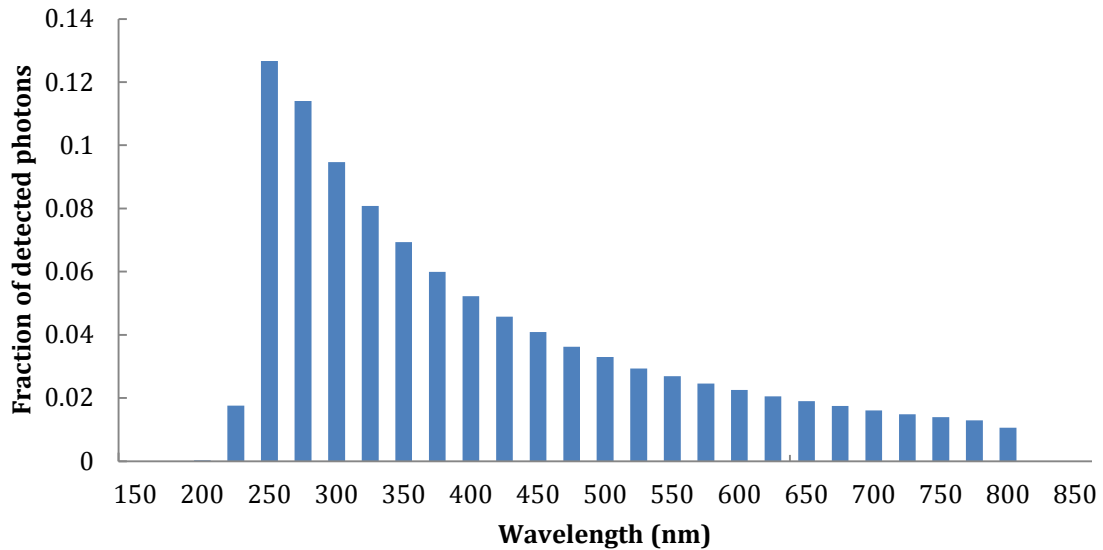


FIGURE 25 *Wavelength spectrum of Cherenkov photons that reach the PMT in a GATE simulation of ^{27}Mg in Al_2O_3*

CONCLUSIONS

The results presented above show that fast neutron activation in the SiO_2 sample likely produced a signal measurable by a PMT that was due to the Cherenkov effect. GATE simulations suggest that the signals seen from Al_2O_3 and MgAl_2O_4 are likely not due to the Cherenkov effect. Subsequent irradiation with an alpha particle source showed that Al_2O_3 and MgAl_2O_4 may fluoresce when exposed to ionizing radiation. ZnS was the only sample that did not produce a measurable signal with the neutron flux used in these experiments. The measured counting efficiencies were all below 40%, and varied depending on transmittance, energy of the reaction product's beta particles, and choice of lower level pulse height discriminator. The light collection of Cherenkov photons produced in each sample was modeled using a GEANT4 based program. The model showed that enough Cherenkov radiation can be produced in the samples to create a measurable signal, and that a PMT with lower background noise and that is sensitive to a wider wavelength spectrum of photons may increase the counting efficiency. Further modeling will reveal how aspects of the technique may be optimized.

FUTURE WORK

Further probing of the detection system will have to be done to ensure that it will give reliable results. The most important test would be to measure the response of each material after exposing it to a simulated criticality event, e.g. a pulsed nuclear reactor. Only then would the true potential of the detection method

be realized. A few of the experiments that could be done to better understand the detection system include: trying PMTs with a wider spectral range, measuring the difference in signal when using different reflectors, coupling the sample to the PMT with optical greases of different indices of refraction, and measuring how the signal changes with samples of the same material but different thickness. It is likely that some of the signal may be due to fluorescence rather than from the Cherenkov effect. While this may not be problematic experimentally, the fluorescence light yield would be helpful to know if future simulations are to be performed. An experiment could be performed to determine how much light is generated by fluorescence. A PMT with a fast response time may be able to distinguish between a pulse due to Cherenkov radiation and a pulse to fluorescence via their decay times. A PMT sees all of the Cherenkov photons from a decay event in one pulse, a few nanoseconds in width. The fluorescence photons from a decay event will be seen as a collection of pulses whose heights decay exponentially over the course of tens of nanoseconds to milliseconds. By recording the decay time for each pulse, the frequency of Cherenkov and fluorescence pulses can be determined.

In addition, although the GATE/GEANT4 simulations gave the expected responses when parameters such as density and index of refraction were varied, and they also helped lead to the realization that some of the samples may fluoresce when exposed to ionizing radiation, the model should be verified more thoroughly. A Cherenkov detector with known characteristics should be simulated by the

GATE/GEANT4 toolkit and the results compared with experiment to show that the GATE/GEANT4 simulations are indeed a good model.

APPLICABILITY FOR A CRITICALITY EVENT

The experiments performed in this research were intended to show the detection and quantification of the fast neutron flux from fission using the technique developed by Bell and Boatner. It has been shown in this research that, with the exception of ZnS, when exposed to a flux of approximately $9400 \text{ neutrons cm}^{-2}\text{s}^{-1}$ the samples produce a signal that is readily measurable. If exposed to an actual criticality event, the samples could become several orders of magnitude more radioactive than seen in this research.

In a criticality event, all of the materials near the source will undergo neutron reactions and become radioactive to some degree. Even though the counting system will be turned on after the event occurs, (preventing prompt gamma rays from interfering) errant gamma rays and energetic beta particles from reaction products surrounding the material and PMT may cause Cherenkov photons to be produced within the sample. The PMT window itself may even become activated. If either of these events occurs, the undesired signal will show up as an additional decay constant in the multichannel scaler spectrum if it has a half-life on the order of the desired reaction product's half-life or as an increase in the background count rate if it has a much longer half-life. These decay constants must be known in order to properly estimate the activity within the sample. Knowledge of all of the most likely

neutron reactions that could take place around the material and PMT will help in determining the proper decay constants. In this research, the sample and PMT were placed in a dark box for counting. A box is not necessary; a thin, opaque covering or coating of some fast neutron insensitive material that would envelope the sample and PMT would be enough. To further reduce background noise produced from reaction products outside of the sample, the material and PMT could be perched on the end of an arm that sticks out from the wall, or even hung from the ceiling. If these placements are not practical, then knowledge of the surroundings is a necessity.

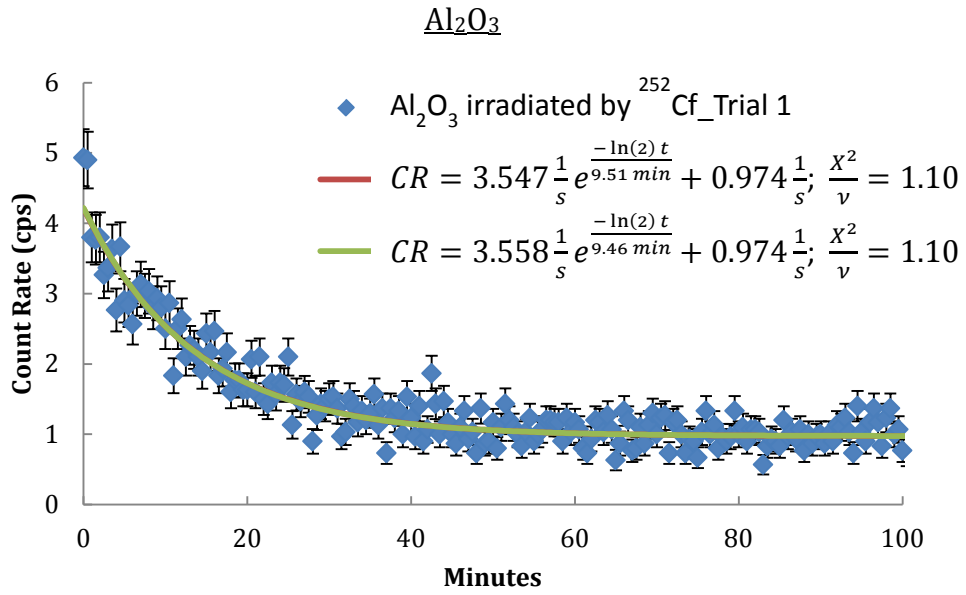
Spectroscopy of the energy spectrum is possible by having many different target nuclides, either in the same medium or by having multiple materials, each with a different target. Using a neutron spectrum unfolding program like SANDII would be a viable solution. SANDII works by taking activities of the reaction products as inputs, and varying the solution spectrum until it is an acceptable solution for all of the input activities (within a certain degree of uncertainty). Understanding the neutron energy spectrum will make it easier to estimate the dose due to neutrons, as the dose changes based on the energy of the neutron.

In conclusion, the Cherenkov effect can be utilized to detect fast fission neutrons in SiO_2 . Capturing the signal from the Cherenkov effect in Al_2O_3 and MgAl_2O_4 was hampered by high background noise. This made it necessary to raise the lower level discriminator, excluding Cherenkov pulses corresponding to few photons, which decreased efficiency. A measurable signal from ZnS was not found

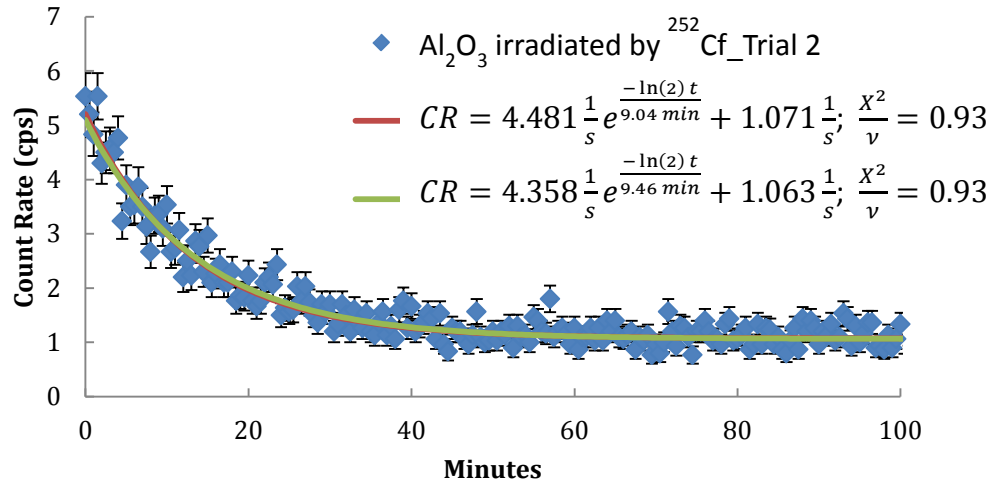
because of the low energy and branching ratio of the beta particles it emitted. Although the detection of fast fission neutrons via the Cherenkov effect was demonstrated in SiO₂ in this research, exposure to an actual criticality event will create many more challenges for operation of the detection system that must be addressed. However, the basic principle of this detection method has been shown here to be effective.

APPENDICES

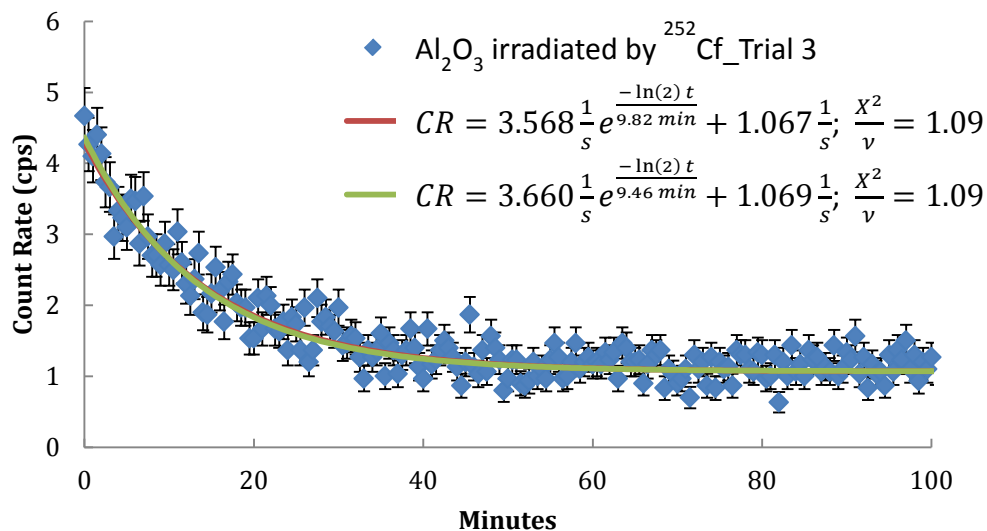
APPENDIX A: RAW DATA



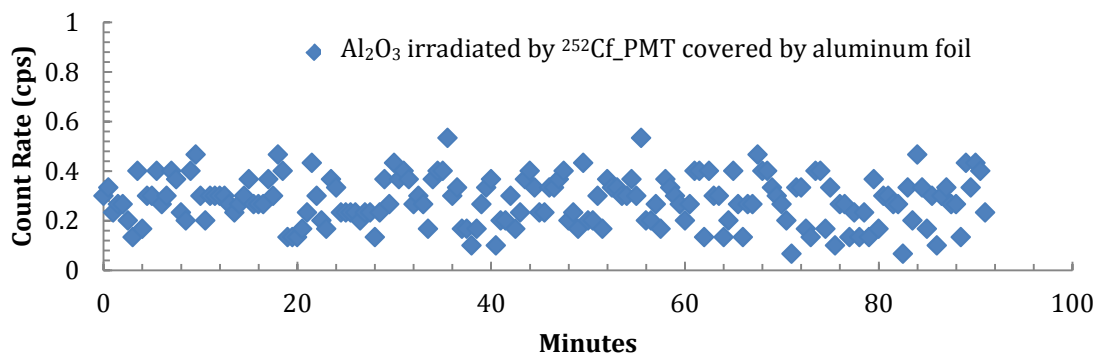
a)



b)



c)



d)

FIGURE 26 a), b), c) Time series data showing the exponential decay of ^{27}Mg produced as a result of neutron irradiation of Al_2O_3 . d) Time series data showing a lack of signal after the Cherenkov photons were prevented from reaching the PMT. The background count rate decreases when the PMT is covered by foil. This suggests that background gamma-ray radiation may be interacting with the Al_2O_3 sample, producing Cherenkov or fluorescence photons.

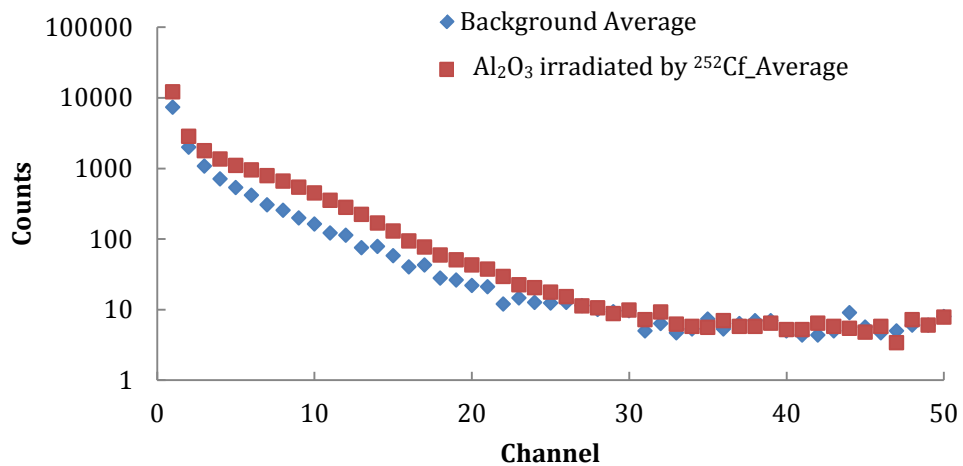
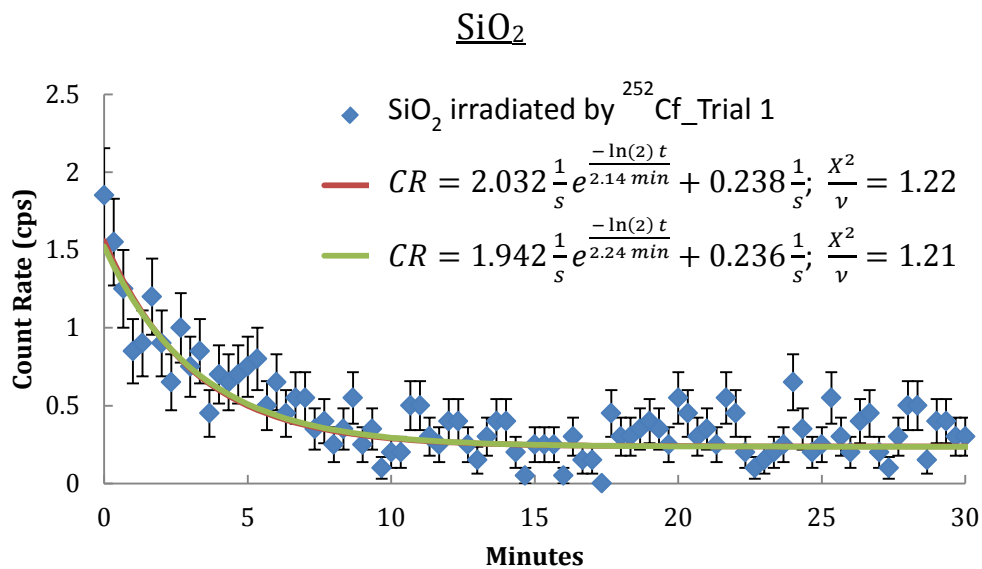
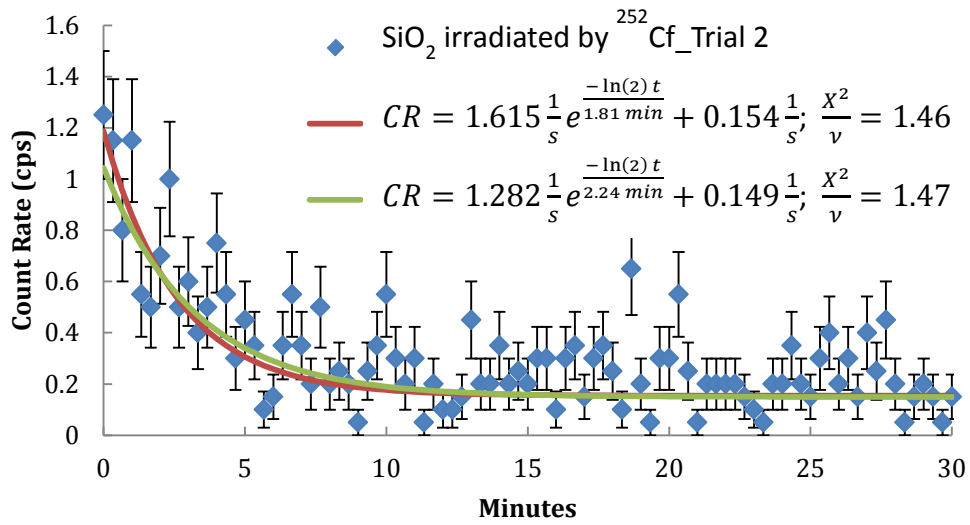


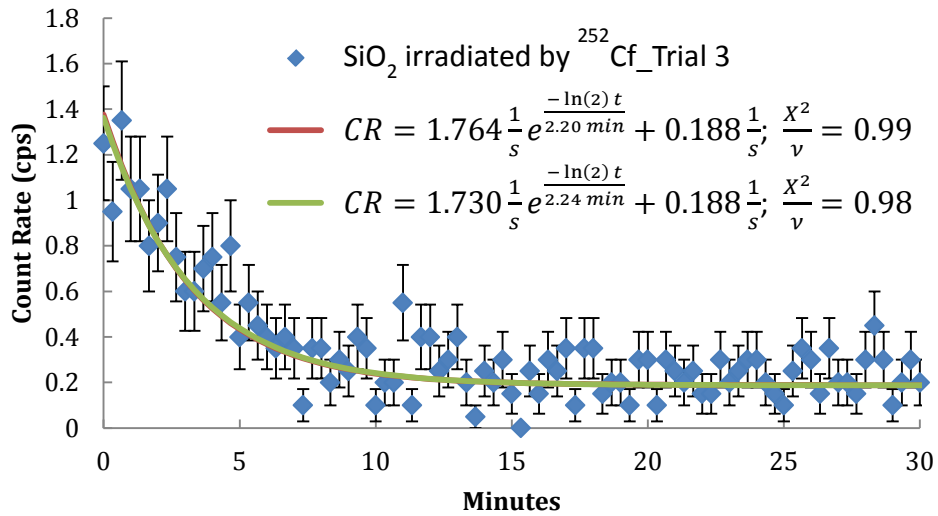
FIGURE 27 Pulse height spectrum of Al_2O_3 after irradiation by ^{252}Cf



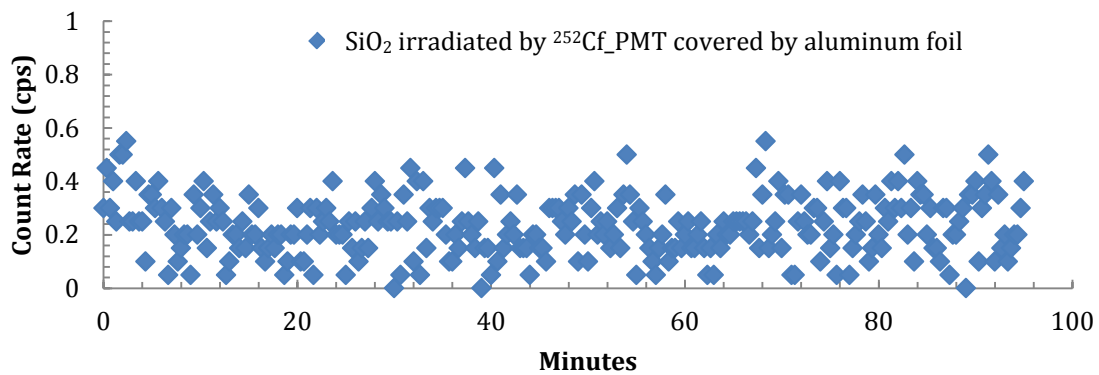
a)



b)



c)



d)

FIGURE 28 a), b), c) Time series data showing the exponential decay of ²⁸Al produced as a result of neutron irradiation of SiO₂. d) Time series data showing a lack of signal after the Cherenkov photons were prevented from reaching the PMT. The background count rates of the covered and uncovered PMT are the same.

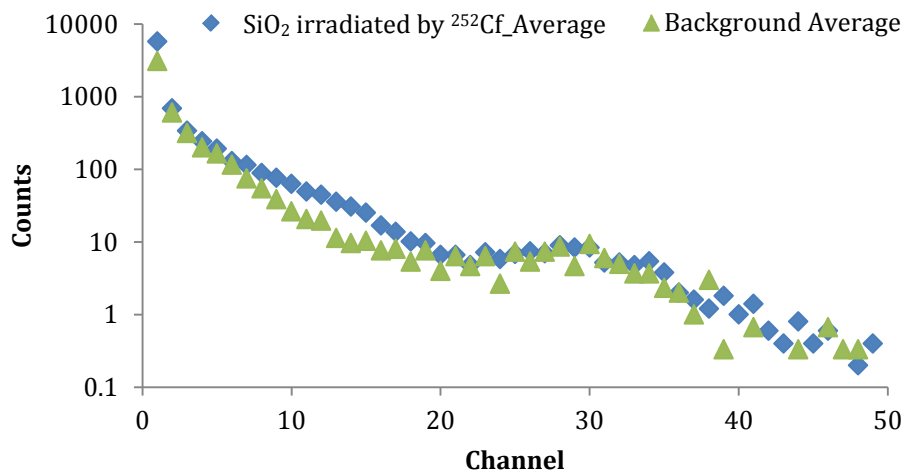
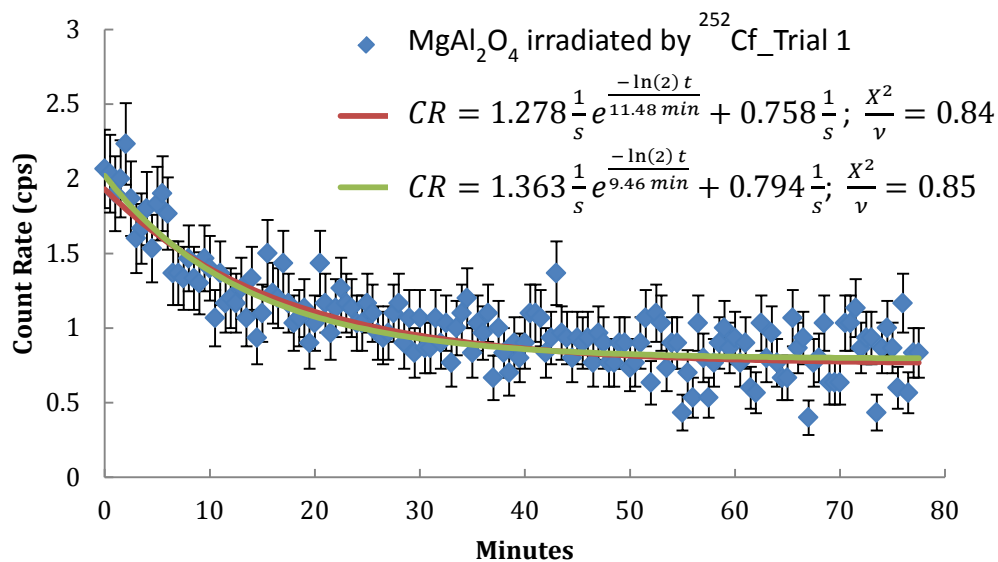
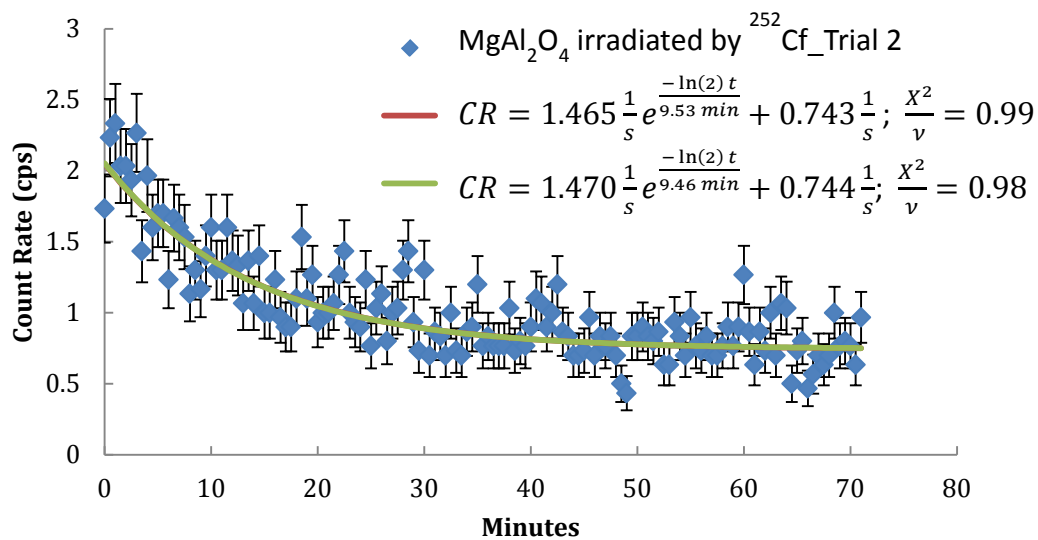


FIGURE 29 Pulse height spectrum of irradiated SiO₂ after irradiation by ²⁵²Cf

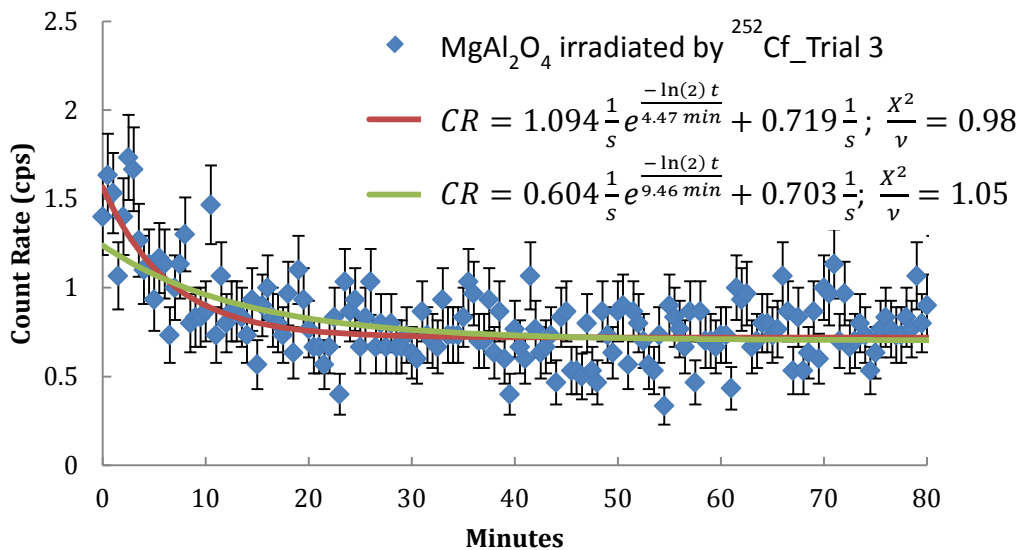
MgAl₂O₄ (30 s bins)



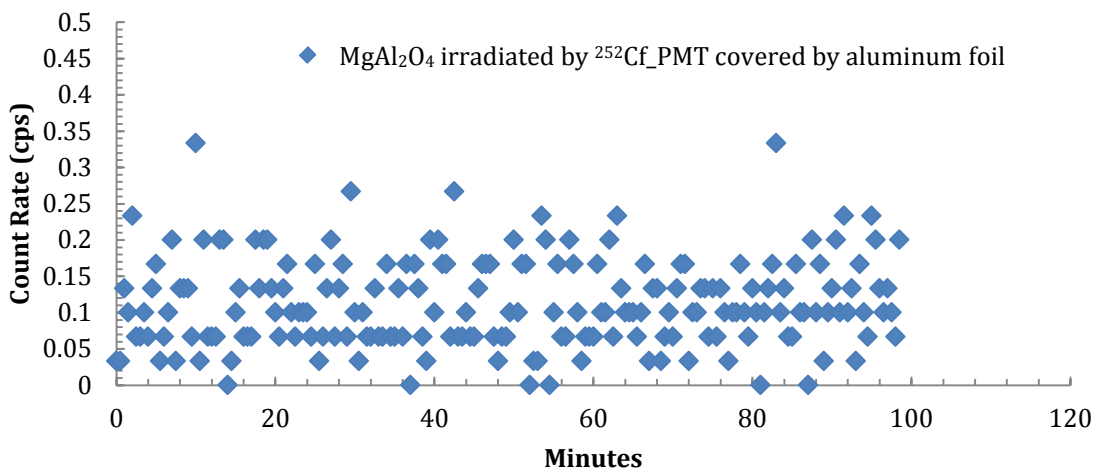
a)



b)



c)



d)

FIGURE 30 a), b), c) Time series data showing the exponential decay of ^{27}Mg produced as a result of neutron irradiation of MgAl_2O_4 . d) Time series data showing a lack of signal after the Cherenkov photons were prevented from reaching the PMT. Just as with Al_2O_3 the background count rate decreases when the PMT is covered by foil. The MgAl_2O_4 sample may be scintillating or producing Cherenkov photons from ambient gamma-ray radiation.

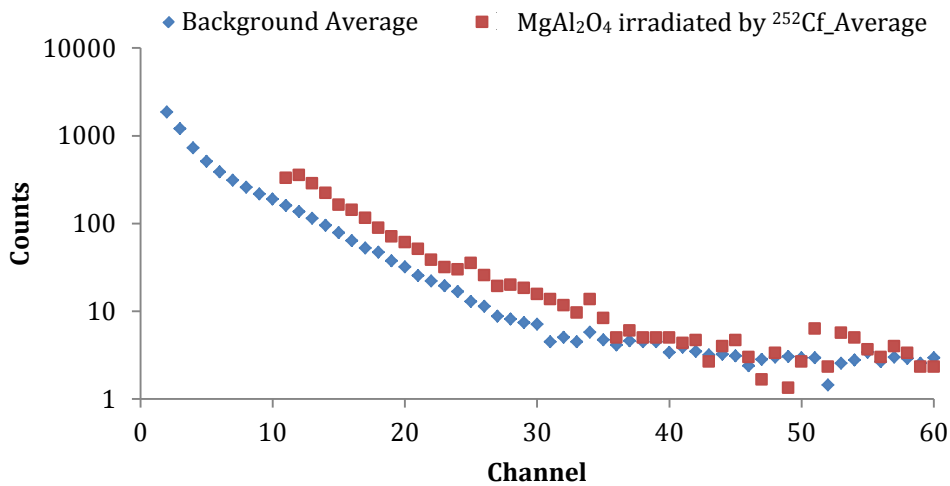
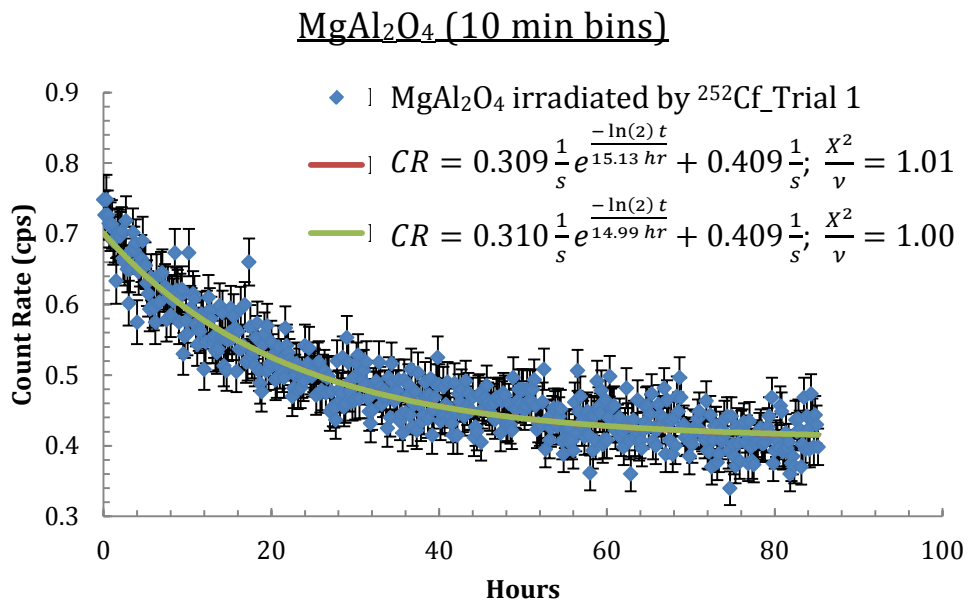
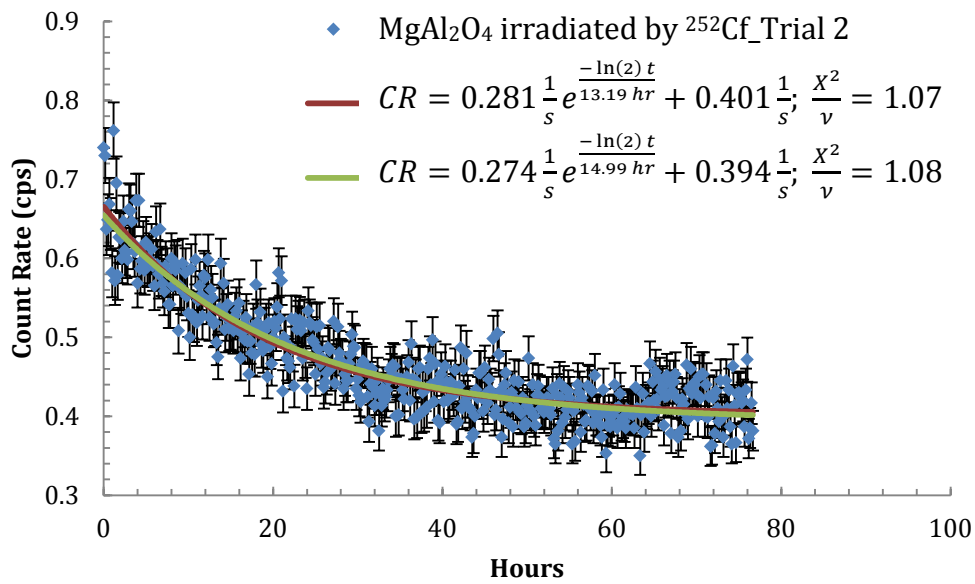


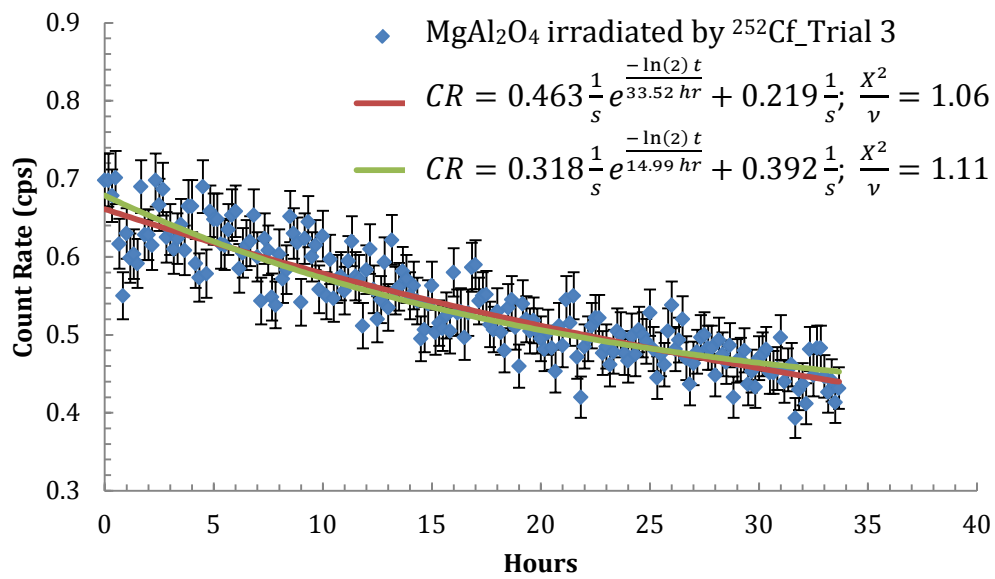
FIGURE 31 Pulse height spectrum of irradiated $MgAl_2O_4$ after irradiation by ^{252}Cf



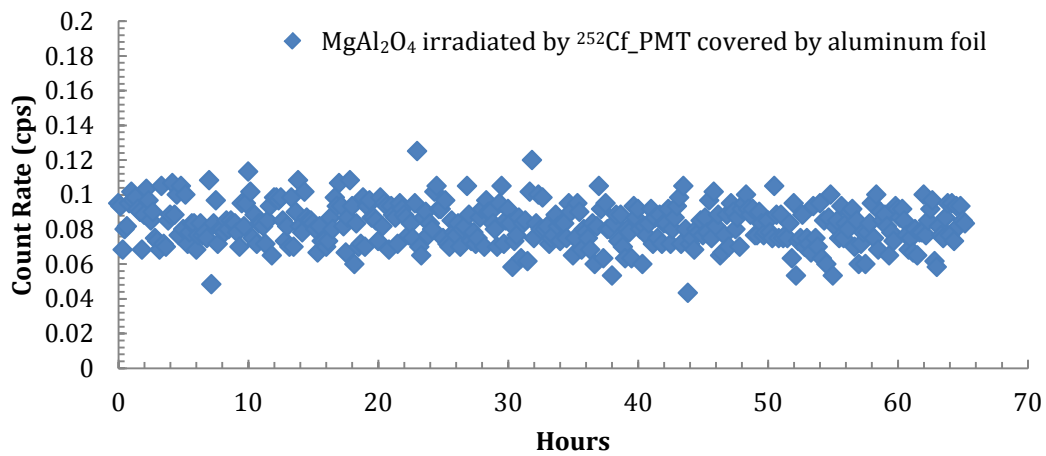
a)



b)



c)



d)
FIGURE 32 a), b), c) Time series data showing the exponential decay of ²⁴Na produced as a result of neutron irradiation of MgAl₂O₄. d) Time series data showing a lack of signal after the Cherenkov photons were prevented from reaching the PMT.

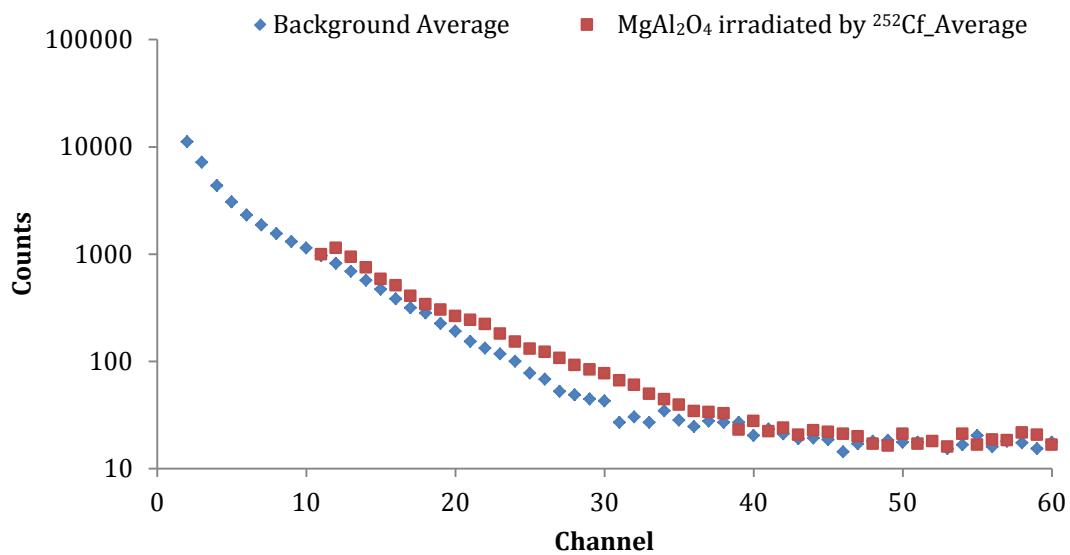


FIGURE 33 Pulse height spectrum of irradiated MgAl₂O₄ after irradiation by ²⁵²Cf

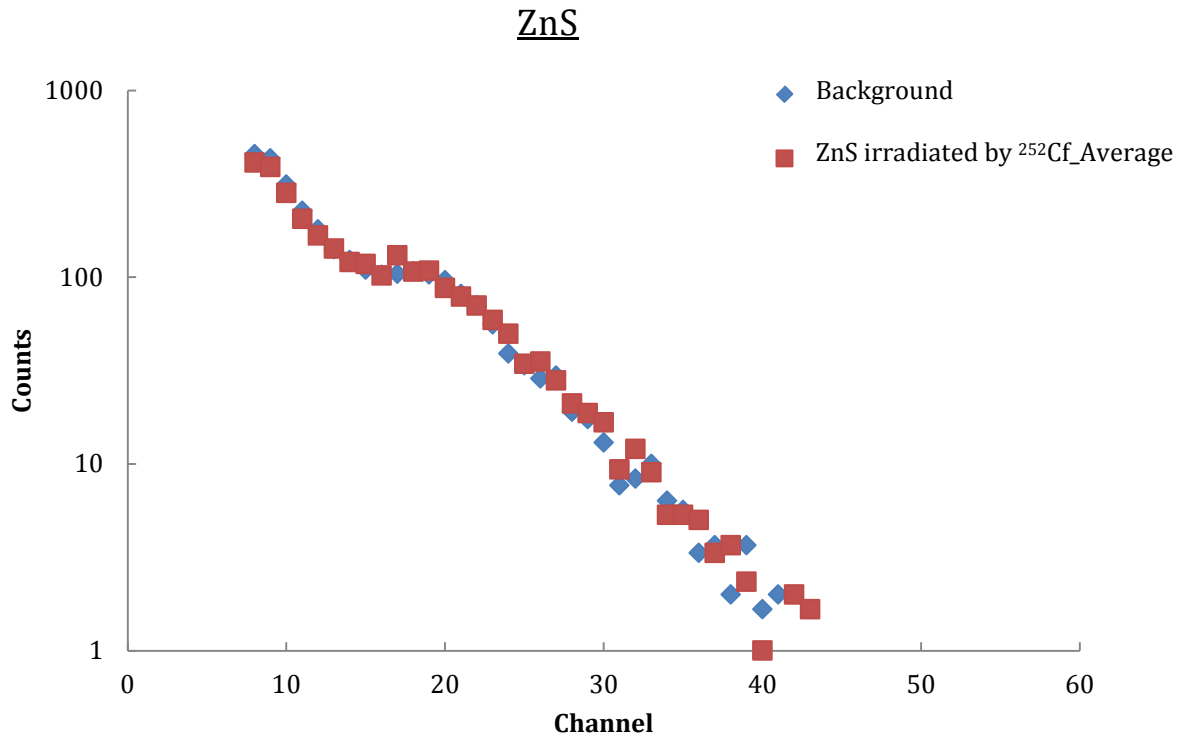


FIGURE 34 Pulse height spectrum of ZnS irradiated by ^{252}Cf vs Background. No signal due to irradiation is visible.

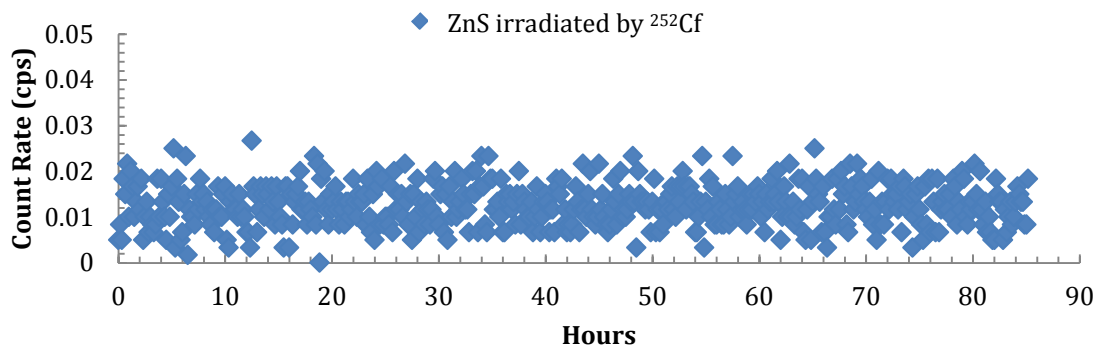


FIGURE 35 Time series data showing a lack of signal from ^{64}Cu in ZnS.

APPENDIX B: INPUT FILES

EXAMPLE MCNP INPUT (Al_2O_3)

```
C CELLS
C INNER CAPSULE
  1 2 -8.03      15 -3 -2
  2 1 -19.97     3 -7 -2 (-4:6:1)
  3 3 -0.000000596  4 -6 -1
C 4 1 -19.97     4 -5 1 -2
C 5 0           5 -6 -2
C 6 1 -19.97     6 -7 -2
C OUTER CAPSULE
  4 2 -8.03      15 -9 2 -8
C 8 2 -8.03      11 -12 -10 $HANDLE AT TOP
  5 2 -8.03      7 -14 -13
  6 2 -8.03      9 -7 2 -13
  7 4 .00127 -16 (13:-9:14)(8:-15:9) (18:-19:20)
    (21:-22:23:-24:26:-25) #10 #11
  8 0           16 $AIR
C SAMPLE CELLS
  9 6 -3.95      -18 19 -20
 10 6 -3.95      20 -29 -28
 11 6 -3.95      20 -29 27 -18
C LEAD
 12 5 -11.34     -21 22 -23 24 25 -26

C SURFACES
C INNERMOST CYLINDER (PLATINUM-RHODIUM)
  1 CZ 0.1588 $CONTAINS ACTUAL CF2O3 POWDER, INNER DIAMETER OF NEXT CYLINDER
  2 CZ 0.2756 $ OUTER DIAMETER OF CYLINDER OUTSIDE POWDER CYLINDER
  3 PZ 0.4572 $BOTTOM OF INNERMOST CYLINDER, BOTTOM OF PLAT-RHOD
  4 PZ 0.8509 $TOP OF PLAT-RHOD BOTTOM CAP, BOTTOM OF CF2O3 CAVITY
  5 PZ 2.3622 $TOP CF2O3 CAVITY, BOTTOM OF AIR(ASSUMING) CAVITY
  6 PZ 2.5400 $TOP OF "AIR" CAVITY, BOTTOM OF PLAT-RHOD CAP
  7 PZ 3.0480 $TOP OF PLAT-RHOD CAP AND ENTIRE INNER CYLINDER
C NEXT CYLINDER (STAINLESS STEEL)
  8 CZ 0.4114 $LITTLE HANDLE AT BOTTOM
  9 PZ 0.127 $TOP OF HANDLE
C NEXT CYLINDER(STAINLESS STEEL TOP HANDLE)
 10 CZ 0.2540 $HANDLE AT TOP OF CAPSULE
 11 PZ 3.2512 $ BOTTOM OF HANDLE
 12 PZ 3.7592 $ TOP OF HANDLE
C NEXT CYLINDER (STAINLESS STEEL)
 13 CZ 0.4699 $OUTERMOST CYLINDER OF CAPSULE
 14 PZ 5.0013 $TOP OF OUTERMOST CYLINDER
C BOTTOM
 15 PZ 0.0001 $LEAD BRICK FLOOR
C WORLD
 16 SO 20.00
 17 PZ 10.00
C OPTICAL SAMPLES (AL2O3)
```

18 C/X 0.8000 1.27 1.27 \$RADIUS OF SAMPLE, CENTERED ON CENTER OF CAPSULE
 19 PX 0.4700 \$ CORRESPONDS TO OUTER RADIUS OF SOURCE CAPSULE
 20 PX 1.2828 \$RADIUS OF SOURCE CAPSULE + THICKNESS OF SAMPLE - CHANNEL
 27 C/X 0.8000 1.27 0.635 \$RADIUS OF OUTER CHANNEL
 28 C/X 0.8000 1.27 0.2667 \$RADIUS OF INNER CHANNEL
 29 PX 1.5368 \$END OF AL2O3 DISC
 C LEAD BLOCK (LENGTH: 3 TIMES LENGTH OF CAPSULE, 2 TIMES LENGTH OF CAPSULE)
 21 PX 5.00 \$ WIDTH SIDE OF BLOCK
 22 PX -5.00 \$ WIDTH SIDE OF BLOCK
 23 PZ 15.00 \$LENGTH SIDE OF BLOCK
 24 PZ -15.00 \$LENGTH SIDE OF BLOCK
 25 PY -5.00 \$DEPTH BOTTOM OF BLOCK
 26 PY -0.4710 \$DEPTH TOP OF BLOCK

C PLATINUM WITH 10% RHODIUM
 M1 78000. -0.90 45103. -0.10 \$ DENSITY = 19.97
 C AKSTEEL 304L STAINLESS STEEL
 M2 12000. -0.0003 25055. -0.02 15031. -0.00045 16000. -0.00030
 14000. -0.0075 24000. -0.20 28000. -0.12 7014. -0.0010
 26000. -0.65

C CALIFORNIUM OXIDE
 M3 98252. 2 8016. 3 \$ DENSITY = 5.96*10^-7
 M4 7014. -0.754 8016. -0.232 18040. -0.014 \$ AIR
 M5 82000. 1

C AL2O3 (SAPPHIRE)
 M6 13027. 2 8016. 3
 M7 13027. 1
 IMP:N 1 6R 0 1 1 1 1
 MODE N

SDEF CEL= 3 POS= 0 0 0.4573 AXS= 0 0 1 EXT= D2 ERG=D1

SP1 -3 1.025 2.926

SI2 0 2.5401

E0 0 0.1 1.89691

- 2.25
- 2.5
- 2.75
- 2.91838
- 3
- 3.25
- 3.5
- 3.65838
- 3.75
- 3.90943
- 4
- 4.25
- 4.5
- 4.75
- 5
- 5.12255
- 5.45192
- 5.50213
- 5.5181
- 5.58916

5.75
5.9261
6
6.25
6.90467
7
7.07584
7.75
8
8.25
8.5
9
10
11
13
15
16
17
18
20
150
C0 0 1
F1:N 16
F4:N 9
FM4 1 6 103
F14:N 10
FM14 1 6 103
F24:N 11
FM24 1 6 103
F34:N 9
F44:N 10
F54:N 11
F64:N 9
FM64 1 7 103
F74:N 10
FM74 1 7 103
F84:N 11
FM84 1 7 103
C AL(N,ALPHA
F94:N 9
FM94 1 7 107
F104:N 10
FM104 1 7 107
F114:N 11
FM114 1 7 107
NPS 100000000
PRINT

EXAMPLE GATE INPUT MACRO (SiO₂)

```

# Open Visualization
#/vis/open OGLSX
#/vis/viewer/reset
#/vis/viewer/set/viewpointThetaPhi 60 60
#/vis/viewer/zoom 1
#/vis/viewer/set/style surface
#/vis/drawVolume
#/tracking/storeTrajectory 1
#/vis/scene/endOfEventAction accumulate
#/vis/viewer/update
#
# Set database
#
#VERBOSITY

/gate/verbose Physic           0
/gate/verbose Cuts             0
/gate/verbose SD               0
/gate/verbose Actions          0
/gate/verbose Actor            0
/gate/verbose Step             0
/gate/verbose Error            0
/gate/verbose Warning          0
/gate/verbose Output           0
/gate/verbose Beam             0
/gate/verbose Volume           0
/gate/verbose Image            0
/gate/verbose Geometry         0
/gate/verbose Core             0

/run/verbose                    0
/event/verbose                  0
/tracking/verbose              0

#/gate/geometry/setMaterialDatabase ./myGateMaterials.db
/gate/geometry/setMaterialDatabase GateMaterials.db
#
#Create world parameters
#
/gate/world/geometry/setXLength 40. cm
/gate/world/geometry/setYLength 40. cm
/gate/world/geometry/setZLength 40. cm
/gate/world/setMaterial Air
#
#Create scanner system
#
/gate/world/daughters/name scanner
/gate/world/daughters/insert box
/gate/scanner/geometry/setXLength 10. cm
/gate/scanner/geometry/setYLength 10. cm
/gate/scanner/geometry/setZLength 10. cm
/gate/scanner/placement/setTranslation 0 0 0 cm
/gate/scanner/setMaterial Air

# Create a new volume - Foil on top of sample
#
/gate/scanner/daughters/name foilHalo
#
# Give sample a cylinder shape
#
/gate/scanner/daughters/insert cylinder

```



```

#
# Change parameters of cylinder
# Half a millimeter between sample and Al foil
#
/gate/foilHalo/geometry/setRmin 0. cm
/gate/foilHalo/geometry/setRmax 1.27 cm
/gate/foilHalo/geometry/setHeight 0.0016 cm
/gate/foilHalo/geometry/setPhiStart 0 radian
/gate/foilHalo/geometry/setDeltaPhi 360 deg
#
#Move foilHalo into place
#
/gate/foilHalo/placement/setTranslation 0. 0. 1. cm
/gate/foilHalo/placement/setMagOfTranslation 2.7858 cm
#
# Set Material
#
/gate/foilHalo/setMaterial Aluminum
#/gate/foilHalo/vis/setColor red
#/gate/geometry/rebuild
#
# Attach foilHalo to scanner
#
#/gate/foilHalo/attachCrystalSD
/gate/systems/scanner/level1/attach foilHalo

#

# Create a new volume - Air on top of sample
#
/gate/scanner/daughters/name airHalo
#
# Give sample a cylinder shape
#
/gate/scanner/daughters/insert cylinder
#
# Change parameters of cylinder
# Half a millimeter between sample and Al foil
#
/gate/airHalo/geometry/setRmin 0. cm
/gate/airHalo/geometry/setRmax 1.27 cm
/gate/airHalo/geometry/setHeight 0.05 cm
/gate/airHalo/geometry/setPhiStart 0 radian
/gate/airHalo/geometry/setDeltaPhi 360 deg
#
#Move airHalo into place
#
/gate/airHalo/placement/setTranslation 0. 0. 1. cm
/gate/airHalo/placement/setMagOfTranslation 2.760 cm
#
# Set Material
#
/gate/airHalo/setMaterial Air
#/gate/airHalo/vis/setColor red
#/gate/geometry/rebuild
#
# Attach airHalo to scanner
#
#/gate/airHalo/attachCrystalSD
/gate/systems/scanner/level1/attach airHalo

#

# Create a new volume - Quartz sample
#
/gate/scanner/daughters/name quartzGlass

```

```

#
# Give sample a cylinder shape
#
/gate/scanner/daughters/insert cylinder
#
# Change parameters of cylinder
#
/gate/quartzGlass/geometry/setRmin 0 cm
/gate/quartzGlass/geometry/setRmax 1.27 cm
/gate/quartzGlass/geometry/setHeight 0.635 cm
/gate/quartzGlass/geometry/setPhiStart 0 radian
/gate/quartzGlass/geometry/setDeltaPhi 360 deg
#
#Move quartzGlass into place
#
/gate/quartzGlass/placement/setTranslation 0. 0. 1. cm
/gate/quartzGlass/placement/setMagOfTranslation 2.4175 cm
#
# Set Material
#
/gate/quartzGlass/setMaterial Quartz
/gate/quartzGlass/vis/setColor red
#/gate/geometry/rebuild
#
# Attach quartzGlass to scanner
#
#/gate/quartzGlass/attachCrystalSD
/gate/systems/scanner/level1/attach quartzGlass

# Create a new volume - Air surrounding sample
#
/gate/scanner/daughters/name perimeterAir
#
# Give sample a cylinder shape
#
/gate/scanner/daughters/insert cylinder
#
# Change parameters of cylinder
# Half a millimeter between sample and Al foil
#
/gate/perimeterAir/geometry/setRmin 1.27 cm
/gate/perimeterAir/geometry/setRmax 1.32 cm
/gate/perimeterAir/geometry/setHeight 0.735 cm
/gate/perimeterAir/geometry/setPhiStart 0 radian
/gate/perimeterAir/geometry/setDeltaPhi 360 deg
#
#Move perimeterAir into place
#
/gate/perimeterAir/placement/setTranslation 0. 0. 1. cm
/gate/perimeterAir/placement/setMagOfTranslation 2.3675 cm
#
# Set Material
#
/gate/perimeterAir/setMaterial Air
#/gate/perimeterAir/vis/setColor red
#/gate/geometry/rebuild
#
# Attach perimeterAir to scanner
#
#/gate/perimeterAir/attachCrystalSD
/gate/systems/scanner/level1/attach perimeterAir

# Create a new volume - Aluminum foil surrounding sample
#
/gate/scanner/daughters/name perimeterFoil

```

```

#
# Give sample a cylinder shape
#
/gate/scanner/daughters/insert cylinder
#
# Change parameters of cylinder
# Half a millimeter between sample and Al foil
# Al foil is 0.0016 cm thick
#
/gate/perimeterFoil/geometry/setRmin 1.32 cm
/gate/perimeterFoil/geometry/setRmax 1.3216 cm
/gate/perimeterFoil/geometry/setHeight 0.735 cm
/gate/perimeterFoil/geometry/setPhiStart 0 radian
/gate/perimeterFoil/geometry/setDeltaPhi 360 deg
#
#Move perimeterFoil into place
#
/gate/perimeterFoil/placement/setTranslation 0. 0. 1. cm
/gate/perimeterFoil/placement/setMagOfTranslation 2.3675 cm
#
# Set Material
#
/gate/perimeterFoil/setMaterial Aluminum
#/gate/perimeterFoil/vis/setColor red
#/gate/geometry/rebuild
#
# Attach perimeterAir to scanner
#
#/gate/perimeterFoil/attachCrystalSD
/gate/systems/scanner/level1/attach perimeterFoil

# Create a new volume - optical grease
#
/gate/scanner/daughters/name opticalGrease
/gate/scanner/daughters/insert cylinder
#
/gate/opticalGrease/geometry/setRmin 0 cm
/gate/opticalGrease/geometry/setRmax 1.27 cm
/gate/opticalGrease/geometry/setHeight 0.1 cm
/gate/opticalGrease/geometry/setPhiStart 0 radian
/gate/opticalGrease/geometry/setDeltaPhi 360 deg
#
#Move opticalGrease into place
#
/gate/opticalGrease/placement/setTranslation 0. 0. 1. cm
/gate/opticalGrease/placement/setMagOfTranslation 2.05 cm
#
# Set Material
#
/gate/opticalGrease/setMaterial siliconeGel
#/gate/opticalGrease/vis/setColor purple
#/gate/geometry/rebuild
# Attach opticalGrease to scanner
#
/gate/opticalGrease/attachCrystalSD
/gate/systems/scanner/level1/attach opticalGrease
#
# Create a new volume - PMT
#
/gate/scanner/daughters/name PMT
#
# Give PMT a cylinder shape
#

```

```

/gate/scanner/daughters/insert cylinder
#
# Change parameters of cylinder
#
/gate/PMT/geometry/setRmin 0 cm
/gate/PMT/geometry/setRmax 1.27 cm
/gate/PMT/geometry/setHeight 0.3 cm
/gate/PMT/geometry/setPhiStart 0 radian
/gate/PMT/geometry/setDeltaPhi 360 deg

/gate/PMT/placement/setTranslation 0. 0. 1. cm
/gate/PMT/placement/setMagOfTranslation 1.85 cm
#
# Set Material
#
/gate/PMT/setMaterial Borosillicate_Glass
/gate/PMT/vis/setColor yellow
/gate/PMT/vis/setVisible
/gate/PMT/vis/forceSolid
#/gate/geometry/rebuild
#
#Attach PMT to scanner system
#
#/gate/PMT/attachCrystalSD
/gate/systems/scanner/level2/attach PMT
#
#Create a new volume-tubeAirPocket
#
/gate/scanner/daughters/name tubeAirPocket
/gate/scanner/daughters/insert cylinder
/gate/tubeAirPocket/geometry/setRmin 0 cm
/gate/tubeAirPocket/geometry/setRmax 1.27 cm
/gate/tubeAirPocket/geometry/setHeight .01 cm
/gate/tubeAirPocket/geometry/setPhiStart 0 radian
/gate/tubeAirPocket/geometry/setDeltaPhi 360 deg
/gate/tubeAirPocket/placement/setTranslation 0. 0. 1. cm
/gate/tubeAirPocket/placement/setMagOfTranslation 1.695 cm
/gate/tubeAirPocket/setMaterial Vacuum
#
#Attach tubeAirPocket to scanner system
#
#/gate/tubeAirPocket/attachCrystalSD
/gate/systems/scanner/level1/attach tubeAirPocket
#
#
# Create a new volume - photocathode
#
/gate/scanner/daughters/name photocathode
/gate/scanner/daughters/insert cylinder
/gate/photocathode/geometry/setRmin 0 cm
/gate/photocathode/geometry/setRmax 1.27 cm
/gate/photocathode/geometry/setHeight 3.38 cm
/gate/photocathode/geometry/setPhiStart 0 radian
/gate/photocathode/geometry/setDeltaPhi 360 deg
/gate/photocathode/setMaterial Vacuum
/gate/systems/scanner/level1/attach photocathode

#
# Add surfaces
#
/gate/quartzGlass/surfaces/name surfOne
/gate/quartzGlass/surfaces/insert opticalGrease
/gate/quartzGlass/surfaces/surfOne/setSurface smooth
#
/gate/opticalGrease/surfaces/name surfTwo

```

```

/gate/opticalGrease/surfaces/insert quartzGlass
/gate/opticalGrease/surfaces/surfTwo/setSurface smooth
#
/gate/opticalGrease/surfaces/name detectionSurf
/gate/opticalGrease/surfaces/insert PMT
/gate/opticalGrease/surfaces/detectionSurf/setSurface perfect_apd

#/gate/PMT/surfaces/name surfFourteen
#/gate/PMT/surfaces/insert opticalGrease
#/gate/PMT/surfaces/surfFourteen/setSurface smooth

/gate/PMT/surfaces/name surfFifteen
/gate/PMT/surfaces/insert tubeAirPocket
/gate/PMT/surfaces/surfFifteen/setSurface smooth

/gate/tubeAirPocket/surfaces/name surfSixteen
/gate/tubeAirPocket/surfaces/insert PMT
/gate/tubeAirPocket/surfaces/surfSixteen/setSurface smooth

/gate/tubeAirPocket/surfaces/name surfThirteen
/gate/tubeAirPocket/surfaces/insert photocathode
/gate/tubeAirPocket/surfaces/surfThirteen/setSurface smooth

/gate/photocathode/surfaces/name surfSeventeen
/gate/photocathode/surfaces/insert tubeAirPocket
/gate/photocathode/surfaces/surfSeventeen/setSurface smooth

/gate/opticalGrease/surfaces/name surfThree
/gate/opticalGrease/surfaces/insert perimeterAir
/gate/opticalGrease/surfaces/surfThree/setSurface smooth

/gate/perimeterAir/surfaces/name surfFour
/gate/perimeterAir/surfaces/insert opticalGrease
/gate/perimeterAir/surfaces/surfFour/setSurface smooth

/gate/perimeterAir/surfaces/name surfFive
/gate/perimeterAir/surfaces/insert perimeterFoil
/gate/perimeterAir/surfaces/surfFive/setSurface reflective

/gate/perimeterFoil/surfaces/name surfSix
/gate/perimeterFoil/surfaces/insert perimeterAir
/gate/perimeterFoil/surfaces/surfSix/setSurface reflective

/gate/quartzGlass/surfaces/name surfSeven
/gate/quartzGlass/surfaces/insert perimeterAir
/gate/quartzGlass/surfaces/surfSeven/setSurface rough

/gate/perimeterAir/surfaces/name surfEight
/gate/perimeterAir/surfaces/insert quartzGlass
/gate/perimeterAir/surfaces/surfEight/setSurface rough

/gate/quartzGlass/surfaces/name surfNine
/gate/quartzGlass/surfaces/insert airHalo
/gate/quartzGlass/surfaces/surfNine/setSurface smooth

/gate/airHalo/surfaces/name surfTen
/gate/airHalo/surfaces/insert quartzGlass
/gate/airHalo/surfaces/surfTen/setSurface smooth

/gate/airHalo/surfaces/name surfEleven
/gate/airHalo/surfaces/insert foilHalo
/gate/airHalo/surfaces/surfEleven/setSurface reflective

/gate/foilHalo/surfaces/name surfTwelve
/gate/foilHalo/surfaces/insert airHalo

```

```

/gate/foilHalo/surfaces/surfTwelve/setSurface      reflective
#
#
#
# Add Physics Processes
#=====
# Electromagnetic processes
#=====

/gate/physics/addProcess PhotoElectric
/gate/physics/processes/PhotoElectric/setModel StandardModel

/gate/physics/addProcess Compton
/gate/physics/processes/Compton/setModel StandardModel

/gate/physics/addProcess GammaConversion
/gate/physics/processes/GammaConversion/setModel StandardModel

/gate/physics/addProcess ElectronIonisation
/gate/physics/processes/ElectronIonisation/setModel StandardModel e-
/gate/physics/processes/ElectronIonisation/setModel StandardModel e+
/gate/physics/processes/ElectronIonisation/setStepFunction e+ 0.2 0.1 mm
/gate/physics/processes/ElectronIonisation/setStepFunction e- 0.2 0.1 mm

/gate/physics/addProcess Bremsstrahlung
/gate/physics/processes/Bremsstrahlung/setModel StandardModel e-
/gate/physics/processes/Bremsstrahlung/setModel StandardModel e+

/gate/physics/addProcess PositronAnnihilation

#gate/physics/addProcess eMultipleScattering
#/gate/physics/processes/eMultipleScattering/setGeometricalStepLimiterType e- distanceToBoundary
#/gate/physics/processes/eMultipleScattering/setGeometricalStepLimiterType e+ distanceToBoundary

/gate/physics/addProcess HadronIonisation
/gate/physics/removeProcess HadronIonisation deuteron
/gate/physics/removeProcess HadronIonisation triton
/gate/physics/removeProcess HadronIonisation He3
/gate/physics/removeProcess HadronIonisation alpha
/gate/physics/removeProcess HadronIonisation GenericIon
/gate/physics/processes/HadronIonisation/setStepFunction proton 0.2 0.05 mm
/gate/physics/processes/HadronIonisation/setStepFunction pi+ 0.2 0.05 mm
/gate/physics/processes/HadronIonisation/setStepFunction pi- 0.2 0.05 mm

/gate/physics/addProcess IonIonisation
/gate/physics/processes/IonIonisation/setStepFunction GenericIon 0.1 0.02 mm
/gate/physics/processes/IonIonisation/setStepFunction alpha 0.1 0.02 mm
/gate/physics/processes/IonIonisation/setStepFunction deuteron 0.1 0.02 mm
/gate/physics/processes/IonIonisation/setStepFunction triton 0.1 0.02 mm
/gate/physics/processes/IonIonisation/setStepFunction He3 0.1 0.02 mm

#=====
# Hadronic processes
#=====

/gate/physics/addProcess HadronElastic GenericIon
/gate/physics/processes/HadronElastic/setModel G4LElastic GenericIon

/gate/physics/addProcess HadronElastic
/gate/physics/processes/HadronElastic/setModel G4HadronElastic
/gate/physics/processes/HadronElastic/setDataSet G4HadronElasticDataSet

```

```

/gate/physics/addProcess ProtonInelastic
/gate/physics/processes/ProtonInelastic/setModel G4BinaryCascade
/gate/physics/processes/ProtonInelastic/G4BinaryCascade/setEmin 170 MeV
/gate/physics/processes/ProtonInelastic/G4BinaryCascade/setEmax 500 GeV
/gate/physics/processes/ProtonInelastic/setModel PreCompound
/gate/physics/processes/ProtonInelastic/PreCompound/setEmin 0 MeV
/gate/physics/processes/ProtonInelastic/PreCompound/setEmax 170 MeV

/gate/physics/addProcess IonInelastic
/gate/physics/processes/IonInelastic/setModel G4BinaryLightIonReaction
/gate/physics/processes/IonInelastic/setModel G4LEDeuteronInelastic deuteron
/gate/physics/processes/IonInelastic/setModel G4LETritonInelastic triton
/gate/physics/processes/IonInelastic/setModel G4LEAlphaInelastic alpha
/gate/physics/processes/IonInelastic/G4BinaryLightIonReaction/setEmin 80 MeV deuteron
/gate/physics/processes/IonInelastic/G4BinaryLightIonReaction/setEmax 20 GeV deuteron
/gate/physics/processes/IonInelastic/G4BinaryLightIonReaction/setEmin 80 MeV triton
/gate/physics/processes/IonInelastic/G4BinaryLightIonReaction/setEmax 20 GeV triton
/gate/physics/processes/IonInelastic/G4BinaryLightIonReaction/setEmin 80 MeV alpha
/gate/physics/processes/IonInelastic/G4BinaryLightIonReaction/setEmax 20 GeV alpha
/gate/physics/processes/IonInelastic/G4LEDeuteronInelastic/setEmin 0 MeV deuteron
/gate/physics/processes/IonInelastic/G4LEDeuteronInelastic/setEmax 80 MeV deuteron
/gate/physics/processes/IonInelastic/G4LETritonInelastic/setEmin 0 MeV triton
/gate/physics/processes/IonInelastic/G4LETritonInelastic/setEmax 80 MeV triton
/gate/physics/processes/IonInelastic/G4LEAlphaInelastic/setEmin 0 MeV alpha
/gate/physics/processes/IonInelastic/G4LEAlphaInelastic/setEmax 80 MeV alpha
/gate/physics/processes/IonInelastic/setDataSet G4IonsShenCrossSection GenericIon
/gate/physics/processes/IonInelastic/setDataSet G4TripathiLightCrossSection deuteron
/gate/physics/processes/IonInelastic/setDataSet G4TripathiLightCrossSection triton
/gate/physics/processes/IonInelastic/setDataSet G4TripathiLightCrossSection alpha

/gate/physics/addProcess PionPlusInelastic
/gate/physics/processes/PionPlusInelastic/setModel G4LEPionPlusInelastic

/gate/physics/addProcess PionMinusInelastic
/gate/physics/processes/PionMinusInelastic/setModel G4LEPionMinusInelastic

/gate/physics/addProcess NeutronCapture
/gate/physics/processes/NeutronCapture/setModel G4LCapture
/gate/physics/addProcess Fission
/gate/physics/processes/Fission/setModel G4LFission
/gate/physics/addProcess NeutronInelastic
/gate/physics/processes/NeutronInelastic/setModel PreCompound

#/gate/physics/addProcess Decay

/gate/physics/addProcess Cerenkov

#=====  

# Options  

#=====

/gate/physics/addProcess RayleighScattering
/gate/physics/processes/RayleighScattering/setModel PenelopeModel
/gate/physics/addProcess MultipleScattering e-
/gate/physics/addProcess MultipleScattering e+

#/gate/physics/addProcess hMultipleScattering alpha
#/gate/physics/addProcess IonIonisation alpha
#/gate/physics/processes/IonIonisation/setStepFunction alpha 0.1 0.02 mm
#/gate/physics/addProcess Scintillation alpha
#/gate/physics/addProcess Scintillation e-
/gate/physics/addProcess OpticalRayleigh
/gate/physics/addProcess OpticalAbsorption
/gate/physics/addProcess OpticalBoundary

```

```

/gate/physics/processList
/gate/physics/processList

/gate/physics/setEMin 0.1 keV
/gate/physics/setEMax 10 GeV
/gate/physics/setDEDXBinning 220
/gate/physics/setLambdaBinning 220

/gate/run/initialize

# Print Physics List
#
#/gate/physics/print physicsProcesses.txt
#
# source:
# Add source (Al-28 from Si-28(n, p)Al-28 reaction)
#
/gate/source/addSource Al28
/gate/source/Al28/gps/particle e-
/gate/source/Al28/setActivity 10 becquerel
/gate/source/Al28/gps/energytype User

# Beta spectrum from Al-28 from NRC's Radiological Toolbox
#
/gate/source/Al28/gps/histname energy
/gate/source/Al28/gps/emin 0.0 MeV
/gate/source/Al28/gps/emax 2.864 MeV

/gate/source/Al28/gps/histpoint      0      74.1
/gate/source/Al28/gps/histpoint      0.003  74.8
/gate/source/Al28/gps/histpoint      0.006  76.4
/gate/source/Al28/gps/histpoint      0.009  78.6
/gate/source/Al28/gps/histpoint      0.012  81.1
/gate/source/Al28/gps/histpoint      0.015  83.6
/gate/source/Al28/gps/histpoint      0.018  86.1
/gate/source/Al28/gps/histpoint      0.021  88.6
/gate/source/Al28/gps/histpoint      0.024  91.1
/gate/source/Al28/gps/histpoint      0.027  93.5
/gate/source/Al28/gps/histpoint      0.03   95.9
/gate/source/Al28/gps/histpoint      0.033  98.3
/gate/source/Al28/gps/histpoint      0.036  101
/gate/source/Al28/gps/histpoint      0.039  103
/gate/source/Al28/gps/histpoint      0.042  105
/gate/source/Al28/gps/histpoint      0.045  108
/gate/source/Al28/gps/histpoint      0.048  110
/gate/source/Al28/gps/histpoint      0.051  112
/gate/source/Al28/gps/histpoint      0.054  114
/gate/source/Al28/gps/histpoint      0.057  116
/gate/source/Al28/gps/histpoint      0.06   119
/gate/source/Al28/gps/histpoint      0.063  121
/gate/source/Al28/gps/histpoint      0.066  123
/gate/source/Al28/gps/histpoint      0.069  125
/gate/source/Al28/gps/histpoint      0.072  127
/gate/source/Al28/gps/histpoint      0.075  129
/gate/source/Al28/gps/histpoint      0.078  131
/gate/source/Al28/gps/histpoint      0.081  134
/gate/source/Al28/gps/histpoint      0.084  136
/gate/source/Al28/gps/histpoint      0.087  138
/gate/source/Al28/gps/histpoint      0.09   140
/gate/source/Al28/gps/histpoint      0.093  142
/gate/source/Al28/gps/histpoint      0.096  144
/gate/source/Al28/gps/histpoint      0.099  146
/gate/source/Al28/gps/histpoint      0.102  148
/gate/source/Al28/gps/histpoint      0.105  150

```

Enabled
Initialized

/gate/source/AI28/gps/histpoint	0.108	152
/gate/source/AI28/gps/histpoint	0.111	154
/gate/source/AI28/gps/histpoint	0.114	156
/gate/source/AI28/gps/histpoint	0.117	158
/gate/source/AI28/gps/histpoint	0.12	160
/gate/source/AI28/gps/histpoint	0.123	162
/gate/source/AI28/gps/histpoint	0.126	164
/gate/source/AI28/gps/histpoint	0.129	166
/gate/source/AI28/gps/histpoint	0.132	168
/gate/source/AI28/gps/histpoint	0.135	170
/gate/source/AI28/gps/histpoint	0.138	172
/gate/source/AI28/gps/histpoint	0.141	174
/gate/source/AI28/gps/histpoint	0.144	176
/gate/source/AI28/gps/histpoint	0.147	178
/gate/source/AI28/gps/histpoint	0.15	180
/gate/source/AI28/gps/histpoint	0.153	182
/gate/source/AI28/gps/histpoint	0.156	184
/gate/source/AI28/gps/histpoint	0.159	186
/gate/source/AI28/gps/histpoint	0.162	187
/gate/source/AI28/gps/histpoint	0.165	189
/gate/source/AI28/gps/histpoint	0.168	191
/gate/source/AI28/gps/histpoint	0.171	193
/gate/source/AI28/gps/histpoint	0.174	195
/gate/source/AI28/gps/histpoint	0.177	197
/gate/source/AI28/gps/histpoint	0.18	199
/gate/source/AI28/gps/histpoint	0.183	201
/gate/source/AI28/gps/histpoint	0.186	203
/gate/source/AI28/gps/histpoint	0.189	205
/gate/source/AI28/gps/histpoint	0.192	207
/gate/source/AI28/gps/histpoint	0.195	209
/gate/source/AI28/gps/histpoint	0.198	211
/gate/source/AI28/gps/histpoint	0.201	212
/gate/source/AI28/gps/histpoint	0.204	214
/gate/source/AI28/gps/histpoint	0.207	216
/gate/source/AI28/gps/histpoint	0.21	218
/gate/source/AI28/gps/histpoint	0.213	220
/gate/source/AI28/gps/histpoint	0.216	222
/gate/source/AI28/gps/histpoint	0.219	224
/gate/source/AI28/gps/histpoint	0.222	226
/gate/source/AI28/gps/histpoint	0.225	228
/gate/source/AI28/gps/histpoint	0.228	229
/gate/source/AI28/gps/histpoint	0.231	231
/gate/source/AI28/gps/histpoint	0.234	233
/gate/source/AI28/gps/histpoint	0.237	235
/gate/source/AI28/gps/histpoint	0.24	237
/gate/source/AI28/gps/histpoint	0.243	239
/gate/source/AI28/gps/histpoint	0.246	241
/gate/source/AI28/gps/histpoint	0.249	242
/gate/source/AI28/gps/histpoint	0.252	244
/gate/source/AI28/gps/histpoint	0.255	246
/gate/source/AI28/gps/histpoint	0.258	248
/gate/source/AI28/gps/histpoint	0.261	250
/gate/source/AI28/gps/histpoint	0.264	252
/gate/source/AI28/gps/histpoint	0.267	254
/gate/source/AI28/gps/histpoint	0.27	255
/gate/source/AI28/gps/histpoint	0.273	257
/gate/source/AI28/gps/histpoint	0.276	259
/gate/source/AI28/gps/histpoint	0.279	261
/gate/source/AI28/gps/histpoint	0.282	263
/gate/source/AI28/gps/histpoint	0.285	265
/gate/source/AI28/gps/histpoint	0.288	266
/gate/source/AI28/gps/histpoint	0.291	268
/gate/source/AI28/gps/histpoint	0.294	270
/gate/source/AI28/gps/histpoint	0.297	272
/gate/source/AI28/gps/histpoint	0.3	274

/gate/source/A128/gps/histpoint	0.303	275
/gate/source/A128/gps/histpoint	0.306	277
/gate/source/A128/gps/histpoint	0.309	279
/gate/source/A128/gps/histpoint	0.312	281
/gate/source/A128/gps/histpoint	0.315	283
/gate/source/A128/gps/histpoint	0.318	285
/gate/source/A128/gps/histpoint	0.321	286
/gate/source/A128/gps/histpoint	0.324	288
/gate/source/A128/gps/histpoint	0.327	290
/gate/source/A128/gps/histpoint	0.33	292
/gate/source/A128/gps/histpoint	0.333	293
/gate/source/A128/gps/histpoint	0.336	295
/gate/source/A128/gps/histpoint	0.339	297
/gate/source/A128/gps/histpoint	0.342	299
/gate/source/A128/gps/histpoint	0.345	301
/gate/source/A128/gps/histpoint	0.348	302
/gate/source/A128/gps/histpoint	0.351	304
/gate/source/A128/gps/histpoint	0.354	306
/gate/source/A128/gps/histpoint	0.357	308
/gate/source/A128/gps/histpoint	0.36	309
/gate/source/A128/gps/histpoint	0.363	311
/gate/source/A128/gps/histpoint	0.366	313
/gate/source/A128/gps/histpoint	0.369	315
/gate/source/A128/gps/histpoint	0.372	316
/gate/source/A128/gps/histpoint	0.375	318
/gate/source/A128/gps/histpoint	0.378	320
/gate/source/A128/gps/histpoint	0.381	322
/gate/source/A128/gps/histpoint	0.384	323
/gate/source/A128/gps/histpoint	0.387	325
/gate/source/A128/gps/histpoint	0.39	327
/gate/source/A128/gps/histpoint	0.393	328
/gate/source/A128/gps/histpoint	0.396	330
/gate/source/A128/gps/histpoint	0.399	332
/gate/source/A128/gps/histpoint	0.402	334
/gate/source/A128/gps/histpoint	0.405	335
/gate/source/A128/gps/histpoint	0.408	337
/gate/source/A128/gps/histpoint	0.411	339
/gate/source/A128/gps/histpoint	0.414	340
/gate/source/A128/gps/histpoint	0.417	342
/gate/source/A128/gps/histpoint	0.42	344
/gate/source/A128/gps/histpoint	0.423	345
/gate/source/A128/gps/histpoint	0.426	347
/gate/source/A128/gps/histpoint	0.429	349
/gate/source/A128/gps/histpoint	0.432	350
/gate/source/A128/gps/histpoint	0.435	352
/gate/source/A128/gps/histpoint	0.438	354
/gate/source/A128/gps/histpoint	0.441	355
/gate/source/A128/gps/histpoint	0.444	357
/gate/source/A128/gps/histpoint	0.447	359
/gate/source/A128/gps/histpoint	0.45	360
/gate/source/A128/gps/histpoint	0.453	362
/gate/source/A128/gps/histpoint	0.456	364
/gate/source/A128/gps/histpoint	0.459	365
/gate/source/A128/gps/histpoint	0.462	367
/gate/source/A128/gps/histpoint	0.465	369
/gate/source/A128/gps/histpoint	0.468	370
/gate/source/A128/gps/histpoint	0.471	372
/gate/source/A128/gps/histpoint	0.474	373
/gate/source/A128/gps/histpoint	0.477	375
/gate/source/A128/gps/histpoint	0.48	377
/gate/source/A128/gps/histpoint	0.483	378
/gate/source/A128/gps/histpoint	0.486	380
/gate/source/A128/gps/histpoint	0.489	381
/gate/source/A128/gps/histpoint	0.492	383
/gate/source/A128/gps/histpoint	0.495	385

/gate/source/A128/gps/histpoint	0.498	386
/gate/source/A128/gps/histpoint	0.501	388
/gate/source/A128/gps/histpoint	0.504	389
/gate/source/A128/gps/histpoint	0.507	391
/gate/source/A128/gps/histpoint	0.51	392
/gate/source/A128/gps/histpoint	0.513	394
/gate/source/A128/gps/histpoint	0.516	396
/gate/source/A128/gps/histpoint	0.519	397
/gate/source/A128/gps/histpoint	0.522	399
/gate/source/A128/gps/histpoint	0.525	400
/gate/source/A128/gps/histpoint	0.528	402
/gate/source/A128/gps/histpoint	0.531	403
/gate/source/A128/gps/histpoint	0.534	405
/gate/source/A128/gps/histpoint	0.537	406
/gate/source/A128/gps/histpoint	0.54	408
/gate/source/A128/gps/histpoint	0.543	409
/gate/source/A128/gps/histpoint	0.546	411
/gate/source/A128/gps/histpoint	0.549	412
/gate/source/A128/gps/histpoint	0.552	414
/gate/source/A128/gps/histpoint	0.555	415
/gate/source/A128/gps/histpoint	0.558	417
/gate/source/A128/gps/histpoint	0.561	418
/gate/source/A128/gps/histpoint	0.564	420
/gate/source/A128/gps/histpoint	0.567	421
/gate/source/A128/gps/histpoint	0.57	423
/gate/source/A128/gps/histpoint	0.573	424
/gate/source/A128/gps/histpoint	0.576	426
/gate/source/A128/gps/histpoint	0.579	427
/gate/source/A128/gps/histpoint	0.582	429
/gate/source/A128/gps/histpoint	0.585	430
/gate/source/A128/gps/histpoint	0.588	431
/gate/source/A128/gps/histpoint	0.591	433
/gate/source/A128/gps/histpoint	0.594	434
/gate/source/A128/gps/histpoint	0.597	436
/gate/source/A128/gps/histpoint	0.6	437
/gate/source/A128/gps/histpoint	0.603	438
/gate/source/A128/gps/histpoint	0.606	440
/gate/source/A128/gps/histpoint	0.609	441
/gate/source/A128/gps/histpoint	0.612	443
/gate/source/A128/gps/histpoint	0.615	444
/gate/source/A128/gps/histpoint	0.618	445
/gate/source/A128/gps/histpoint	0.621	447
/gate/source/A128/gps/histpoint	0.624	448
/gate/source/A128/gps/histpoint	0.627	450
/gate/source/A128/gps/histpoint	0.63	451
/gate/source/A128/gps/histpoint	0.633	452
/gate/source/A128/gps/histpoint	0.636	454
/gate/source/A128/gps/histpoint	0.639	455
/gate/source/A128/gps/histpoint	0.642	456
/gate/source/A128/gps/histpoint	0.645	458
/gate/source/A128/gps/histpoint	0.648	459
/gate/source/A128/gps/histpoint	0.651	460
/gate/source/A128/gps/histpoint	0.654	462
/gate/source/A128/gps/histpoint	0.657	463
/gate/source/A128/gps/histpoint	0.66	464
/gate/source/A128/gps/histpoint	0.663	465
/gate/source/A128/gps/histpoint	0.666	467
/gate/source/A128/gps/histpoint	0.669	468
/gate/source/A128/gps/histpoint	0.672	469
/gate/source/A128/gps/histpoint	0.675	471
/gate/source/A128/gps/histpoint	0.678	472
/gate/source/A128/gps/histpoint	0.681	473
/gate/source/A128/gps/histpoint	0.684	474
/gate/source/A128/gps/histpoint	0.687	476
/gate/source/A128/gps/histpoint	0.69	477

/gate/source/A128/gps/histpoint	0.693	478
/gate/source/A128/gps/histpoint	0.696	479
/gate/source/A128/gps/histpoint	0.699	480
/gate/source/A128/gps/histpoint	0.702	482
/gate/source/A128/gps/histpoint	0.705	483
/gate/source/A128/gps/histpoint	0.708	484
/gate/source/A128/gps/histpoint	0.711	485
/gate/source/A128/gps/histpoint	0.714	486
/gate/source/A128/gps/histpoint	0.717	488
/gate/source/A128/gps/histpoint	0.72	489
/gate/source/A128/gps/histpoint	0.723	490
/gate/source/A128/gps/histpoint	0.726	491
/gate/source/A128/gps/histpoint	0.729	492
/gate/source/A128/gps/histpoint	0.732	494
/gate/source/A128/gps/histpoint	0.735	495
/gate/source/A128/gps/histpoint	0.738	496
/gate/source/A128/gps/histpoint	0.741	497
/gate/source/A128/gps/histpoint	0.744	498
/gate/source/A128/gps/histpoint	0.747	499
/gate/source/A128/gps/histpoint	0.75	500
/gate/source/A128/gps/histpoint	0.753	501
/gate/source/A128/gps/histpoint	0.756	502
/gate/source/A128/gps/histpoint	0.759	504
/gate/source/A128/gps/histpoint	0.762	505
/gate/source/A128/gps/histpoint	0.765	506
/gate/source/A128/gps/histpoint	0.768	507
/gate/source/A128/gps/histpoint	0.771	508
/gate/source/A128/gps/histpoint	0.774	509
/gate/source/A128/gps/histpoint	0.777	510
/gate/source/A128/gps/histpoint	0.78	511
/gate/source/A128/gps/histpoint	0.783	512
/gate/source/A128/gps/histpoint	0.786	513
/gate/source/A128/gps/histpoint	0.789	514
/gate/source/A128/gps/histpoint	0.792	515
/gate/source/A128/gps/histpoint	0.795	516
/gate/source/A128/gps/histpoint	0.798	517
/gate/source/A128/gps/histpoint	0.801	518
/gate/source/A128/gps/histpoint	0.804	519
/gate/source/A128/gps/histpoint	0.807	520
/gate/source/A128/gps/histpoint	0.81	521
/gate/source/A128/gps/histpoint	0.813	522
/gate/source/A128/gps/histpoint	0.816	523
/gate/source/A128/gps/histpoint	0.819	524
/gate/source/A128/gps/histpoint	0.822	525
/gate/source/A128/gps/histpoint	0.825	526
/gate/source/A128/gps/histpoint	0.828	527
/gate/source/A128/gps/histpoint	0.831	528
/gate/source/A128/gps/histpoint	0.834	529
/gate/source/A128/gps/histpoint	0.837	530
/gate/source/A128/gps/histpoint	0.84	531
/gate/source/A128/gps/histpoint	0.843	531
/gate/source/A128/gps/histpoint	0.846	532
/gate/source/A128/gps/histpoint	0.849	533
/gate/source/A128/gps/histpoint	0.852	534
/gate/source/A128/gps/histpoint	0.855	535
/gate/source/A128/gps/histpoint	0.858	536
/gate/source/A128/gps/histpoint	0.861	537
/gate/source/A128/gps/histpoint	0.864	538
/gate/source/A128/gps/histpoint	0.867	538
/gate/source/A128/gps/histpoint	0.87	539
/gate/source/A128/gps/histpoint	0.873	540
/gate/source/A128/gps/histpoint	0.876	541
/gate/source/A128/gps/histpoint	0.879	542
/gate/source/A128/gps/histpoint	0.882	543
/gate/source/A128/gps/histpoint	0.885	543

/gate/source/A128/gps/histpoint	0.888	544
/gate/source/A128/gps/histpoint	0.891	545
/gate/source/A128/gps/histpoint	0.894	546
/gate/source/A128/gps/histpoint	0.897	547
/gate/source/A128/gps/histpoint	0.9	547
/gate/source/A128/gps/histpoint	0.903	548
/gate/source/A128/gps/histpoint	0.906	549
/gate/source/A128/gps/histpoint	0.909	550
/gate/source/A128/gps/histpoint	0.912	550
/gate/source/A128/gps/histpoint	0.915	551
/gate/source/A128/gps/histpoint	0.918	552
/gate/source/A128/gps/histpoint	0.921	552
/gate/source/A128/gps/histpoint	0.924	553
/gate/source/A128/gps/histpoint	0.927	554
/gate/source/A128/gps/histpoint	0.93	555
/gate/source/A128/gps/histpoint	0.933	555
/gate/source/A128/gps/histpoint	0.936	556
/gate/source/A128/gps/histpoint	0.939	557
/gate/source/A128/gps/histpoint	0.942	557
/gate/source/A128/gps/histpoint	0.945	558
/gate/source/A128/gps/histpoint	0.948	559
/gate/source/A128/gps/histpoint	0.951	559
/gate/source/A128/gps/histpoint	0.954	560
/gate/source/A128/gps/histpoint	0.957	561
/gate/source/A128/gps/histpoint	0.96	561
/gate/source/A128/gps/histpoint	0.963	562
/gate/source/A128/gps/histpoint	0.966	562
/gate/source/A128/gps/histpoint	0.969	563
/gate/source/A128/gps/histpoint	0.972	564
/gate/source/A128/gps/histpoint	0.975	564
/gate/source/A128/gps/histpoint	0.978	565
/gate/source/A128/gps/histpoint	0.981	565
/gate/source/A128/gps/histpoint	0.984	566
/gate/source/A128/gps/histpoint	0.987	566
/gate/source/A128/gps/histpoint	0.99	567
/gate/source/A128/gps/histpoint	0.993	567
/gate/source/A128/gps/histpoint	0.996	568
/gate/source/A128/gps/histpoint	0.999	569
/gate/source/A128/gps/histpoint	1.002	569
/gate/source/A128/gps/histpoint	1.005	570
/gate/source/A128/gps/histpoint	1.008	570
/gate/source/A128/gps/histpoint	1.011	571
/gate/source/A128/gps/histpoint	1.014	571
/gate/source/A128/gps/histpoint	1.017	571
/gate/source/A128/gps/histpoint	1.02	572
/gate/source/A128/gps/histpoint	1.023	572
/gate/source/A128/gps/histpoint	1.026	573
/gate/source/A128/gps/histpoint	1.029	573
/gate/source/A128/gps/histpoint	1.032	574
/gate/source/A128/gps/histpoint	1.035	574
/gate/source/A128/gps/histpoint	1.038	575
/gate/source/A128/gps/histpoint	1.041	575
/gate/source/A128/gps/histpoint	1.044	575
/gate/source/A128/gps/histpoint	1.047	576
/gate/source/A128/gps/histpoint	1.05	576
/gate/source/A128/gps/histpoint	1.053	577
/gate/source/A128/gps/histpoint	1.056	577
/gate/source/A128/gps/histpoint	1.059	577
/gate/source/A128/gps/histpoint	1.062	578
/gate/source/A128/gps/histpoint	1.065	578
/gate/source/A128/gps/histpoint	1.068	578
/gate/source/A128/gps/histpoint	1.071	579
/gate/source/A128/gps/histpoint	1.074	579
/gate/source/A128/gps/histpoint	1.077	579
/gate/source/A128/gps/histpoint	1.08	580

/gate/source/A128/gps/histpoint	1.278	583
/gate/source/A128/gps/histpoint	1.281	583
/gate/source/A128/gps/histpoint	1.284	583
/gate/source/A128/gps/histpoint	1.287	583
/gate/source/A128/gps/histpoint	1.29	582
/gate/source/A128/gps/histpoint	1.293	582
/gate/source/A128/gps/histpoint	1.296	582
/gate/source/A128/gps/histpoint	1.299	582
/gate/source/A128/gps/histpoint	1.302	581
/gate/source/A128/gps/histpoint	1.305	581
/gate/source/A128/gps/histpoint	1.308	581
/gate/source/A128/gps/histpoint	1.311	581
/gate/source/A128/gps/histpoint	1.314	580
/gate/source/A128/gps/histpoint	1.317	580
/gate/source/A128/gps/histpoint	1.32	580
/gate/source/A128/gps/histpoint	1.323	579
/gate/source/A128/gps/histpoint	1.326	579
/gate/source/A128/gps/histpoint	1.329	579
/gate/source/A128/gps/histpoint	1.332	578
/gate/source/A128/gps/histpoint	1.335	578
/gate/source/A128/gps/histpoint	1.338	578
/gate/source/A128/gps/histpoint	1.341	577
/gate/source/A128/gps/histpoint	1.344	577
/gate/source/A128/gps/histpoint	1.347	577
/gate/source/A128/gps/histpoint	1.35	576
/gate/source/A128/gps/histpoint	1.353	576
/gate/source/A128/gps/histpoint	1.356	575
/gate/source/A128/gps/histpoint	1.359	575
/gate/source/A128/gps/histpoint	1.362	575
/gate/source/A128/gps/histpoint	1.365	574
/gate/source/A128/gps/histpoint	1.368	574
/gate/source/A128/gps/histpoint	1.371	573
/gate/source/A128/gps/histpoint	1.374	573
/gate/source/A128/gps/histpoint	1.377	572
/gate/source/A128/gps/histpoint	1.38	572
/gate/source/A128/gps/histpoint	1.383	571
/gate/source/A128/gps/histpoint	1.386	571
/gate/source/A128/gps/histpoint	1.389	571
/gate/source/A128/gps/histpoint	1.392	570
/gate/source/A128/gps/histpoint	1.395	570
/gate/source/A128/gps/histpoint	1.398	569
/gate/source/A128/gps/histpoint	1.401	569
/gate/source/A128/gps/histpoint	1.404	568
/gate/source/A128/gps/histpoint	1.407	568
/gate/source/A128/gps/histpoint	1.41	567
/gate/source/A128/gps/histpoint	1.413	566
/gate/source/A128/gps/histpoint	1.416	566
/gate/source/A128/gps/histpoint	1.419	565
/gate/source/A128/gps/histpoint	1.422	565
/gate/source/A128/gps/histpoint	1.425	564
/gate/source/A128/gps/histpoint	1.428	564
/gate/source/A128/gps/histpoint	1.431	563
/gate/source/A128/gps/histpoint	1.434	562
/gate/source/A128/gps/histpoint	1.437	562
/gate/source/A128/gps/histpoint	1.44	561
/gate/source/A128/gps/histpoint	1.443	561
/gate/source/A128/gps/histpoint	1.446	560
/gate/source/A128/gps/histpoint	1.449	559
/gate/source/A128/gps/histpoint	1.452	559
/gate/source/A128/gps/histpoint	1.455	558
/gate/source/A128/gps/histpoint	1.458	557
/gate/source/A128/gps/histpoint	1.461	557
/gate/source/A128/gps/histpoint	1.464	556
/gate/source/A128/gps/histpoint	1.467	556
/gate/source/A128/gps/histpoint	1.47	555

/gate/source/A128/gps/histpoint	1.473	554
/gate/source/A128/gps/histpoint	1.476	553
/gate/source/A128/gps/histpoint	1.479	553
/gate/source/A128/gps/histpoint	1.482	552
/gate/source/A128/gps/histpoint	1.485	551
/gate/source/A128/gps/histpoint	1.488	551
/gate/source/A128/gps/histpoint	1.491	550
/gate/source/A128/gps/histpoint	1.494	549
/gate/source/A128/gps/histpoint	1.497	548
/gate/source/A128/gps/histpoint	1.5	548
/gate/source/A128/gps/histpoint	1.503	547
/gate/source/A128/gps/histpoint	1.506	546
/gate/source/A128/gps/histpoint	1.509	545
/gate/source/A128/gps/histpoint	1.512	545
/gate/source/A128/gps/histpoint	1.515	544
/gate/source/A128/gps/histpoint	1.518	543
/gate/source/A128/gps/histpoint	1.521	542
/gate/source/A128/gps/histpoint	1.524	541
/gate/source/A128/gps/histpoint	1.527	541
/gate/source/A128/gps/histpoint	1.53	540
/gate/source/A128/gps/histpoint	1.533	539
/gate/source/A128/gps/histpoint	1.536	538
/gate/source/A128/gps/histpoint	1.539	537
/gate/source/A128/gps/histpoint	1.542	537
/gate/source/A128/gps/histpoint	1.545	536
/gate/source/A128/gps/histpoint	1.548	535
/gate/source/A128/gps/histpoint	1.551	534
/gate/source/A128/gps/histpoint	1.554	533
/gate/source/A128/gps/histpoint	1.557	532
/gate/source/A128/gps/histpoint	1.56	531
/gate/source/A128/gps/histpoint	1.563	530
/gate/source/A128/gps/histpoint	1.566	530
/gate/source/A128/gps/histpoint	1.569	529
/gate/source/A128/gps/histpoint	1.572	528
/gate/source/A128/gps/histpoint	1.575	527
/gate/source/A128/gps/histpoint	1.578	526
/gate/source/A128/gps/histpoint	1.581	525
/gate/source/A128/gps/histpoint	1.584	524
/gate/source/A128/gps/histpoint	1.587	523
/gate/source/A128/gps/histpoint	1.59	522
/gate/source/A128/gps/histpoint	1.593	521
/gate/source/A128/gps/histpoint	1.596	520
/gate/source/A128/gps/histpoint	1.599	519
/gate/source/A128/gps/histpoint	1.602	518
/gate/source/A128/gps/histpoint	1.605	517
/gate/source/A128/gps/histpoint	1.608	516
/gate/source/A128/gps/histpoint	1.611	515
/gate/source/A128/gps/histpoint	1.614	514
/gate/source/A128/gps/histpoint	1.617	513
/gate/source/A128/gps/histpoint	1.62	512
/gate/source/A128/gps/histpoint	1.623	511
/gate/source/A128/gps/histpoint	1.626	510
/gate/source/A128/gps/histpoint	1.629	509
/gate/source/A128/gps/histpoint	1.632	508
/gate/source/A128/gps/histpoint	1.635	507
/gate/source/A128/gps/histpoint	1.638	506
/gate/source/A128/gps/histpoint	1.641	505
/gate/source/A128/gps/histpoint	1.644	504
/gate/source/A128/gps/histpoint	1.647	503
/gate/source/A128/gps/histpoint	1.65	502
/gate/source/A128/gps/histpoint	1.653	501
/gate/source/A128/gps/histpoint	1.656	500
/gate/source/A128/gps/histpoint	1.659	499
/gate/source/A128/gps/histpoint	1.662	498
/gate/source/A128/gps/histpoint	1.665	497

/gate/source/A128/gps/histpoint	1.668	495
/gate/source/A128/gps/histpoint	1.671	494
/gate/source/A128/gps/histpoint	1.674	493
/gate/source/A128/gps/histpoint	1.677	492
/gate/source/A128/gps/histpoint	1.68	491
/gate/source/A128/gps/histpoint	1.683	490
/gate/source/A128/gps/histpoint	1.686	489
/gate/source/A128/gps/histpoint	1.689	488
/gate/source/A128/gps/histpoint	1.692	486
/gate/source/A128/gps/histpoint	1.695	485
/gate/source/A128/gps/histpoint	1.698	484
/gate/source/A128/gps/histpoint	1.701	483
/gate/source/A128/gps/histpoint	1.704	482
/gate/source/A128/gps/histpoint	1.707	481
/gate/source/A128/gps/histpoint	1.71	479
/gate/source/A128/gps/histpoint	1.713	478
/gate/source/A128/gps/histpoint	1.716	477
/gate/source/A128/gps/histpoint	1.719	476
/gate/source/A128/gps/histpoint	1.722	475
/gate/source/A128/gps/histpoint	1.725	473
/gate/source/A128/gps/histpoint	1.728	472
/gate/source/A128/gps/histpoint	1.731	471
/gate/source/A128/gps/histpoint	1.734	470
/gate/source/A128/gps/histpoint	1.737	469
/gate/source/A128/gps/histpoint	1.74	467
/gate/source/A128/gps/histpoint	1.743	466
/gate/source/A128/gps/histpoint	1.746	465
/gate/source/A128/gps/histpoint	1.749	464
/gate/source/A128/gps/histpoint	1.752	462
/gate/source/A128/gps/histpoint	1.755	461
/gate/source/A128/gps/histpoint	1.758	460
/gate/source/A128/gps/histpoint	1.761	459
/gate/source/A128/gps/histpoint	1.764	457
/gate/source/A128/gps/histpoint	1.767	456
/gate/source/A128/gps/histpoint	1.77	455
/gate/source/A128/gps/histpoint	1.773	453
/gate/source/A128/gps/histpoint	1.776	452
/gate/source/A128/gps/histpoint	1.779	451
/gate/source/A128/gps/histpoint	1.782	450
/gate/source/A128/gps/histpoint	1.785	448
/gate/source/A128/gps/histpoint	1.788	447
/gate/source/A128/gps/histpoint	1.791	446
/gate/source/A128/gps/histpoint	1.794	444
/gate/source/A128/gps/histpoint	1.797	443
/gate/source/A128/gps/histpoint	1.8	442
/gate/source/A128/gps/histpoint	1.803	440
/gate/source/A128/gps/histpoint	1.806	439
/gate/source/A128/gps/histpoint	1.809	438
/gate/source/A128/gps/histpoint	1.812	436
/gate/source/A128/gps/histpoint	1.815	435
/gate/source/A128/gps/histpoint	1.818	434
/gate/source/A128/gps/histpoint	1.821	432
/gate/source/A128/gps/histpoint	1.824	431
/gate/source/A128/gps/histpoint	1.827	429
/gate/source/A128/gps/histpoint	1.83	428
/gate/source/A128/gps/histpoint	1.833	427
/gate/source/A128/gps/histpoint	1.836	425
/gate/source/A128/gps/histpoint	1.839	424
/gate/source/A128/gps/histpoint	1.842	423
/gate/source/A128/gps/histpoint	1.845	421
/gate/source/A128/gps/histpoint	1.848	420
/gate/source/A128/gps/histpoint	1.851	418
/gate/source/A128/gps/histpoint	1.854	417
/gate/source/A128/gps/histpoint	1.857	415
/gate/source/A128/gps/histpoint	1.86	414

/gate/source/A128/gps/histpoint	1.863	413
/gate/source/A128/gps/histpoint	1.866	411
/gate/source/A128/gps/histpoint	1.869	410
/gate/source/A128/gps/histpoint	1.872	408
/gate/source/A128/gps/histpoint	1.875	407
/gate/source/A128/gps/histpoint	1.878	405
/gate/source/A128/gps/histpoint	1.881	404
/gate/source/A128/gps/histpoint	1.884	403
/gate/source/A128/gps/histpoint	1.887	401
/gate/source/A128/gps/histpoint	1.89	400
/gate/source/A128/gps/histpoint	1.893	398
/gate/source/A128/gps/histpoint	1.896	397
/gate/source/A128/gps/histpoint	1.899	395
/gate/source/A128/gps/histpoint	1.902	394
/gate/source/A128/gps/histpoint	1.905	392
/gate/source/A128/gps/histpoint	1.908	391
/gate/source/A128/gps/histpoint	1.911	389
/gate/source/A128/gps/histpoint	1.914	388
/gate/source/A128/gps/histpoint	1.917	386
/gate/source/A128/gps/histpoint	1.92	385
/gate/source/A128/gps/histpoint	1.923	383
/gate/source/A128/gps/histpoint	1.926	382
/gate/source/A128/gps/histpoint	1.929	380
/gate/source/A128/gps/histpoint	1.932	379
/gate/source/A128/gps/histpoint	1.935	377
/gate/source/A128/gps/histpoint	1.938	376
/gate/source/A128/gps/histpoint	1.941	374
/gate/source/A128/gps/histpoint	1.944	373
/gate/source/A128/gps/histpoint	1.947	371
/gate/source/A128/gps/histpoint	1.95	370
/gate/source/A128/gps/histpoint	1.953	368
/gate/source/A128/gps/histpoint	1.956	367
/gate/source/A128/gps/histpoint	1.959	365
/gate/source/A128/gps/histpoint	1.962	364
/gate/source/A128/gps/histpoint	1.965	362
/gate/source/A128/gps/histpoint	1.968	361
/gate/source/A128/gps/histpoint	1.971	359
/gate/source/A128/gps/histpoint	1.974	358
/gate/source/A128/gps/histpoint	1.977	356
/gate/source/A128/gps/histpoint	1.98	355
/gate/source/A128/gps/histpoint	1.983	353
/gate/source/A128/gps/histpoint	1.986	351
/gate/source/A128/gps/histpoint	1.989	350
/gate/source/A128/gps/histpoint	1.992	348
/gate/source/A128/gps/histpoint	1.995	347
/gate/source/A128/gps/histpoint	1.998	345
/gate/source/A128/gps/histpoint	2.001	344
/gate/source/A128/gps/histpoint	2.004	342
/gate/source/A128/gps/histpoint	2.007	340
/gate/source/A128/gps/histpoint	2.01	339
/gate/source/A128/gps/histpoint	2.013	337
/gate/source/A128/gps/histpoint	2.016	336
/gate/source/A128/gps/histpoint	2.019	334
/gate/source/A128/gps/histpoint	2.022	333
/gate/source/A128/gps/histpoint	2.025	331
/gate/source/A128/gps/histpoint	2.028	329
/gate/source/A128/gps/histpoint	2.031	328
/gate/source/A128/gps/histpoint	2.034	326
/gate/source/A128/gps/histpoint	2.037	325
/gate/source/A128/gps/histpoint	2.04	323
/gate/source/A128/gps/histpoint	2.043	321
/gate/source/A128/gps/histpoint	2.046	320
/gate/source/A128/gps/histpoint	2.049	318
/gate/source/A128/gps/histpoint	2.052	317
/gate/source/A128/gps/histpoint	2.055	315

/gate/source/AI28/gps/histpoint	2.058	314
/gate/source/AI28/gps/histpoint	2.061	312
/gate/source/AI28/gps/histpoint	2.064	310
/gate/source/AI28/gps/histpoint	2.067	309
/gate/source/AI28/gps/histpoint	2.07	307
/gate/source/AI28/gps/histpoint	2.073	305
/gate/source/AI28/gps/histpoint	2.076	304
/gate/source/AI28/gps/histpoint	2.079	302
/gate/source/AI28/gps/histpoint	2.082	301
/gate/source/AI28/gps/histpoint	2.085	299
/gate/source/AI28/gps/histpoint	2.088	297
/gate/source/AI28/gps/histpoint	2.091	296
/gate/source/AI28/gps/histpoint	2.094	294
/gate/source/AI28/gps/histpoint	2.097	293
/gate/source/AI28/gps/histpoint	2.1	291
/gate/source/AI28/gps/histpoint	2.103	289
/gate/source/AI28/gps/histpoint	2.106	288
/gate/source/AI28/gps/histpoint	2.109	286
/gate/source/AI28/gps/histpoint	2.112	285
/gate/source/AI28/gps/histpoint	2.115	283
/gate/source/AI28/gps/histpoint	2.118	281
/gate/source/AI28/gps/histpoint	2.121	280
/gate/source/AI28/gps/histpoint	2.124	278
/gate/source/AI28/gps/histpoint	2.127	276
/gate/source/AI28/gps/histpoint	2.13	275
/gate/source/AI28/gps/histpoint	2.133	273
/gate/source/AI28/gps/histpoint	2.136	272
/gate/source/AI28/gps/histpoint	2.139	270
/gate/source/AI28/gps/histpoint	2.142	268
/gate/source/AI28/gps/histpoint	2.145	267
/gate/source/AI28/gps/histpoint	2.148	265
/gate/source/AI28/gps/histpoint	2.151	263
/gate/source/AI28/gps/histpoint	2.154	262
/gate/source/AI28/gps/histpoint	2.157	260
/gate/source/AI28/gps/histpoint	2.16	259
/gate/source/AI28/gps/histpoint	2.163	257
/gate/source/AI28/gps/histpoint	2.166	255
/gate/source/AI28/gps/histpoint	2.169	254
/gate/source/AI28/gps/histpoint	2.172	252
/gate/source/AI28/gps/histpoint	2.175	250
/gate/source/AI28/gps/histpoint	2.178	249
/gate/source/AI28/gps/histpoint	2.181	247
/gate/source/AI28/gps/histpoint	2.184	246
/gate/source/AI28/gps/histpoint	2.187	244
/gate/source/AI28/gps/histpoint	2.19	242
/gate/source/AI28/gps/histpoint	2.193	241
/gate/source/AI28/gps/histpoint	2.196	239
/gate/source/AI28/gps/histpoint	2.199	237
/gate/source/AI28/gps/histpoint	2.202	236
/gate/source/AI28/gps/histpoint	2.205	234
/gate/source/AI28/gps/histpoint	2.208	233
/gate/source/AI28/gps/histpoint	2.211	231
/gate/source/AI28/gps/histpoint	2.214	229
/gate/source/AI28/gps/histpoint	2.217	228
/gate/source/AI28/gps/histpoint	2.22	226
/gate/source/AI28/gps/histpoint	2.223	225
/gate/source/AI28/gps/histpoint	2.226	223
/gate/source/AI28/gps/histpoint	2.229	221
/gate/source/AI28/gps/histpoint	2.232	220
/gate/source/AI28/gps/histpoint	2.235	218
/gate/source/AI28/gps/histpoint	2.238	217
/gate/source/AI28/gps/histpoint	2.241	215
/gate/source/AI28/gps/histpoint	2.244	213
/gate/source/AI28/gps/histpoint	2.247	212
/gate/source/AI28/gps/histpoint	2.25	210

/gate/source/AI28/gps/histpoint	2.253	209
/gate/source/AI28/gps/histpoint	2.256	207
/gate/source/AI28/gps/histpoint	2.259	205
/gate/source/AI28/gps/histpoint	2.262	204
/gate/source/AI28/gps/histpoint	2.265	202
/gate/source/AI28/gps/histpoint	2.268	201
/gate/source/AI28/gps/histpoint	2.271	199
/gate/source/AI28/gps/histpoint	2.274	197
/gate/source/AI28/gps/histpoint	2.277	196
/gate/source/AI28/gps/histpoint	2.28	194
/gate/source/AI28/gps/histpoint	2.283	193
/gate/source/AI28/gps/histpoint	2.286	191
/gate/source/AI28/gps/histpoint	2.289	189
/gate/source/AI28/gps/histpoint	2.292	188
/gate/source/AI28/gps/histpoint	2.295	186
/gate/source/AI28/gps/histpoint	2.298	185
/gate/source/AI28/gps/histpoint	2.301	183
/gate/source/AI28/gps/histpoint	2.304	182
/gate/source/AI28/gps/histpoint	2.307	180
/gate/source/AI28/gps/histpoint	2.31	179
/gate/source/AI28/gps/histpoint	2.313	177
/gate/source/AI28/gps/histpoint	2.316	175
/gate/source/AI28/gps/histpoint	2.319	174
/gate/source/AI28/gps/histpoint	2.322	172
/gate/source/AI28/gps/histpoint	2.325	171
/gate/source/AI28/gps/histpoint	2.328	169
/gate/source/AI28/gps/histpoint	2.331	168
/gate/source/AI28/gps/histpoint	2.334	166
/gate/source/AI28/gps/histpoint	2.337	165
/gate/source/AI28/gps/histpoint	2.34	163
/gate/source/AI28/gps/histpoint	2.343	162
/gate/source/AI28/gps/histpoint	2.346	160
/gate/source/AI28/gps/histpoint	2.349	159
/gate/source/AI28/gps/histpoint	2.352	157
/gate/source/AI28/gps/histpoint	2.355	155
/gate/source/AI28/gps/histpoint	2.358	154
/gate/source/AI28/gps/histpoint	2.361	152
/gate/source/AI28/gps/histpoint	2.364	151
/gate/source/AI28/gps/histpoint	2.367	149
/gate/source/AI28/gps/histpoint	2.37	148
/gate/source/AI28/gps/histpoint	2.373	146
/gate/source/AI28/gps/histpoint	2.376	145
/gate/source/AI28/gps/histpoint	2.379	144
/gate/source/AI28/gps/histpoint	2.382	142
/gate/source/AI28/gps/histpoint	2.385	141
/gate/source/AI28/gps/histpoint	2.388	139
/gate/source/AI28/gps/histpoint	2.391	138
/gate/source/AI28/gps/histpoint	2.394	136
/gate/source/AI28/gps/histpoint	2.397	135
/gate/source/AI28/gps/histpoint	2.4	133
/gate/source/AI28/gps/histpoint	2.403	132
/gate/source/AI28/gps/histpoint	2.406	130
/gate/source/AI28/gps/histpoint	2.409	129
/gate/source/AI28/gps/histpoint	2.412	127
/gate/source/AI28/gps/histpoint	2.415	126
/gate/source/AI28/gps/histpoint	2.418	125
/gate/source/AI28/gps/histpoint	2.421	123
/gate/source/AI28/gps/histpoint	2.424	122
/gate/source/AI28/gps/histpoint	2.427	120
/gate/source/AI28/gps/histpoint	2.43	119
/gate/source/AI28/gps/histpoint	2.433	118
/gate/source/AI28/gps/histpoint	2.436	116
/gate/source/AI28/gps/histpoint	2.439	115
/gate/source/AI28/gps/histpoint	2.442	113
/gate/source/AI28/gps/histpoint	2.445	112

/gate/source/AI28/gps/histpoint	2.448	111
/gate/source/AI28/gps/histpoint	2.451	109
/gate/source/AI28/gps/histpoint	2.454	108
/gate/source/AI28/gps/histpoint	2.457	107
/gate/source/AI28/gps/histpoint	2.46	105
/gate/source/AI28/gps/histpoint	2.463	104
/gate/source/AI28/gps/histpoint	2.466	102
/gate/source/AI28/gps/histpoint	2.469	101
/gate/source/AI28/gps/histpoint	2.472	99.8
/gate/source/AI28/gps/histpoint	2.475	98.4
/gate/source/AI28/gps/histpoint	2.478	97.1
/gate/source/AI28/gps/histpoint	2.481	95.8
/gate/source/AI28/gps/histpoint	2.484	94.5
/gate/source/AI28/gps/histpoint	2.487	93.2
/gate/source/AI28/gps/histpoint	2.49	91.9
/gate/source/AI28/gps/histpoint	2.493	90.6
/gate/source/AI28/gps/histpoint	2.496	89.3
/gate/source/AI28/gps/histpoint	2.499	88
/gate/source/AI28/gps/histpoint	2.502	86.8
/gate/source/AI28/gps/histpoint	2.505	85.5
/gate/source/AI28/gps/histpoint	2.508	84.2
/gate/source/AI28/gps/histpoint	2.511	83
/gate/source/AI28/gps/histpoint	2.514	81.7
/gate/source/AI28/gps/histpoint	2.517	80.5
/gate/source/AI28/gps/histpoint	2.52	79.3
/gate/source/AI28/gps/histpoint	2.523	78
/gate/source/AI28/gps/histpoint	2.526	76.8
/gate/source/AI28/gps/histpoint	2.529	75.6
/gate/source/AI28/gps/histpoint	2.532	74.4
/gate/source/AI28/gps/histpoint	2.535	73.2
/gate/source/AI28/gps/histpoint	2.538	72
/gate/source/AI28/gps/histpoint	2.541	70.8
/gate/source/AI28/gps/histpoint	2.544	69.6
/gate/source/AI28/gps/histpoint	2.547	68.5
/gate/source/AI28/gps/histpoint	2.55	67.3
/gate/source/AI28/gps/histpoint	2.553	66.2
/gate/source/AI28/gps/histpoint	2.556	65
/gate/source/AI28/gps/histpoint	2.559	63.9
/gate/source/AI28/gps/histpoint	2.562	62.7
/gate/source/AI28/gps/histpoint	2.565	61.6
/gate/source/AI28/gps/histpoint	2.568	60.5
/gate/source/AI28/gps/histpoint	2.571	59.4
/gate/source/AI28/gps/histpoint	2.574	58.3
/gate/source/AI28/gps/histpoint	2.577	57.2
/gate/source/AI28/gps/histpoint	2.58	56.1
/gate/source/AI28/gps/histpoint	2.583	55
/gate/source/AI28/gps/histpoint	2.586	54
/gate/source/AI28/gps/histpoint	2.589	52.9
/gate/source/AI28/gps/histpoint	2.592	51.8
/gate/source/AI28/gps/histpoint	2.595	50.8
/gate/source/AI28/gps/histpoint	2.598	49.8
/gate/source/AI28/gps/histpoint	2.601	48.7
/gate/source/AI28/gps/histpoint	2.604	47.7
/gate/source/AI28/gps/histpoint	2.607	46.7
/gate/source/AI28/gps/histpoint	2.61	45.7
/gate/source/AI28/gps/histpoint	2.613	44.7
/gate/source/AI28/gps/histpoint	2.616	43.7
/gate/source/AI28/gps/histpoint	2.619	42.7
/gate/source/AI28/gps/histpoint	2.622	41.8
/gate/source/AI28/gps/histpoint	2.625	40.8
/gate/source/AI28/gps/histpoint	2.628	39.9
/gate/source/AI28/gps/histpoint	2.631	38.9
/gate/source/AI28/gps/histpoint	2.634	38
/gate/source/AI28/gps/histpoint	2.637	37.1
/gate/source/AI28/gps/histpoint	2.64	36.2

/gate/source/A128/gps/histpoint	2.643	35.3
/gate/source/A128/gps/histpoint	2.646	34.4
/gate/source/A128/gps/histpoint	2.649	33.5
/gate/source/A128/gps/histpoint	2.652	32.6
/gate/source/A128/gps/histpoint	2.655	31.8
/gate/source/A128/gps/histpoint	2.658	30.9
/gate/source/A128/gps/histpoint	2.661	30.1
/gate/source/A128/gps/histpoint	2.664	29.2
/gate/source/A128/gps/histpoint	2.667	28.4
/gate/source/A128/gps/histpoint	2.67	27.6
/gate/source/A128/gps/histpoint	2.673	26.8
/gate/source/A128/gps/histpoint	2.676	26
/gate/source/A128/gps/histpoint	2.679	25.2
/gate/source/A128/gps/histpoint	2.682	24.5
/gate/source/A128/gps/histpoint	2.685	23.7
/gate/source/A128/gps/histpoint	2.688	22.9
/gate/source/A128/gps/histpoint	2.691	22.2
/gate/source/A128/gps/histpoint	2.694	21.5
/gate/source/A128/gps/histpoint	2.697	20.8
/gate/source/A128/gps/histpoint	2.7	20.1
/gate/source/A128/gps/histpoint	2.703	19.4
/gate/source/A128/gps/histpoint	2.706	18.7
/gate/source/A128/gps/histpoint	2.709	18
/gate/source/A128/gps/histpoint	2.712	17.3
/gate/source/A128/gps/histpoint	2.715	16.7
/gate/source/A128/gps/histpoint	2.718	16
/gate/source/A128/gps/histpoint	2.721	15.4
/gate/source/A128/gps/histpoint	2.724	14.8
/gate/source/A128/gps/histpoint	2.727	14.2
/gate/source/A128/gps/histpoint	2.73	13.6
/gate/source/A128/gps/histpoint	2.733	13
/gate/source/A128/gps/histpoint	2.736	12.4
/gate/source/A128/gps/histpoint	2.739	11.9
/gate/source/A128/gps/histpoint	2.742	11.3
/gate/source/A128/gps/histpoint	2.745	10.8
/gate/source/A128/gps/histpoint	2.748	10.3
/gate/source/A128/gps/histpoint	2.751	9.76
/gate/source/A128/gps/histpoint	2.754	9.26
/gate/source/A128/gps/histpoint	2.757	8.77
/gate/source/A128/gps/histpoint	2.76	8.29
/gate/source/A128/gps/histpoint	2.763	7.83
/gate/source/A128/gps/histpoint	2.766	7.38
/gate/source/A128/gps/histpoint	2.769	6.94
/gate/source/A128/gps/histpoint	2.772	6.52
/gate/source/A128/gps/histpoint	2.775	6.1
/gate/source/A128/gps/histpoint	2.778	5.7
/gate/source/A128/gps/histpoint	2.781	5.32
/gate/source/A128/gps/histpoint	2.784	4.94
/gate/source/A128/gps/histpoint	2.787	4.58
/gate/source/A128/gps/histpoint	2.79	4.23
/gate/source/A128/gps/histpoint	2.793	3.9
/gate/source/A128/gps/histpoint	2.796	3.58
/gate/source/A128/gps/histpoint	2.799	3.27
/gate/source/A128/gps/histpoint	2.802	2.97
/gate/source/A128/gps/histpoint	2.805	2.69
/gate/source/A128/gps/histpoint	2.808	2.42
/gate/source/A128/gps/histpoint	2.811	2.17
/gate/source/A128/gps/histpoint	2.814	1.93
/gate/source/A128/gps/histpoint	2.817	1.7
/gate/source/A128/gps/histpoint	2.82	1.49
/gate/source/A128/gps/histpoint	2.823	1.29
/gate/source/A128/gps/histpoint	2.826	1.1
/gate/source/A128/gps/histpoint	2.829	0.931
/gate/source/A128/gps/histpoint	2.832	0.774
/gate/source/A128/gps/histpoint	2.835	0.632

/gate/source/Al28/gps/histpoint	2.838	0.503
/gate/source/Al28/gps/histpoint	2.841	0.389
/gate/source/Al28/gps/histpoint	2.844	0.289
/gate/source/Al28/gps/histpoint	2.847	0.204
/gate/source/Al28/gps/histpoint	2.85	0.134
/gate/source/Al28/gps/histpoint	2.853	0.0784
/gate/source/Al28/gps/histpoint	2.856	0.0375
/gate/source/Al28/gps/histpoint	2.859	0.0115
/gate/source/Al28/gps/histpoint	2.862	0.000422
/gate/source/Al28/gps/histpoint	2.865	0
/gate/source/Al28/gps/histpoint	2.868	0

#/gate/source/Al28/gps/arbint Lin

/gate/source/Al28/setForcedUnstableFlag false

#/gate/source/Al28/setForcedHalfLife 134.5 s

/gate/source/Al28/gps/angtype iso

#

/gate/source/Al28/gps/type Volume

/gate/source/Al28/gps/shape Cylinder

/gate/source/Al28/gps/radius 1.27 cm

/gate/source/Al28/gps/halfz 0.3175 cm

/gate/source/Al28/gps/centre 0. 0. 2.4175 cm

/gate/source/list

#

#Output

#

#/gate/output/root/enable

#/gate/output/root/setFileName rootOutput

#/gate/output/root/setRootHitFlag 1

#/gate/output/root/setRootSinglesFlag 0

#/gate/output/root/setRootOpticalFlag 1

#

/gate/output/ascii/enable

/gate/output/ascii/setFileName asciiQuartz_beta_Output

/gate/output/ascii/setOutFileHitsFlag 1

/gate/output/ascii/setOutFileSinglesFlag 0

#

/gate/output/analysis/enable

/gate/output/fastanalysis/enable

#

Random Number Generator

#

/gate/random/setEngineName MersenneTwister

/gate/random/setEngineSeed auto

#

Run Gate

#

/gate/application/setTimeSlice 100000 s

/gate/application/setTimeStart 0 s

/gate/application/setTimeStop 100000 s

/gate/application/startDAQ

APPENDIX C: ^{252}Cf SOURCE INFORMATION



U.S. Department
of Transportation
Research and
Special Programs
Administration

IAEA CERTIFICATE OF COMPETENT AUTHORITY
SPECIAL FORM RADIOACTIVE MATERIALS
CERTIFICATE NUMBER USA/0018/S, REVISION 6

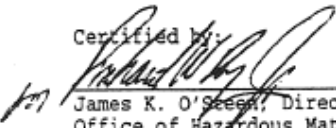
400 Seventh Street S.W.
Washington D.C. 20590

This certifies that the sources described have been demonstrated to meet the regulatory requirements for special form radioactive material as prescribed in the regulations of the International Atomic Energy Agency and the United States of America² for the transport of radioactive materials.

1. Source Identification - SR-CF-100 series neutron source manufactured by either the Savannah River Laboratory or the Oak Ridge National Laboratory (ORNL).
2. Source Description - The source described by this certificate is a welded, double encapsulation constructed of a platinum-rhodium alloy inner capsule and a stainless steel or Zircalloy-2 outer capsule. The external dimensions are 9.4 mm (0.37") in diameter x 38 mm (1.5") long (illustration attached).
3. Radioactive Contents - This source consists of not more than 0.192 TBq (5.2 Ci) of Cf-252 as an oxide.
4. Quality Assurance - Records of Quality Assurance activities required by Paragraph 209 of the IAEA regulations¹ shall be maintained and made available to the authorized officials for at least three years after the last shipment authorized by this certificate. Consignors and consignees in the United States exporting or importing shipments under this certificate shall satisfy the requirements of Subpart H of 10 CFR 71.
5. Expiration Date - This certificate expires November 1, 2000.

This certificate is issued in accordance with paragraph 703 of the IAEA Regulations and Section 173.476 of Title 49 of the Code of Federal Regulations, in response to the petition and information dated October 17, 1995 submitted by U.S. Department of Energy, Washington, DC, and in consideration of other information on file in this Office.

Certified by:


James K. O'Steen, Director
Office of Hazardous Materials
Technology

NOV - 3 1995

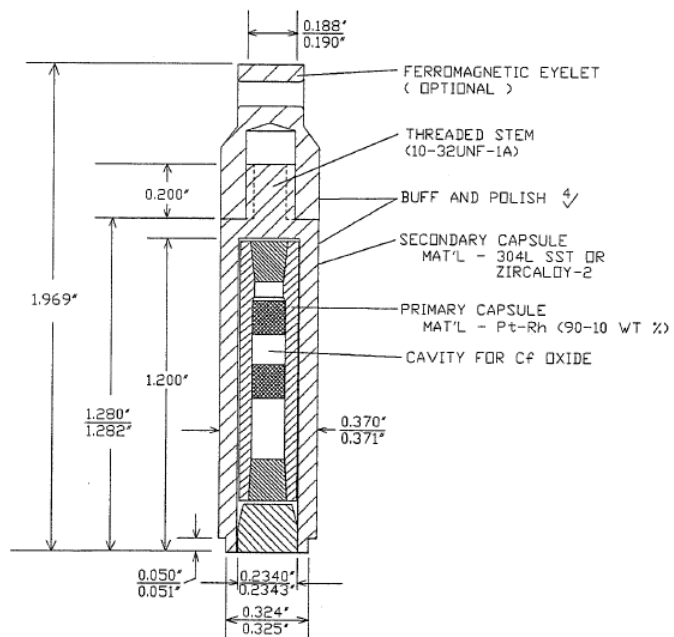
(DATE)

Revision 6 - Issued to incorporate the 1985 Edition of the IAEA regulations, and to add ORNL as an authorized fabricator of the SR-CF-100 series source, and to extend the expiration date.

Table 1

Neutron Source	SR-Cf-194Z
Sample Identification	CX-CF191
Date of Analysis	March 5, 1982
<u>Nuclide</u>	<u>Isotopic Composition (atom %)</u>
^{249}Cf	2.400
^{250}Cf	7.920
^{251}Cf	2.250
^{252}Cf	87.220
^{253}Cf	0.101
^{254}Cf	0.026
Date of Final Purification	July 13, 1982
Date of Encapsulation (Primary Capsule)	June 16, 1984
(Secondary Reencapsulation)	June 19, 1984
Date of Original Assay	June 19, 1984
Calculated Fraction of Neutrons from ^{252}Cf	0.98987 ^a
^{252}Cf Content, μg	5.17 ^a

^aValues decayed to March 31, 1997.



SR-Cf-100 Series ²⁵²Cf capsule

APPENDIX D: GAMMA RAY SPECTRA

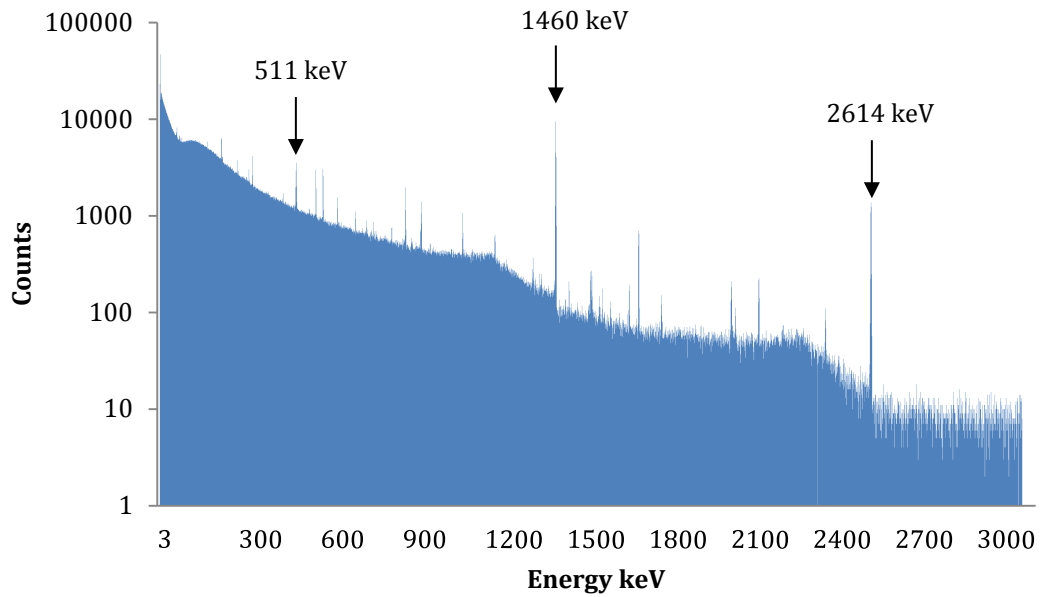


FIGURE 36 *Three day background count. The 511 keV peak from positron annihilation, 1460 keV peak from ^{40}K , and 2614 keV peak from ^{208}Tl are present.*

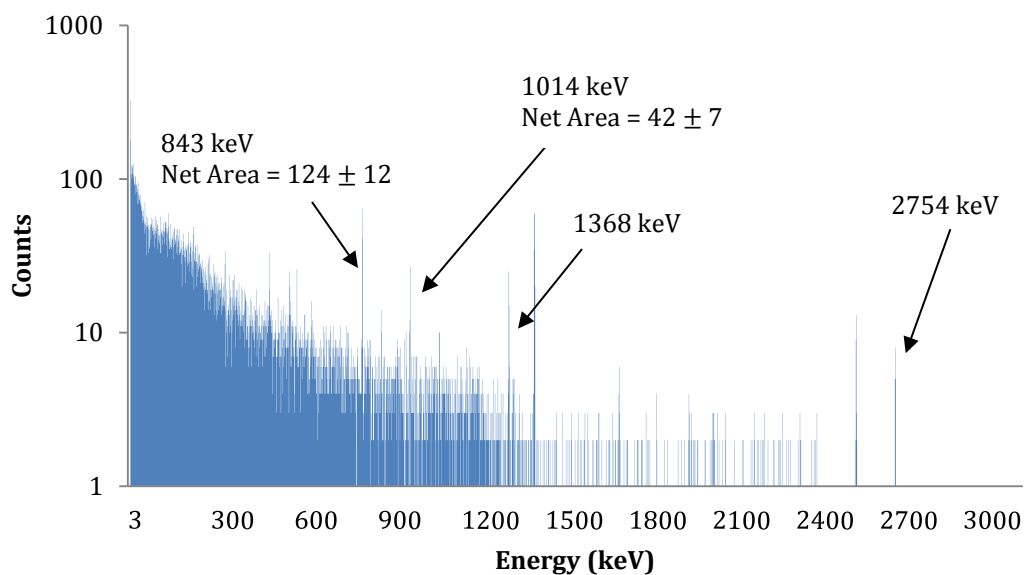


FIGURE 37 Al_2O_3 irradiated by ^{252}Cf and counted for 30 minutes. The gamma ray peaks from the decay of ^{27}Mg and ^{24}Na are present.

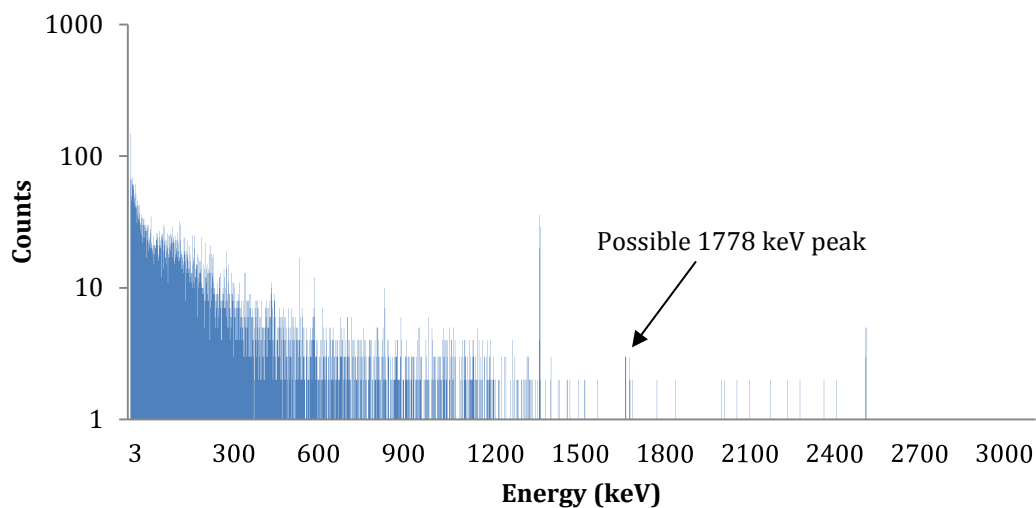


FIGURE 38 SiO_2 irradiated by ^{252}Cf and counted for 15 minutes. Counts were present at 1778 keV, however MAESTRO (the MCA software) was not able to distinguish them from background.

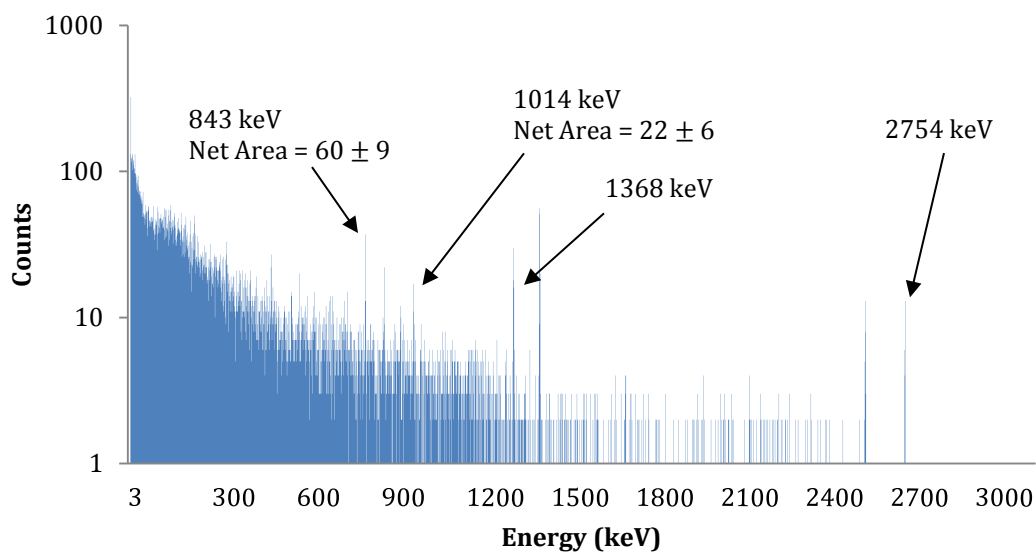


FIGURE 39 MgAl_2O_4 irradiated by ^{252}Cf and counted for 30 minutes. The gamma ray peaks from the decay of ^{27}Mg and ^{24}Na are present.

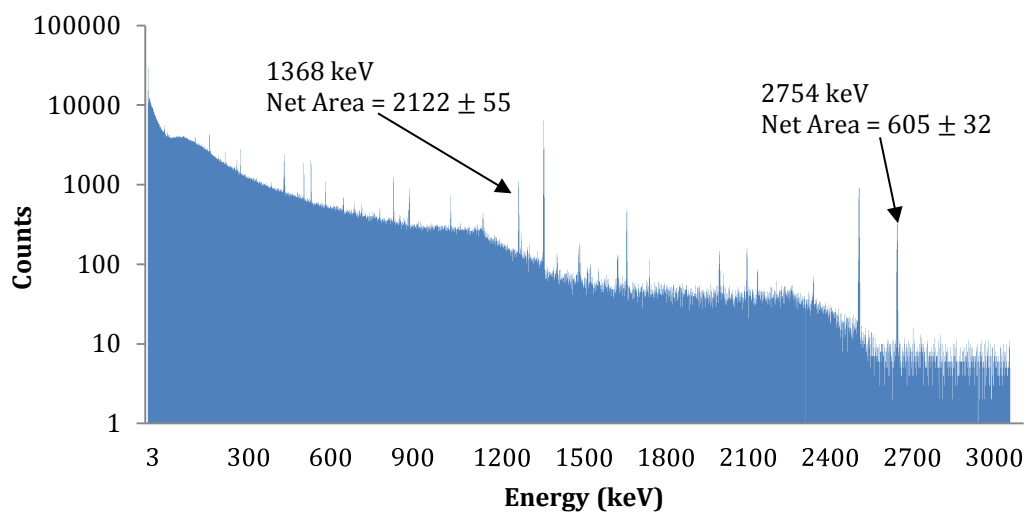


FIGURE 40 MgAl_2O_4 irradiated by ^{252}Cf and counted for 2 days. The gamma ray peaks from the decay of ^{24}Na are present.

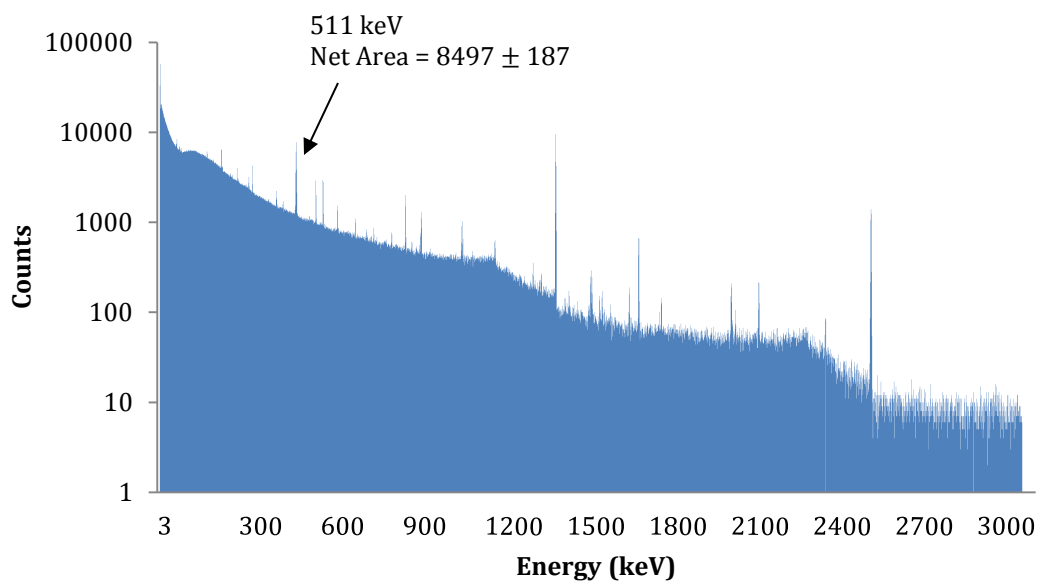


FIGURE 41 *ZnS irradiated by ^{252}Cf and counted for 3 days. The 511 keV gamma ray peak from positron annihilation is present; the net area from the 3 day background count was subtracted out of the net area value.*

APPENDIX E: SPECTROFLUOROMETER MEASUREMENTS

A Photon Technology International Spectrofluorometer (PMT model number 710) was used to measure the wavelength of photons emitted by samples while they were exposed to a 20 mCi $^{90}\text{Sr}/^{90}\text{Y}$ rectangular source and subsequently an Amptek Mini X-ray tube that emitted a 40 keV x-ray flux of approximately 10^6 x-rays per square millimeters at 30 cm. A view of the geometry is show in Figure 42. The $^{90}\text{Sr}/^{90}\text{Y}$ source emits beta particles that are energetic enough (2280 keV) to cause the samples to emit Cherenkov photons and fluorescence photons. The 40 keV x-rays from the x-ray tube are not energetic enough to cause the samples to emit Cherenkov photons, but may produce fluorescence photons in the sample. The goal was to isolate the wavelength of the Cherenkov photons and the fluorescence photons. If possible, a wavelength filter may be used to filter the signal from the two different processes.

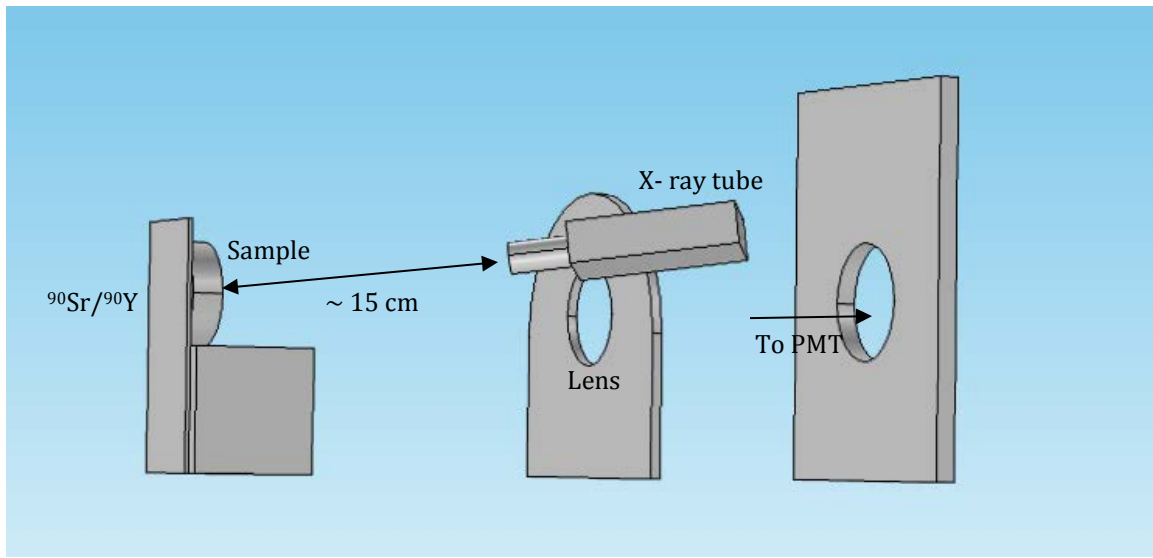
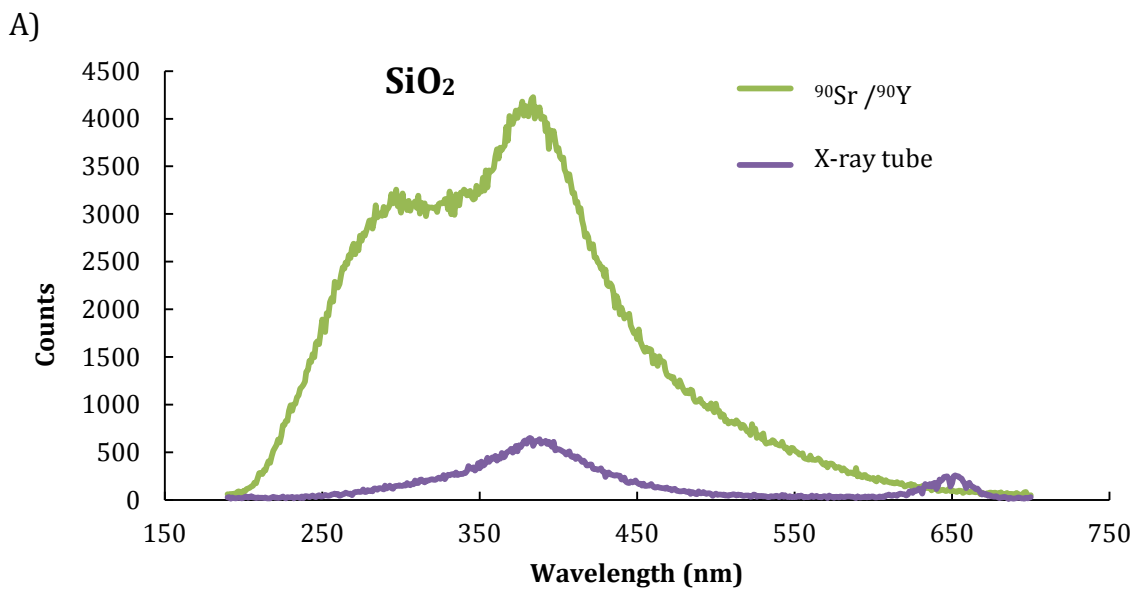
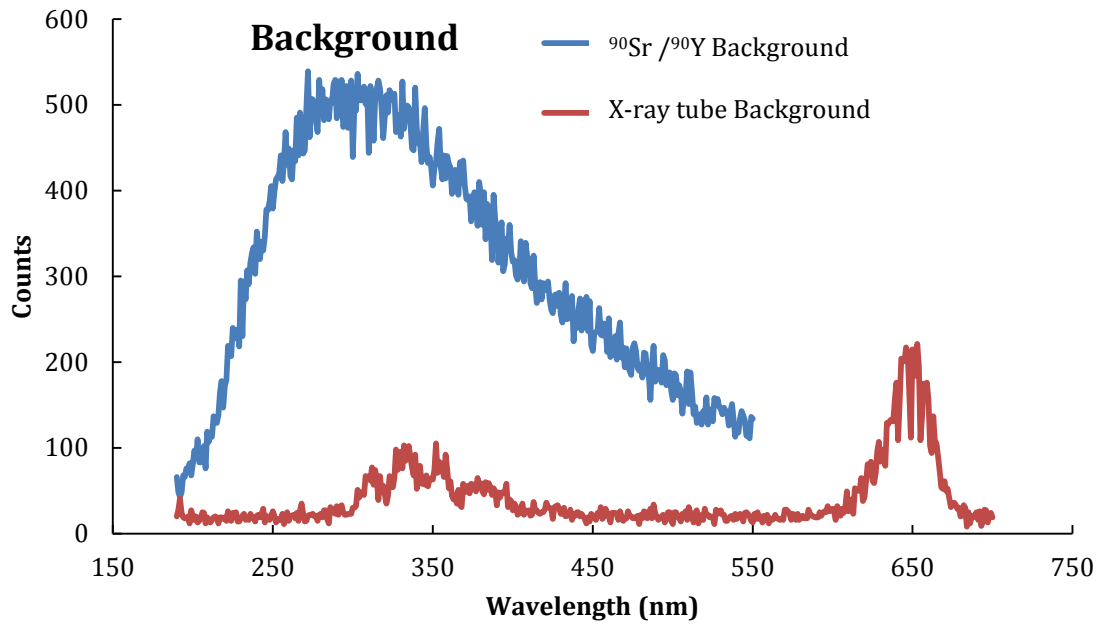


FIGURE 42 *Geometry of the spectrofluoroscopic measurements taken of the samples. The $^{90}\text{Sr}/^{90}\text{Y}$ source and the x-ray tube did not irradiate the samples simultaneously.*

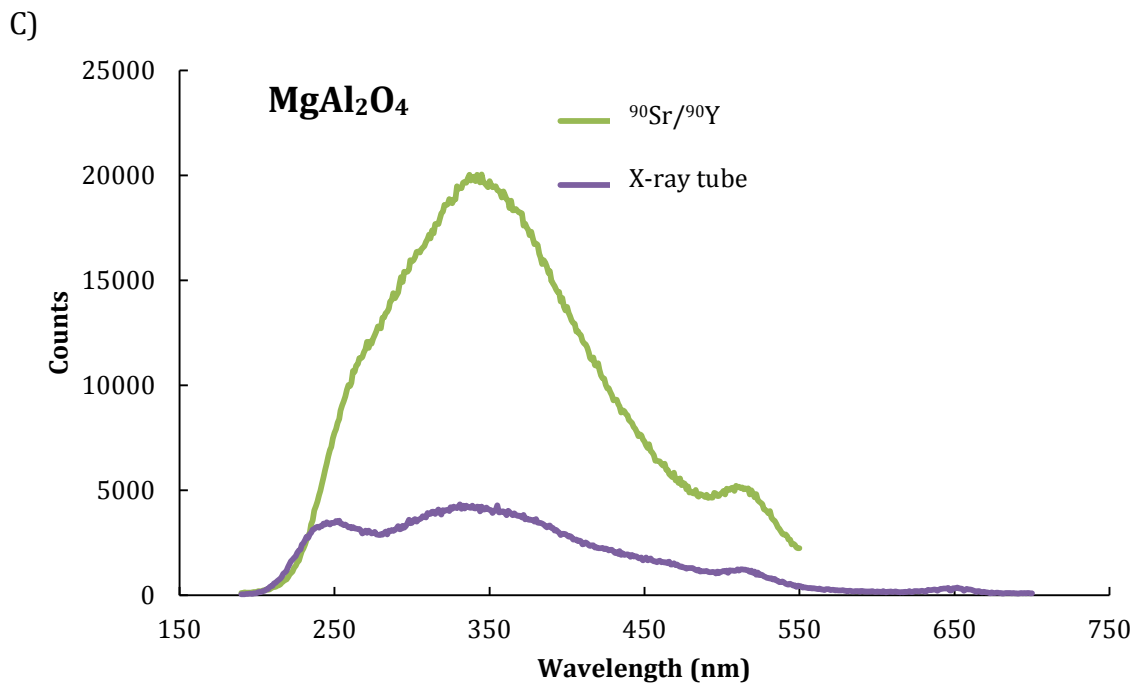
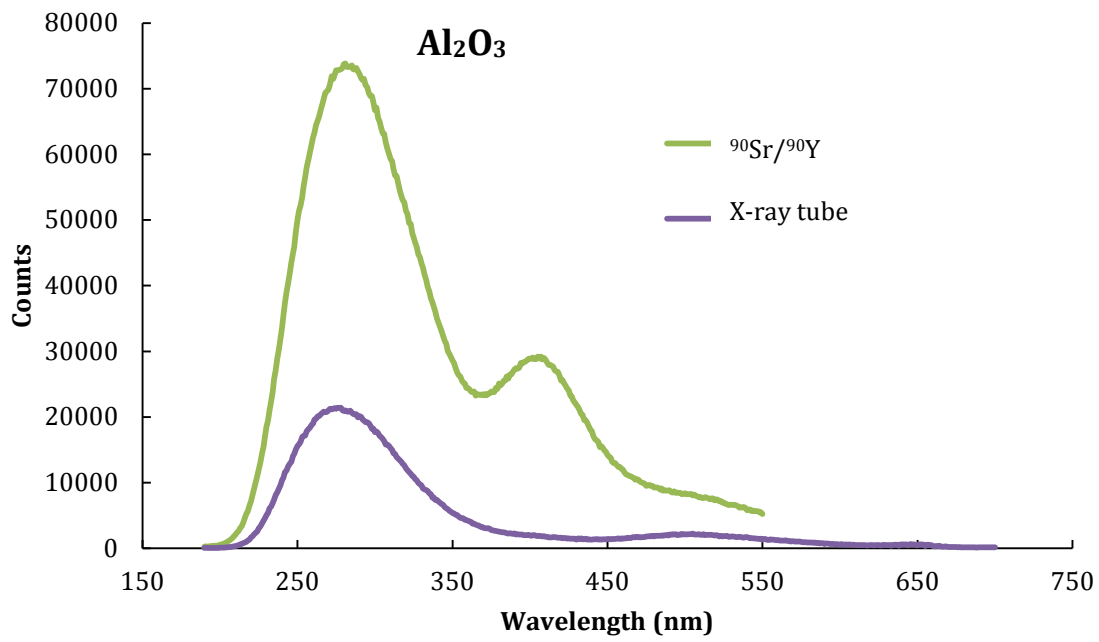
The results of the spectrofluorosity measurements are shown in Figure 43. Both the spectrum of SiO_2 irradiated by $^{90}\text{Sr}/^{90}\text{Y}$ and the spectrum of ZnS irradiated by $^{90}\text{Sr}/^{90}\text{Y}$ clearly have counts present at about 290 nm and 420 nm that are not present in the x-ray tube spectrum. The extra counts may be due to Cherenkov radiation. There was not a significant difference between the the $^{90}\text{Sr}/^{90}\text{Y}$ and x-ray tube spectra for Al_2O_3 and MgAl_2O_4 . It is possible that the signal from fluorescence may have overwhelmed the signal from Cherenkov radiation in those two samples. This coincides with results from Figure 22 which show that the Al_2O_3 and MgAl_2O_4 samples are likely to fluoresce when exposed to ionizing radiation.

The results presented in Figure 43 show that it may be possible to differentiate the Cherenkov photon signal from fluorescence signal if a proper

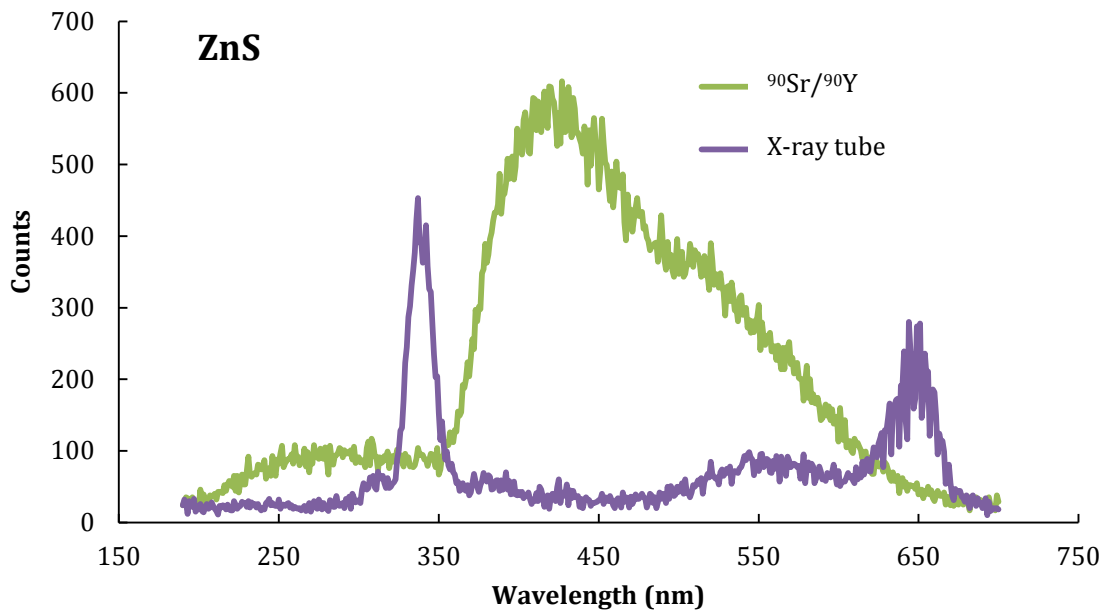
choice of wavelength filter is used when counting. However, more experiments must be undertaken to find more accurate and precise measurements of these wavelengths.



B)



D)



E)
FIGURE 43 Wavelength spectra of A) Background (only the source, no sample) B) SiO_2 C) Al_2O_3 D) MgAl_2O_4 , and E) ZnS when irradiated by a $^{90}\text{Sr}/^{90}\text{Y}$ source and a 40 keV x-ray source (left y-axis). The $^{90}\text{Sr}/^{90}\text{Y}$ source spectrum should be a combination of Cherenkov and fluorescence photons while the x-ray source spectrum should only contain fluorescence photons.

APPENDIX F: NEUTRON REACTION TARGET SEARCH PROGRAM

A computer program written in the computer language C# was developed to search the National Nuclear Data Center's neutron cross section data (National Nuclear Data Center 2013) and the Table of RadioIsotopes database (LBNL Isotopes Project Nuclear Data Dissemination Home Page 2005) for target isotopes that would meet the specific criteria suitable for the purposes of neutron activation analysis using the Cherenov effect. A picture of the program interface is shown in Figure 44. The user specifies a minimum cross section value within a neutron energy range that a desired target must possess, a minimum natural abundance of the target nuclide, and the desired decay type, minimum decay energy, minimum decay branching ratio, and half-life range of the resultant reaction product. The output displays a list of neutron reactions that meet the specified criteria. A flow chart of the program execution is shown in Figure 45.

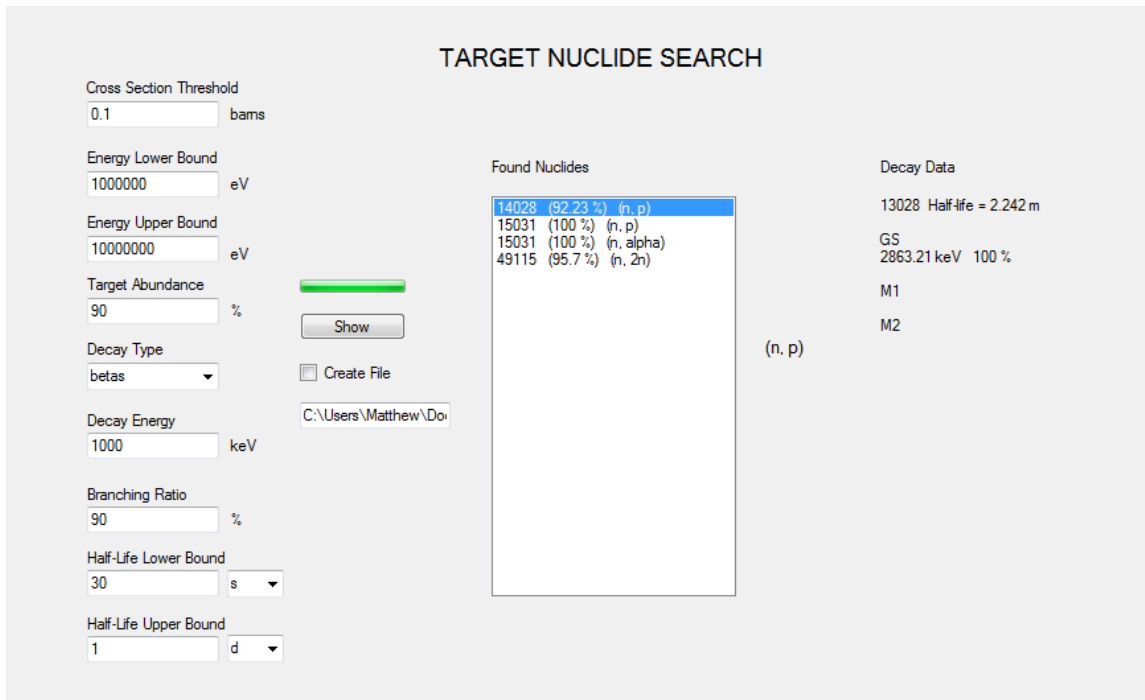
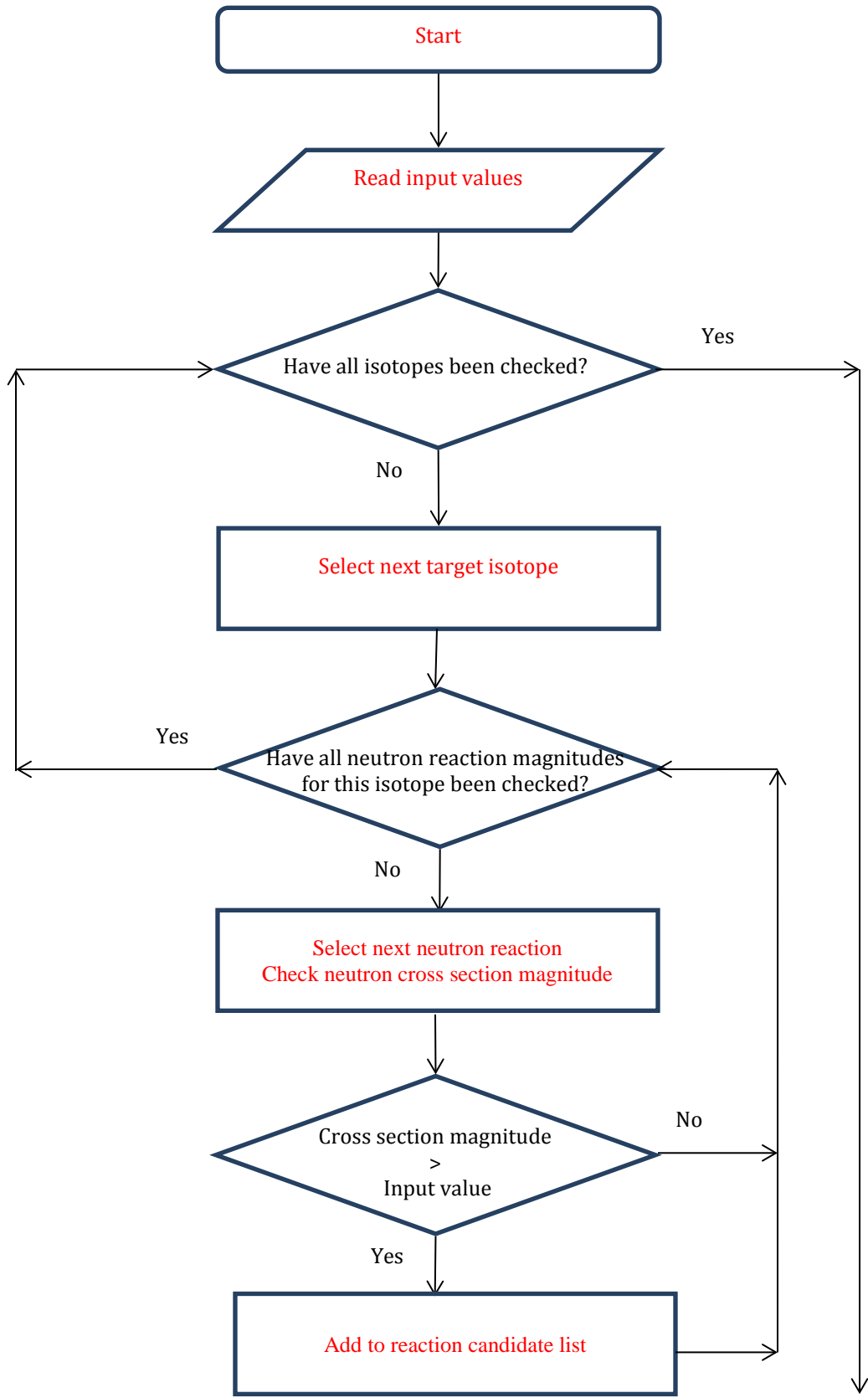


FIGURE 44 User interface for target reaction search tool used for finding neutron reactions for Cherenkov based neutron activation analysis. The program takes the specified criteria of the target nuclide and reaction product and outputs a list of reactions that meet those criteria



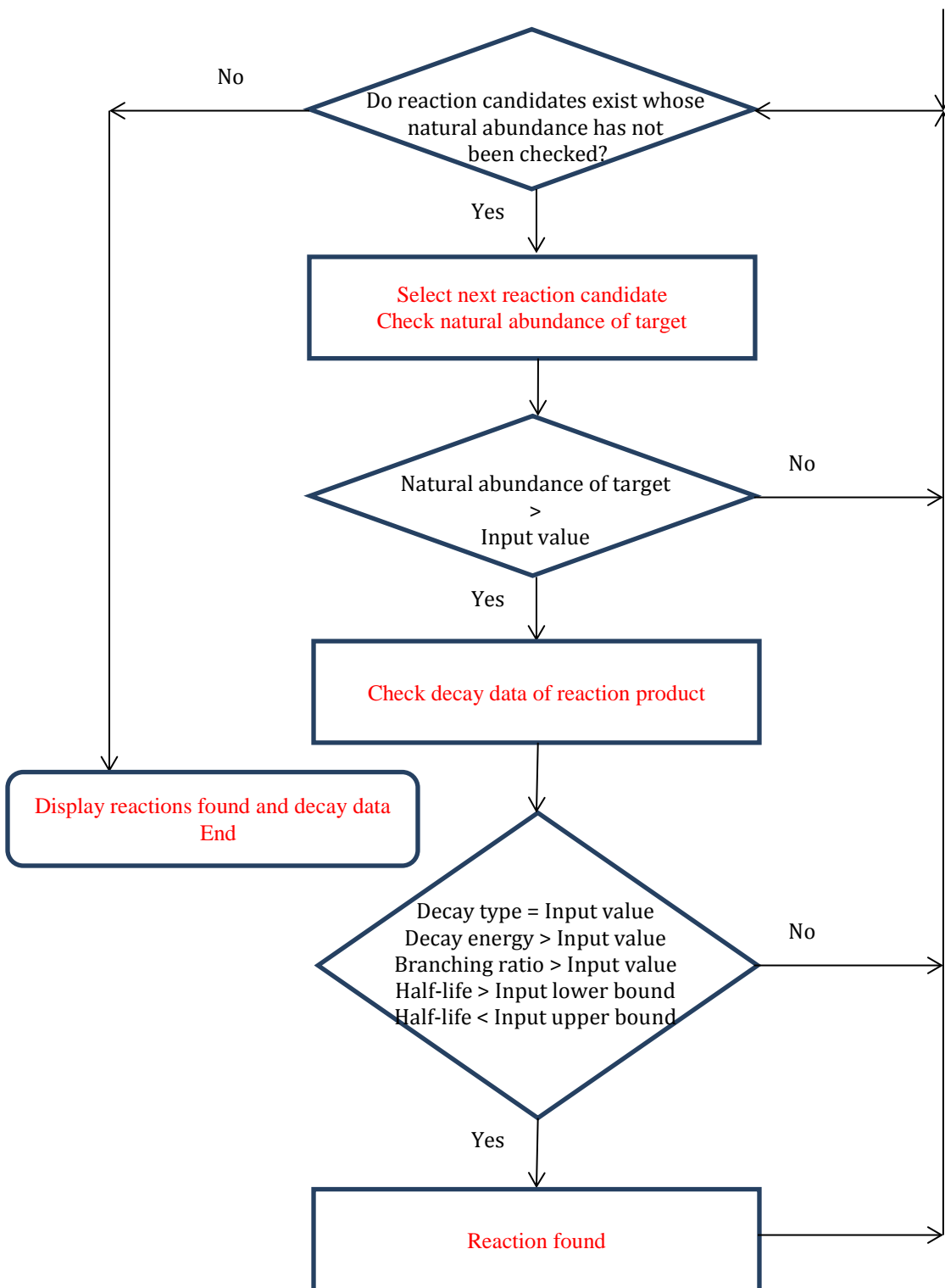


FIGURE 45 Flow chart describing the execution of the target reaction search tool used for finding reactions for Cherenkov based neutron activation analysis.

REFERENCES

- Bass et. al. *Handbook of Optics*. Vol. II. New York: McGraw-Hill, 1995.
- Bell, Zane, and Lynn Boatner. "Neutron Detection via the Cherenkov Effect." *IEEE*, 2010: 3800-3806.
- Currie, Lloyd A. "Limits for Qualitative Detection and Quantitative Determination." *Analytical Chemistry*, 1968: 586 - 593.
- Frank, I. M., and I. E. Tamm. "Coherent visible radiation of fast electrons passing through matter." *Proceedings of the USSR Academy of Sciences*, 1937: 109-114.
- Hamamatsu Photonics K.K., Electron Tube Center. "Photomultiplier Tubes R6094, R6095." Hamamatsu, August 1996.
- Jelley, J. V. *CERENKOV RADIATION and its applications*. New York: Permagon Press, 1958.
- Kerr, George D., and Gloria T. Mei. *Technical Basis for Nuclear Accident Dosimetry at Oak Ridge National Laboratory*. Oak Ridge: Oak Ridge National Laboratory, 1993.
- Knoll, Glenn. *Radiation Detection and Measurement*. Hoboken, NJ: John Wiley and Sons, Inc., 2012.
- "LBNL Isotopes Project Nuclear Data Dissemination Home Page." March 22 22, 2005. <http://ie.lbl.gov/toi.html> (accessed 2013).
- Marquardt, Donald. "An Algorithm for Least-Squares Estimation of Nonlinear Parameters." *SIAM Journal on Applied Mathematics*, 1963: 431-441.
- McLaughlin. *A Review of Criticality Accidents*. Los Alamos: Los Alamos National Laboratory, 2000, 53-56.
- National Nuclear Data Center*. 2013. <http://www.nndc.bnl.gov/sigma/>.
- Ortec. "MAESTRO-32 MCA Emulator for Microsoft Windows XP Professional SP3 and Windows 7 x32 and x64: A65-BW Software User's Manual, Software Version 7.0." Advanced Measurement Technology, Inc., 2012.
- Radioactive Material Packaging*. 2014. <http://rampac.energy.gov/docs/certificates/1030018.PDF> (accessed 2014).
- Rathbone, B. A. "Hanford External Dosimetry Technical Basis Manual PNL-MA-842." Pacific Northwest National Laboratory, 2010.
- Taylor, John R. *Classical Mechanics*. Sausalito: University Science Books, 2005.
- U.S. Department of Energy. "DOE Standard Radiological Control." U.S. Department of Energy, 2008, 5-5, 5-6.

X-5 Monte Carlo Team. "MCNP — A General Monte Carlo N-Particle Transport Code, Version 5." Vol. 1. Los Alamos: Los Alamos National Laboratory, April 24, 2003. H-3.